

Technische Universität München
Lehrstuhl für Technische Chemie II

Kinetic studies on alkane hydroisomerization over bifunctional catalysts

Christian Woltz

Vollständiger Abdruck der von der Fakultät für Chemie der Technischen Universität
München zur Erlangung des akademischen Grades eines

Doktors der Naturwissenschaften (Dr.rer.nat.)

genehmigten Dissertation.

Vorsitzende: Univ.-Prof. Dr. Sevil Weinkauf

Prüfer der Dissertation:

1. Univ.-Prof. Dr. Johannes A. Lercher
2. Priv.-Doz. Dr. Peter Härter

Die Dissertation wurde am 19.9.2005 bei der Technischen Universität München
eingereicht und durch die Fakultät für Chemie am 28.10.2005 angenommen.

Acknowledgements:

The work presented is the result of a number of fruitful, critical, lengthy, interesting and sulphurous discussions among a couple of people.

First I would like to thank Prof. Johannes A. Lercher for giving me the chance to work in an interesting research field, offering me various opportunities in apparatus and scientific promotion manner with sufficient freedom and independency for structuring my work and for enabling me to attend national and international conferences where I could present my results and meet people from industry and research.

Thanks Andy for your daily help, corrections, discussions and introduction into the Austrian language.

My time in Munich would not have been half the fun without all the crazy people from the TC2 team. Thanks for the nice working atmosphere, personal communication, help with the setups, daily trouble shooting, great soccer matches and for pitching in correction when time ran away at the end of the thesis.

Furthermore I would like to express my gratitude to Xaver who helped me a lot, especially with the setups at the beginning of my work. His long experience and knowledge was very advantageous for efficiently fixing things with the parallelized plants. I am also grateful for all the students involved in the work within the scope of their diploma thesis, semester thesis, internships or lab slavery. Thanks Josef, Stephan, Helge, Till, Saskia, Christoph, Zemin, Martin R., Martin S., Matija and Long.

Finally I would like to thank my parents for enabling me my long education and encouraging and supporting me to finish the thesis. Thanks also to my grandmas. I am sure the group will miss the marvelous cakes. I specially would like to thank Sahne for her support, sympathy and love.

The Bundesministerium für Bildung und Forschung is gratefully acknowledged for financing the project.

Christian

August 2005

Jedes Ding erscheint zuerst lächerlich,
dann wird es bekämpft,
schließlich ist es selbstverständlich

Artur Schopenhauer (22.2.1788 - 21.9.1860)

1	Chapter 1: Introduction	
1.1	General background	2
1.2	Legislation requirements	3
1.3	Catalyst development	4
1.4	Isomerization process	5
1.5	Isomerization mechanism	6
1.6	Zeolites	8
1.7	Catalyst deactivation and effect of sulfur on catalytic activity	10
1.8	Scope of the thesis	12
2	Chapter 2: Experimental	
2.1	Introduction	17
2.2	20-fold parallel plug-flow reactor	17
2.3	Temperature programmed desorption studies	20
2.4	Acknowledgements	22
3	Chapter 3: Kinetic studies on pentane hydroisomerization of Pt/H-BEA	
3.1	Abstract	24
3.2	Introduction	24
3.3	Experimental	26
3.3.1	Catalyst preparation	26
3.3.2	Atomic adsorption spectroscopy (AAS)	26
3.3.3	Transition electron microscopy (TEM)	26
3.3.4	Hydrogen Chemisorption	26
3.3.5	Temperature programmed desorption (TPD)	27
3.3.6	IR spectroscopy	27
3.3.7	Kinetic studies	27
3.4	Results and Discussion	28
3.4.1	Physical chemical properties of Pt/H-Beta	28
3.4.2	Determination of the equilibrium constant	32
3.4.3	Kinetic studies on isomerization stability and activity	33
3.4.4	Catalyst selectivity	35
3.4.5	Kinetic approach	36
3.5	Conclusions	42
3.6	Acknowledgements	42
4	Chapter 4: Improving bifunctional zeolites <i>via</i> gas phase sulfation: Effect of temperature during sulfation	
4.1	Abstract	46
4.2	Introduction	46
4.3	Experimental	48
4.3.1	Catalyst preparation	48
4.3.2	Hydrogen chemisorption	48
4.3.3	X-ray absorption spectroscopy (XAS)	49
4.3.4	Ion-Chromatography	49
4.3.5	N ₂ adsorption	50
4.3.6	Temperature programmed desorption (TPD)	50

4.3.7	IR spectroscopy.....	50
4.3.8	Temperature programmed reduction studies.....	51
4.3.9	Kinetic studies.....	51
4.4	Results.....	51
4.4.1	Preparation procedure and sulfation loading.....	51
4.4.2	Characterization of metal particles.....	53
4.4.3	Characterization of zeolite and sulfate compound.....	55
4.4.4	Nature and reactivity of sulfate species under reaction conditions.....	58
4.4.5	Hydroisomerization of pentane.....	60
4.5	Discussion.....	65
4.5.1	Influence of sulfur treatment on metal properties.....	65
4.5.2	Impact of the sulfur treatment on the acidic properties.....	66
4.5.3	Catalytic properties.....	68
4.6	Conclusions.....	70
4.7	Acknowledgements.....	71
5	Chapter 5: Preparing improved bifunctional zeolite based catalysts by sulfate modification: The role of Pt concentration and the preparation conditions	
5.1	Abstract.....	75
5.2	Introduction.....	75
5.3	Experimental.....	76
5.3.1	Catalyst preparation.....	76
5.3.2	²⁷ Al magic angle spinning nuclear magnetic resonance spectroscopy (MAS-NMR).....	77
5.3.3	Ion-Chromatography.....	78
5.3.4	Hydrogen chemisorption.....	78
5.3.5	Temperature programmed oxidation studies.....	78
5.3.6	X-ray absorption spectroscopy (XAS).....	79
5.3.7	IR spectroscopy.....	79
5.3.8	Catalytic test reactions.....	80
5.4	Results.....	81
5.4.1	Physiochemical characterization.....	81
5.4.2	Characterization of metallic properties.....	84
5.4.3	Characterization of acidic properties.....	86
5.5	Kinetic experiments.....	90
5.5.1	neo-pentane hydrogenolysis.....	91
5.5.2	n-pentane hydroisomerization.....	91
5.6	Discussion.....	95
5.6.1	Metallic properties.....	95
5.6.2	Acidic properties.....	96
5.6.3	Kinetic results.....	99
5.7	Conclusions.....	102
5.8	Acknowledgements.....	103
6	Chapter 6: Acidity and activity enhancement of zeolite Beta and Mordernite by gasphase sulfation and modification with tungsten precursor	
6.1	Abstract.....	107
6.2	Introduction.....	107
6.3	Experimental.....	109

6.3.1	Sample preparation.....	110
6.3.2	N ₂ adsorption.....	110
6.3.3	Temperature programmed desorption (TPD).....	110
6.3.4	IR spectroscopy.....	111
6.3.5	Thermal gravimetry.....	111
6.3.6	Catalytic studies.....	111
6.4	Results.....	112
6.4.1	Influence of tungsten precursor on zeolite acidity.....	112
6.4.2	Acidic characterization of zeolite mordenite.....	117
6.4.3	Activity studies.....	120
6.5	Discussion.....	123
6.5.1	Influence of tungsten precursor and subsequent sulfation process on the acidic properties.....	123
6.5.2	Influence of tungsten precursor and subsequent sulfation process on the adsorption and catalytic properties.....	124
6.5.3	Influence of different sulfation precursors on the acidic properties of zeolite MOR.....	125
6.5.4	Influence of different sulfation precursors on isomerization activity of zeolite MOR.....	127
6.6	Conclusion.....	128
6.7	Acknowledgements.....	129
7	Chapter 7: Summary	
7.1	Summary.....	133
7.2	Zusammenfassung.....	136
	Curriculum Vitae.....	140

Chapter 1

1 INTRODUCTION

1.1 General background

According to biogenetic theory, oil is composed of compressed hydrocarbons and was formed millions of years ago in a process that began when aquatic plant and animal remains were covered by layers of sediment and exposed to extreme pressure and high temperatures. The oil industry began to develop over five thousand years ago. In the Middle East, oil seeping up through the ground was used for waterproofing boats and baskets, in paints, lighting and even for medication. The modern oil industry dates back about 150 years, when the production of kerosene by simple atmospheric distillation was the major purpose. Two major events changed this situation: (i) the invention of the electric light decreased the demand for kerosene, and (ii) the invention of the internal combustion engine created a demand for diesel fuel and gasoline (naphtha). Although a use for all fractions of petroleum produced in a refinery can be found, the greatest demand is for gasoline which is present in crude oil to a content of only 25-35%. Transportation demands require that over 50% of the crude oil is converted into gasoline. Therefore catalytic cracking (breaking down large molecules), hydroprocessing (breaking down large molecules and converting aromatics to cyclic alkanes, olefins to alkanes), alkylation (forming longer molecules from smaller ones) and catalytic reforming (converting short carbon chain molecule fraction into high-octane gasoline components e.g. by isomerization) is performed to maximize the amount and quality of gasoline. All these processes involve catalysts. Cracking, alkylation and isomerization are reactions catalysed by acids. Solid acid-base catalysts have a number of advantages (e.g. non-corrosive, environmentally benign, easy separation from products) over liquid Brønsted and Lewis acidic and base catalysts. Thus more than three hundreds of solid acids and bases have been developed over the last 40 years [1]. In particular, the contribution of zeolites to industrial application is found to be of major importance. However in case of acid-base bifunctional catalysts, only few commercial processes have been developed. Since the simultaneous cooperation of weak acid sites with weak base sites on a solid surface is powerful to exhibit high catalytic activity, selectivity and catalyst lifetime, they are expected to become more important for industrial application in the future [1].

1.2 Legislation requirements

Interest in the isomerization process heightened with the phase out of tetra ethyl lead in the mid 1970s. Following the phase-out of leaded gasoline due to the Clean Air Act Amendments (CAAA) [2] in Europe (1992) and in the US (1995), oxygenates (fuel additives containing oxygen like methyl tertiary-butyl ether (MTBE) (RON:110); ethyl tertiary-butyl ether (ETBE) (RON:112); Ethanol (RON:115)) were in commercial use as octane boosters in premium gasoline to a content of up to 10 vol%. Recently oxygenates have been suspected to emit toxic formaldehyde (from methanol) or peroxyacetyl nitrate (from ethanol). The European Program on Emission, Fuel and Engine Technologies (EPEFE) developed a set of conclusions towards improving the environmental sustainability of gasoline by lowering the olefin, aromatic, oxygen and sulfur content. Aromatic and olefin react with NO_x emission to form ozone, thus contributing to smog formation. Benzene concentration levels average 2.7% in Europe due to its carcinogenicity [3]. Therefore in many plants refiners have fractionated out lighter naphta from reformer feed to minimize benzene yield. In Europe the aromatic content e.g. is limited since Jan. 1st 2005 to a content of 35 vol% instead of the formerly common 42 vol.%.

On the other hand the reduction of the aromatic content has a negative impact on the octane number of the gasoline, which is a figure of merit representing the resistance of gasoline to premature detonation when exposed to heat and pressure in the combustion chamber of an internal-combustion engine. Such detonations are wasteful for the energy in the fuel, reduce engine performance and potentially damage the engine.

Light iso-alkanes are promising compounds for the production of environmentally friendly gasoline. Iso-alkanes appear in the naphta fraction of crude oil only to a low content. The fact that they possess advanced octane numbers compared to the linear alkane offers the possibility of enhancing the gasoline quality through hydroisomerization reaction. Another advantage of these gasoline blending compounds is that the refinery streams comprehends low olefin, aromatic and sulfur contents. An overview of the combustion properties of paraffins, olefins and aromatics is given in Table 1.

Table 1: Octan numbers for different hydrocarbons.

	Hydrocarbons	RON ¹⁾	MON ²⁾
Paraffins	n-butane	93	
	n-pentane	62	62
	2-methylbutane	92	90
	2,2-dimethylpropane	85	80
	n-hexane	25	26
	2,2-dimethylpentane	92	93
	n-heptane	0	0
	2,2-dimethylpentane	93	96
	2,2,3-trimethylpentane	100	100
Olefins	1-pentene	91	77
	2-methyl-2-butene	97	85
Aromatics	Benzene	>100	>100
	Toluene	>100	>100

¹⁾: RON - Research Octane Number: Indicates petrol's anti-knock performance at lower engine speed and typical acceleration conditions.

²⁾: MON - Motor Octane Number: Indicates anti-knock performance of fuel under higher engine speed and higher load conditions.

1.3 Catalyst development

At the beginning of 20th century the production of gasoline was performed by thermal cracking. At a temperature level of 450-500°C, the larger hydrocarbon molecules become unstable and tend to break up spontaneously into smaller molecules of all possible sizes and types. One of the first improvements in petrochemical production was the process developed by Eugene Houdry (1892-1962) who introduced active clay as a catalyst to produce high-octane “Nu-Blue Sunoco” gasoline in 1937. Later on, the synthetic catalyst amorphous silica alumina (ASA) was developed which was commonly used until 1960, when it was slightly modified by incorporation of some crystalline material (zeolite catalyst). A breakthrough was achieved when platinum loaded catalyst was used in the early 1950s. From then on catalyst lifetime was enhanced dramatically as the platinum reduced the deactivation by hydrogenation of coke precursors.

The first hydro- isomerization unit was introduced in 1953 by UOP, followed in 1965 by the first BP unit, while in 1970 the first Shell hydro-isomerization (HYSOMER) unit was started up. All these processes take place in the gas phase on a fixed bed catalyst containing platinum on a solid carrier. In the late 1950s and early 1960s, chlorinated platinum loaded alumina was used as a catalyst. The major advantage of this catalyst was its low temperature activity ($T < 200^{\circ}\text{C}$) due to its high acidity. However the catalysts were sensitive towards water and oxygenates and in addition had corrosive properties. Furthermore chlorine addition during the reaction is necessary to guarantee catalyst stability. In the Hysomer process zeolite based catalysts were used which had the major advantage to be resistant against feed impurities. Expensive drying facilities are therefore not necessary and hydrogen chloride does not need to be removed from the effluent stream. However higher operation temperatures are necessary compared to the chlorinated samples due to their low acidity. Industrially applied zeolites used today are Pt-containing, modified synthetic (large-pore) mordenite [4] e.g. HS10 of UOP, or HYSOPAR from Süd-Chemie. As higher hydrogen to hydrocarbon ratios are needed recycle compressors and separators are required for this technology. In recent time as an alternative catalyst Pt loaded sulfated zirconia was commercialized for the n-butane isomerization. This catalyst stands in between the activity of the above mentioned catalyst but suffers from the loss of sulphate groups resulting in a lower catalyst life time.

1.4 Isomerization process

Besides the catalyst used, the operation characteristics of an isomerization plant severely influence isomerization rates and yields. A typical process scheme of a conventional once-through isomerization unit from UOP is given in Figure 1. Butane, pentane and hexane as feed as well as hydrogen pass through dryers towards the isomerization reactors. Either one or two reactors can be used depending on the catalyst applied and the required octane numbers. In case of two reactors the first reactor is operated at a high temperature in order to obtain high reaction rates while the second reactor is operated at a lower temperature to take advantage of the more favourable equilibrium distribution and therefore enhances the selectivity. In order to further increase the isomerization yield, it is possible to perform n- and iso- alkane separation by e.g. molecular sieves adsorption or fractionation column. In case of zeolite catalyst and sulfated mixed oxides dryers and chlorine injection are not necessary. For zeolitic isomerization

units fire feed heaters instead of hot oil or steam is necessary in order to obtain the operating temperature [5].

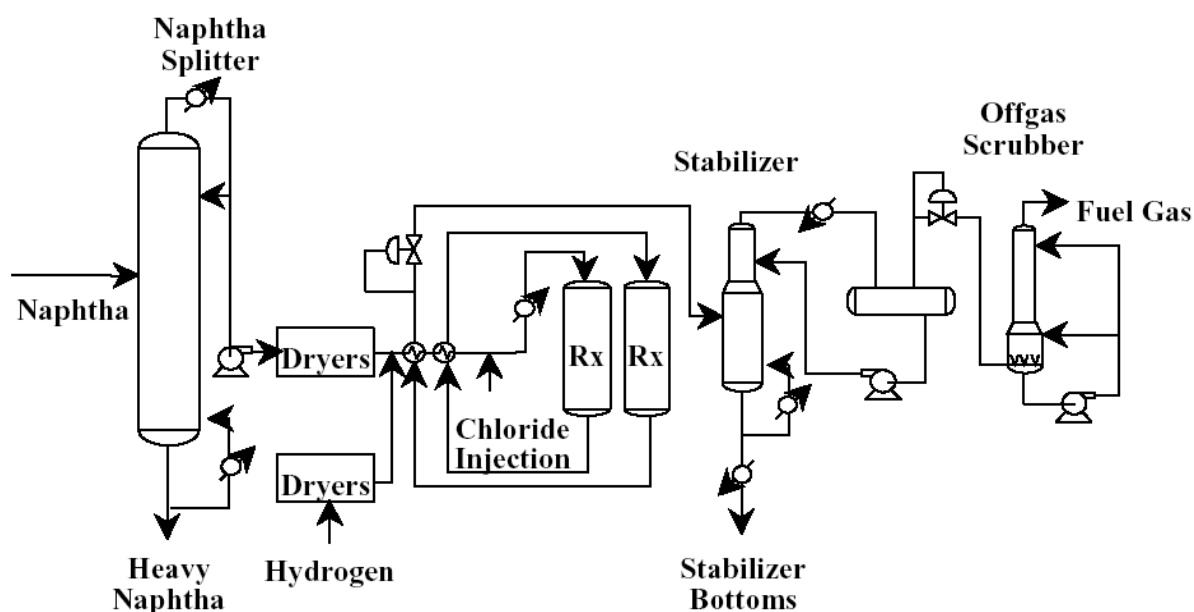


Figure 1: Process scheme of isomerization unit (UOP).

1.5 Isomerization mechanism

A bifunctional catalyst consisting a noble metal and acidic function most effectively catalyses alkane isomerization [6, 7]. The classical mechanism proceeds *via* an olefin intermediate that is formed through a dehydrogenation step on the metal site. As the olefin concentration under hydroisomerization conditions is rather low, due to the equilibrium position of the strongly endothermic dehydrogenation step, it has to be guaranteed that a sufficient number of olefins is presented to be converted to form a carbocation on the acidic sites. As hydrocarbons are very weak bases, the equilibrium concentration of carbocations on the acidic sites of *e.g.* a zeolite is rather low as well. In general two types of carbocation are known: A three-coordinated carbenium ion and a very unstable five-coordinated carbonium ion [8]. Carbenium ions can be formed in 3 different ways: Hydrid abstraction on Lewis acid sites, protonation of an alkane followed by hydrogen removal and protonation of an olefin. The presence of olefins on a bifunctional catalyst offers the protonation of the olefinic intermediate rather than the direct protonation of an alkane which is energetically much more unfavorable [9]. Therefore isomerization route via alkene intermediate occurs much faster than the route via direct activation of an alkane.

Weisz for example showed that alkenes were highly active for isomerization reaction on Pt-free silica-alumina, while alkanes were not [10]. A number of publications reported an increase in the isomerization rate with increasing Pt content [11, 12] which can be explained by a limitation of olefins on the surface. Due to the formation of strong covalent bonds the enthalpy of protonation (ΔH_{prot}) and activation energy of the isomerization step ($E_{\text{A, isom}}$) is expected to be accordingly high since this involves the lengthening of the C-O bond [13, 14]. Skeletal isomerization reaction is believed to follow the rearrangement of a carbenium ion through a cyclo-alkyl intermediate [15, 16]. The iso-paraffinic carbenium ion is subsequently converted to an olefin by loss of a proton to the acid site. In the last step the iso-olefin intermediate is rapidly hydrogenated to become the iso-alkane product. Figure 2 shows the isomerization mechanism on a bifunctional catalyst which was first proposed by Weisz [17].

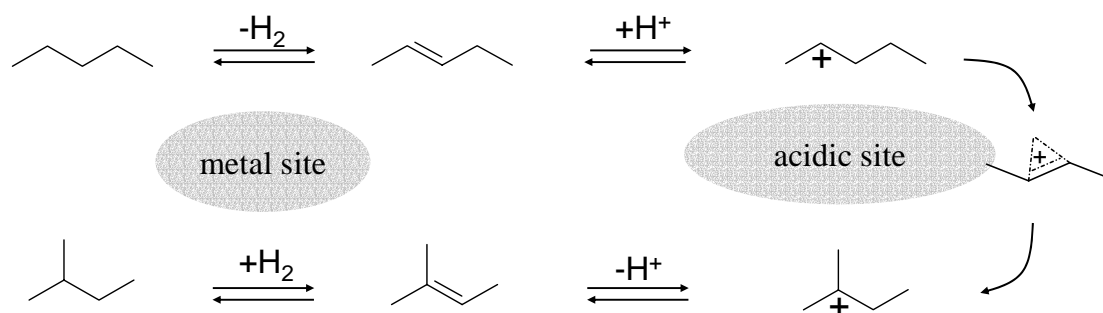


Figure 2: Isomerization mechanism.

It was observed that the rate for the isomerization reaction strongly depends on the chain length of the involved alkanes. The longer the chain length, the more stabilized the associated carbenium ion and the faster the isomerization reaction. While high activity of longer chain alkanes can be easily reached, achieving high isomerization selectivity becomes more and more difficult with increasing chain length. In general two possible side reactions can occur. Since the reaction mechanism proceeds via the formation of carbocationic intermediates consecutive hydrocracking reactions can compete with the isomerization reactions on the acid sites. Furthermore, hydrogenolysis reactions on the metal sites can occur and lower the isomerization selectivity. The balance between hydrogenation and acid function determines strongly whether acid or metal catalysed reactions are predominate and thus determine the nature of the products formed [18].

Three mechanisms for alkane cracking have been established. Non-catalytic thermal cracking proceeds via primary radical occurring only at high temperatures, protolytic α -

cracking involving a carbonium ion and β -cracking proceeding through a carbenium ion. None of the hydroisomerization reactions equilibrate completely because they compete with consecutive hydrocracking reaction that composes the isomers [19], [20]. The currently accepted mechanisms for catalytic cracking under hydroisomerization conditions are similar in that they involve carbenium ions and a β -scission step. β -scission of a C-C bond at the beta position relative to the cationic site forms a smaller alkene and another carbenium ion [21]. The probability of a molecule undergoing a hydrocracking reaction increases with an increasing degree of branching because of the higher stability of the carbocation [22].

Hydrogenolysis reaction is a non selective cracking reaction on the metal site. Particle size effects often play a role in such reactions and can lead either to a reduction (pathetic structure sensitivity) or an enhancement (antipathetic structure sensitivity) of the turnover frequency with increasing particle size or even go through a maximum [23]. In general two effects can be responsible for the change in catalytic activity with changing particle size. The reduction of particle size changes the geometric properties leading to a change in surface atom coordination. Furthermore electronic effects occur as the difference in the energy levels of the valence electrons changes. Geometric and electronic influences often cannot be separated as independent parameters [24].

1.6 Zeolites

Zeolites are crystalline aluminosilicates with precisely defined microporous structures. Industrially they are applied in three major fields: detergents (A-type zeolite), adsorbents and desiccants (A-and X-types) and finally catalysts (especially Y-type) which cover about 50% of the world market for synthetic zeolites [25]. The most important process for zeolites in catalysis are hydrocracking of heavy petroleum distillates, octane number enhancement of light gasoline, the synthesis of ethylbenzene, the disproportionation of toluene into benzene and xylene and isomerization of xylenes [26]. The pores and cages have molecular dimensions, which makes it possible to discriminate between molecules of different sizes, hence zeolites are also known as molecular sieves featuring shape selective properties. In case of reforming reactions, unfavorable side reactions like polymerization can be prevented as the bulky transition state intermediates do not fit into the cages. The channel like structure allows fast intracrystall transport proceeding.

Aluminium and Silicon atoms (T-atoms) are tetrahedrally coordinated to four bridging oxygen atoms. Zeolites are classified according to their pore size which depends on the number of oxygen atoms in the aperture ring which can contain 8-member (small pore zeolite), 10-member (medium pore zeolite) and 12-member oxygen rings (large pore zeolite). When Si^{4+} is replaced by Al^{3+} in the zeolite framework, the negative AlO_4^- building block has to be compensated by a counter ion. Brønsted acidity (H^+ -donator) can be introduced by using protons as compensation ion, thus making the material a solid acid. The concentration of Brønsted sites is therefore directly related to the number of framework Al atoms per unit cell (Figure 3). The strength of the acid sites depends on the polarization of the OH band and therefore is influenced by the angle between the two bridging T-O bonds and the distance between the T-atoms connected to the bridging oxygen. Therefore the acid strength depends on the structure of the three-dimensional network and on the local atomic environment [27]. Since aluminium carries a lower charge than the silicon atoms, the electronegativity of the material is strongly dependent on the ratio between the silicon and aluminum atoms in the framework. A higher amount of silicon atoms in the framework causes a strengthening of the Brønsted acidic OH bond and with it a lower deprotonation energy (higher acid strength). Consequentially the number of Brønsted acid sites decreases.

Zeolites are not thermodynamically stable materials. High temperature, concentrated mineral acids and alkalines or steam can destroy the structure of the zeolite causing the aluminum atoms to leave the framework. These extra framework aluminum sites feature Lewis acidic character (electron acceptor).

The large pore BEA zeolite is a potential catalyst for various acid catalyzed reactions like FCC additive to FAU zeolite [28], alkylation [29, 30] or acylation [31]. Beta zeolite was first synthesized by Mobil Oil Corporation in 1967. In Figure 4 the structure of zeolite Beta (BEA) is shown. It has a three dimensional channel system constructed of 12-member rings constituted of perpendicular straight channels (0.66 x 0.67 nm aperture) and of a sinusoidal channel (0.56 x 0.56 aperture) [32]. H-BEA zeolite is an intergrowth hybrid of two distinct structures named polymorphs A and B [32]. Unsatisfied linkages are present in the region connecting the two polymorphs inducing a stacking disorder with a high concentration of internal defects [33]. H-BEA has at least two different types of Lewis acid sites, attributed to extraframework aluminum species or to aluminum in defect position and Brønsted acidic bridging hydroxyl groups shown in Figure 3.

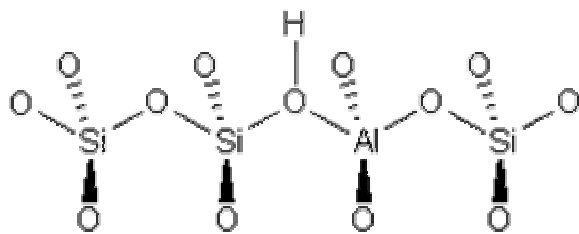


Figure 3: Brønsted acid site.

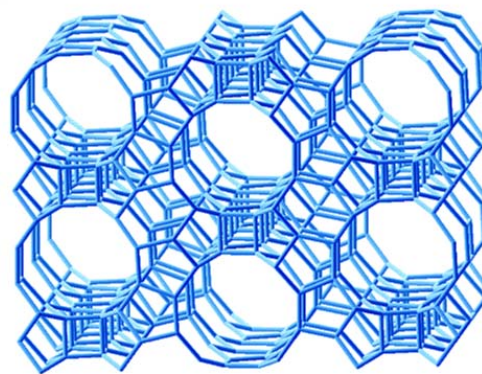


Figure 4: Zeolite BEA view along [100].

1.7 Catalyst deactivation and effect of sulfur on catalytic activity

Catalyst deactivation is the loss of activity and/or selectivity over run time. Many paths of catalyst decay exist such as coking, sintering, phase transformation, pore/void blockage, volatilization of active component and poisoning. Poisoning is the strong chemisorption of reactants on active sites, thus its influence on catalytic activity depends on its adsorption strength relative to the other reactants [34]. Poisoning can either lead to a physical blocking or can electronically modify the active sites. Furthermore a restructuring of the surface can occur and the adsorbed poison can block access of adsorbed species to each other and slow down surface diffusion.

One of the most common poisons on metal containing catalyst is sulphur which directly blocks the metal particles (*e.g.* by the formation of PtS) and can causes metal sintering. In case of platinum the migration and growth of metal particles can be prevented by using chemical anchoring by transition metal cations such as Fe^{3+} , Cr^{3+} or Ni^{2+} [35, 36]. Furtheron, an enhancement in S-tolerance of noble metals is often reported when supporting the metal on acidic carriers. The increasing sulfur resistance was attributed to the modification of the electronic properties of the metal atoms resulting from interaction with Brønsted acidic sites leading to the formation of electron deficient metal sites which lower the strength of the M-S bond [37, 38, 39].

Besides, sulfur can also have beneficial effects on catalytic activity of metal catalyzed reactions. SO_2 inhibits the oxidation of reactive hydrocarbons (such as alkenes) [40] but enhances the one of saturated ones at elevated temperatures [41]. In the catalytic oxidation

of VOC (volatile organic compounds) it was also shown that small amounts of SO_2 can promote the oxidation of hydrocarbons [42, 43]. The enhancement of the activity of the metal catalysed reaction is affiliated with the formation of surface sulfate species. For propane combustion it was argued that the chemisorption properties are enhanced by the formation of surface sulphate on alumina [41], on platinum [44] or the platinum-alumina interface [45]. In [46] the activity enhancement for the propane oxidation was assigned to the formation of electronegative sulfate deposits which lie in close proximity to the edge of a Pt particle. The perimeter sites at the Pt/support interface were suggested to initiate the C-H- bond activation though leading to an enhanced activity. Additionally in studies of SO_2 oxidation over automotive catalyst the effect of surface sulfation on $\gamma\text{-Al}_2\text{O}_3$ is known and associated with the formation of SO_3 modifying catalytic activity [47].

Treatment with sulfur compounds can additionally effects the acidic properties of the catalysts. Treatment with H_2S *e.g.* leads to a blocking of Brønsted and Lewis acidic groups in zeolite ZSM5 or Y [48, 49]. Nucleophilic sulfur such as thiophen was shown to have a negative effect on activity and selectivity for the acid catalyzed hydroisomerization reaction [50].

However acidic properties can also be enhanced in case that the treatment with sulfur compounds involves the formation of sulfate species. Acidity generation on metal oxides such as Al_2O_3 , Fe_2O_3 , SnO_2 or TiO_2 using diverse sulfur precursors was observed in *e.g.* [51, 52, 53]. Well known is also the beneficial effect of aqueous sulfation of ZrO_2 which can lead to the formation of so-called superacid solids [54, 55]. Sulfated metal oxides find application in alkane isomerization and cracking [56] and more recently in liquid alkylation and acylation [57]. Contrary to zirconia for which granulate forming is a difficult procedure [58], alumina is widely used in industry as support of catalyst due to its high surface area, thermal stability and the fact that it can be used without a binder. Surface sulfation on $\gamma\text{-Al}_2\text{O}_3$ through H_2S and SO_2 in the absence of oxygen was reported from the Claus-process, where it is suggested that surface thiosulfate and sulfate species are formed as key species in the catalytic cycle [59]. Alumina was also proposed as a SO_x transfer catalyst for the removal of SO_x during the regeneration of fluidized catalytic cracking (FFC) [60]. The formation of Brønsted acidity on sulfated alumina was observed by pyridine adsorption and ascribed due to Al-O- SO_3H species [61, 62]. In contrast to sulfated zirconia the sulfated alumina remained only weakly acid strength [63]. In [64] the origin of the strong added protonic acidity of alumina containing an admixture of basic alumina sulfate was suggested to either be due to an enhanced dissociation of water on the surface

of sulfate species or to an inductive effect of the sulfate groups on neighboring hydroxyls enhancing their protonic mobility. A sulfur oxide species of chelating organic sulfate structure was proposed to be responsible for the generation of strong acidity on sulfated F_2O_3 [51]. Saur postulated that Brønsted acidity arises in the presence of OH groups or water when $(M_3O_3)S=O$ species are converted to $(M_2O_2)SOOH$ [53]. The presence of Brønsted acid sites on sulfated alumina was furthermore evidenced by *e.g.* the skeletal isomerization of 4-methyl pentan 2-ol [62] or cumene cracking [64].

1.8 Scope of the thesis

The importance of the isomerization reaction for upgrading light naphtha fraction (C_4 - C_6) has increased due to a growing demand for premium gasoline grades and more restricted regulations on gasoline composition. The enhancement of the octane number by isomerization offers the possibility of meeting the required octane demands without the excessive addition of blended octane boosters like MTBE, oxygenates or aromatics. The production of high octane fuel requires highly active, selective, stable and harmless catalysts.

The aim of the thesis is to provide a substantiated knowledge of the isomerization reaction proceeding on a bifunctional zeolite catalyst and a way of optimizing isomerization activity and selectivity.

Chapter 2 presents the multi-fold setups that were built for the investigation of catalytic activity and the acidity measurements.

Chapter 3 describes the acidic and metallic properties of a Pt loaded H-BEA with different metal loadings. The role of Pt on isomerization activity, selectivity and stability is researched. Mechanistic studies were performed during deactivation run under helium atmosphere. The kinetic relevant step of the reaction is identified by a kinetic approach and basic kinetic parameters are determined.

In Chapter 4 a high metal loaded zeolite BEA was functionalized with sulfate groups. The effect of sulfation on the critical attributes of the catalyst, namely metal and acid sites is characterized in detail. Further on sulfate stability, the acidic properties of the sulfate species and the effect of sulfation on the zeolite framework is studied. The isomerization activity and selectivity of the sulfated materials is compared to the untreated sample.

Chapter 5 deals with the influence of preparation conditions and the role of Pt during the sulfation process. The variation of the metal content enabled to research catalysts with a metal to acid site ratio (Pt_S/H^+_{BAS}) which are more closely related to industrial application. The nature of the sulfur species and the processes occurring during sulfidation and oxidation are investigated. The characterization of the accessible metal particle and its electronic structure are emphasized in order to study the activity of the metal particles and the occurrence of dehydrogenation limitation. In addition the origin of the side reaction and the effect of the sulfation process on isomerization selectivity is addressed.

In first part of Chapter 6 the effect of a tungsten promoter was investigated on catalyst acidity and isomerization activity. The modification of the acidic and adsorption properties is described in detail. Additionally the sulfation process is applied on the tungsten modified samples showing that the combination of both acidity promoters can be combined. In the second part of the chapter the effect of different sulfation precursors on the acidic properties of zeolite MOR and thermal dealuminated MOR was studied. Besides the effect of the incorporation of sulfates species on the accessibility and diffusivity in the restricted pore system of MOR is researched.

Finally, Chapter 7 will give a summary and draw the main conclusion of the overall thesis.

REFERENCES

- [1] K. Tanabe, W.F. Hölderich, *Appl. Catal A: General* 181, 399 (1999).
- [2] CAA90, US Public Law 101-549.
- [3] Report Jacobs Consultancy: "Environmental Legislation and the impact on gasoline" J.H. Jenkins.
- [4] Cusher, N. A. (1997) in *Handbook of Petroleum Refining Processes*, ed. Myers, R. A. (McGraw-Hill, New York), p. 915.
- [5] M.J. Cleveland, C.D. Gosling, UOP LLC and J. Utley and J.E.Elstein Flying J. Inc. presentation 1999 NPRA Annual Meeting.
- [6] G.A. Mills, H.Heinemannm, T.H. Milliken, A.G. Oblad, *Ind. Eng. Chem.* 45, 134 (1953).
- [7] P.B. Weisz, *Adv. Catal.*13, 137 (1962).

-
- [8] K. Hiraoka, P. Kebarle, *J. Am. Chem. Soc.* 98, 6119 (1976).
- [9] P.A. Jacobs, J.A. Martens, *Stud. Surface. Sci. Catal.* 58, 445 (1991).
- [10] P.B. Weisz, E.W. Swegler, *Science* 126, 31 (1957).
- [11] F. Alvarez, F.R. Ribeiro, G. Perot, C. Thomazeau, M. Giusnet, *J. Catal.* 162, 179 (1996).
- [12] R. Ravishankar, S. Sivasanker, *Appl. Catal. A: Gen.* 142, 47 (1996).
- [13] V.B. Kazansky, M.V. Frash, R.A. van Santen, *Appl. Catal. A: Gen.* 146, 225 (1996).
- [14] V.B. Kazansky, I.N. Senchenya, *J. Catal. Lett.* 8, 317 (1991).
- [15] M. Saunders, P. Vogel, E.L. Hagen, J. Rosenfeld, *Acc. Chem. Soc.* 98, 3734 (1976).
- [16] E. Blomsma, J.A. Martens, P.A. Jacobs, *J. Catal.* 159, 323 (1996).
- [17] P.B. Weisz, „advances in Catalysis and Related Subjects“ (D.D. Eley, P.W. Selwood, and P.B. Weisz, Eds.) Vol 13, p.137. Academic Press, New York, 1962.
- [18] G.G. Martens, G.B. Marin, *AIChE Journal* Vol 47, No7 p.1607.
- [19] W.O. Haag, R.M. Dessau, in *Proc. 8th Int Congress on Catalysis, Berlin Vol. 2*, Dechema, Frankfurt am Main, 1984, p305.
- [20] S. Kötter, H. Knötzinger, B.C. Gates, *Micro. Meso. Mater.* 35, 11 (2000).
- [21] P.J. Hay, A. Redondo, Y. Guo, *Catal. Today* 50, 517 (1999).
- [22] T.L.M. Maesen, S. Calero, M. Schenk, B. Smit, *J. Catal.* 221, 241 (2004).
- [23] M. Che, C.O. Bennett, *Advances in catalysis, Volumen 36* (p.55ff).
- [24] B. Coq, F. Figueras, *Coord. Chem. Rev.* 178, 1753 (1998).
- [25] C. Marcilly, *Oil & Gas Science and Technology – Rev. IFP*, Vol 56 (2001) No. 5, pp. 499.
- [26] J. Weitkamp, *Solid State Ionics* 131, 175 (2000).
- [27] C. Busco, A. Barbaglia, M. Broyer, V. Bolis, G.M. Foddanu, P. Ugliengo, *thermochimica acta*, 418 3 (2004).
- [28] T. Maesen, B. Marcus, *Stud. Surf. Sci. Catal.* 137,1 (2001).
- [29] K.P. de Jong, C.M.A.M. Mesters, D.G.R. Peferoen, P.T.M. van Brugge, C. de Groot, *Chem. Eng. Sci.* 51, 2053 (1996).
- [30] G. Bellusi, G. Pazzunconi, C. Pereg, G. Girotti, G. Terzoni, *J. Catal.* 157, 227 (1995).
- [31] K. Smith, Z. Zhenhua, P.K.G. Hodgson, *J. Mol. Catal.* 134, 121 (1998).
- [32] J.B. Higgins, R.B. LaPierre, J.L. Schlenker, A.C. Rohrman, J.D. Wood, G.T. Kerr, W.J. Rohrbaugh, *Zeolite* 8, 446 (1988).
- [33] J.P. Marques, I. Gener, P. Ayrault, J. C. Bordado, J. M. Lopes, F.R. Ribeiro, M. Guisnet, *C.R. Chimie* 8, 399 (2005).
- [34] C.H. Bartholomew, *Appl. Catal. A: Gen.* 212, 17 (2001).
- [35] M.S. Tzou, H.J. Jiang, W.M.H. Sachtler, *Appl. Catal. A: Gen.* 20, 231 (1986).

-
- [36] D.E. Resasco, V.A. Durante, J. Kim, G. Larsen, G.L. Haller, *Stud. Surf. Sci. Catal.* 83, 321 (1994).
- [37] S.T. Homeyer, W.M.H. Sachtler, *Stud. Surf. Sci. Catal.* 40, 975 (1989).
- [38] J.K. Lee, H.K. Rhee, *J. Catal.* 177, 208 (1998).
- [39] D.C. Koningsberger, J. de Graaf, B.L. Mojet, D.E. Ramaker, J.T. Miller, *Appl. Catal. A: Gen.* 191, 205 (2000).
- [40] J.C. Summers, K. Baron, *J. Catal.* 57, 380 (1979).
- [41] H.C. Yao, H.K. Stepien, H.S. Gandhi, *J. Catal.* 67, 231 (1979).
- [42] C.P. Hubbard, K. Otto, H.S. Gandhi, K.Y.S. Ng, *J. Catal.* 144, 484 (1993).
- [43] A. Hinz, M. Skoglungh, E. Fridell, A. Andersson, *J. Catal.* 201, 247 (2001).
- [44] K. Wilson, C. Hardacre, R.M. Lambert, *J. Phy. Chem.* 99, 13755, (1995).
- [45] J.A.F. Lee, K. Wilson, R.M. Lambert, C.P. Hubbard, R.G. Hurley, R.W. McCabe, H.S. Gandhi, *J. Catal.* 184, 491 (1997).
- [46] R. Burch, E. Halpin, M. Hayes, K. Ruth, J.A. Sullivan, *Appl. Catal. A: Gen* 19, 199 (1998).
- [47] H.S. Gandhi, M. Shelef, *Appl. Catal. A: Gen.* 77, 175 (1991).
- [48] C.L. Garci, J.A. Lercher, *J. Phys. Chem.* 96, 2231 (1992).
- [49] T.I. Koranyi, F. Moreau, V.V. Rozanov, E.A. Rozanova, *J. Mol. Struct.* 410, 103 (1997).
- [50] S. Gopal, P. G. Smirniotis, *Appl. Catal. A: Gen.* 247, 113 (2003).
- [51] K. Arata, M. Hino, *Appl. Catal. A: Gen.* 59, 197 (1990).
- [52] T. Yamaguchi, T. Jin, K. Tanabe, *J. Phy. Chem.* 90, 3148 (1986).
- [53] O. Saur, M. Bensitel, A.B. Mohammed Saad, J.C. Lavalley, C. P. Tripp, B.A. Morrow, *J. Catal.* 99, 104 (1986).
- [54] M. Hino, S. Kobayashi, K. Arata, *J. Am. Chem. Soc.* 101, 6439 (1979).
- [55] V.V.F. Holm, G.C. Bailey, US Patent 3032599 (1962).
- [56] Q.H. Xia, K. Hidajat, S. Kawi, *J. Catal.* 211, 566 (2002).
- [57] M. Hino, K. Arata, *Appl. Catal. Lett.* 30, 25 (1995).
- [58] T.-S. Yang, T.-H. Chang, C.-T. Yeh, *J. Mol. Catal. A: Chem.* 115, 39 (1997).
- [59] P.D. Clark, N.I. Dowling, M. Huang, O. Okemona, G.D. Butlin, R. Hou, W.S. Kijlstra, *Appl. Catal. A: Gen* 235, 61 (2002).
- [60] S. Andersson, R. Pompe, N.-G. Vannerberg, *Appl. Catal.* 16, 49 (1985).
- [61] A. Auroux, A. Gervasini, *Adsorpt. Sci. Technol.* Vol 21. No. 8 (2003).
- [62] M.L. Guzman-Castillo, E. Lopez-Salinas, J.J. Fripiat, J. Sanchez-Valente, F. Hernandez-Beltran, A. Rodriguez-Hernandez, J. Navarrete-Bolanos, *J. Catal.* 200, 317 (2003).
- [63] D.E. Gawthrope, A.F. Lee, K. Wilson, *Phy. Chem. Chem. Phys.* 6, 3907 (2004).
- [64] W. Przystajko, R. Fiedorow, I.G. Dalla Lana, *Appl. Catal.* 15, 265 (1985).

Chapter 2

2 EXPERIMENTAL

2.1 Introduction

The combination of experimental parallelization with fast analysis allows testing a considerably larger number of solid catalysts compared to traditional methods using single reactors.

The current research in heterogeneous catalysis makes a distinction between two complementary methodologies in the high-throughput approach [1]: (i) primary screening techniques are designed to quickly isolate active materials out of a large number of possible candidates; (ii) secondary screening focuses on a much lower number of samples. Catalysts are tested under more realistic conditions and advanced analytic tools are used which allows to obtain a higher data quality and information depth. Hence the target of primary screening is the discovery of new materials through systematic exploration of combination of elements for preparation of multicomponent materials. Secondary screening targets the optimization of already-existing formulations [2].

The following chapter will give a detailed description of the 20-fold parallel reactor that was built for kinetic studies of the hydroisomerization reaction and the 6-fold temperature programmed desorption setup which was implemented for the parallelized measurement of catalyst acidity and adsorption properties.

2.2 20-fold parallel plug-flow reactor

The kinetic investigations on alkane hydroisomerization were carried out using a 20-fold parallel flow reactor system. The setup allows to investigate the catalytic activity and selectivity in a pressure range between 1 and 50 bar, flow rates between 5 and 100 ml/min and a temperature range up to 450°C. Flow and pressure are controlled for each reactor individually by using electronic mass flow (MFC) and back pressure regulators (BPR) (Bronkhorst High-Tech B.V.). The individual control of the single reactors facilitates on the one hand a high degree of freedom in choosing the reaction conditions in one run and on the other hand a high reproducibility for the measurements as the actual settings for each reactor are monitored and adjusted. The analysis of the bypass and product stream is carried out using a HP-micro gaschromatograph (GC M200, Agilent Technologies). The separation of the gas mixture is conducted for the species C₁ to C₆ (including isomers) in

100s using two columns (Portplot U with Backflush, and OV1). The single reactors are screened sequentially by controlling the flow with the help of two electronic 10-port valves connected to an electronic 4-port valve. The hydrocarbon feed is set by a liquid mass flow controller with subsequent evaporator (Controlled-Evaporator-Mixer C.E.M, Bronkhorst High-Tech B.V.) which is operated at a temperature of 120°C. The electronic equipment including temperature controller, mass flow and back-pressure regulator, evaporator-mixer, control module for multi position valves and micro GC is connected to a computer and is controlled by HPvee programs which allows to automatically vary all mentioned reaction conditions. Figure 1 and Figure 2 shows two pictures of the setup. A heated acryl box which is flushed with nitrogen is installed around the lines in order to prevent condensation of the feed stream. Hydrogen detectors are installed which shut down the gas supply and heating system in case critical hydrogen concentration is exceeded.

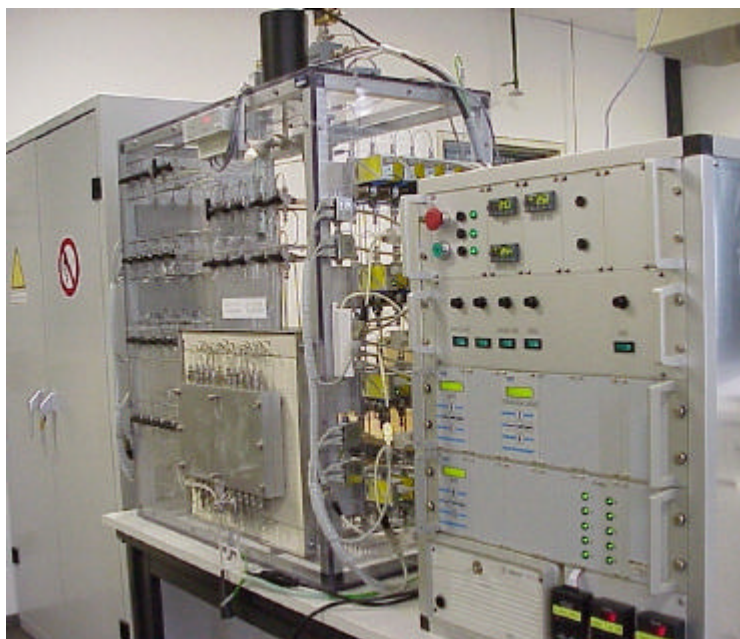


Figure 1: Setup front view.

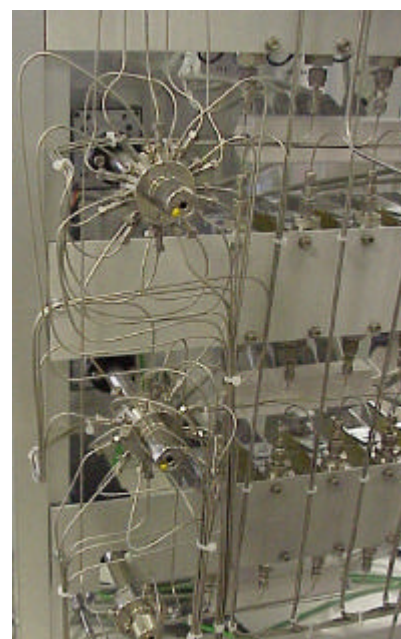


Figure 2: Multi-position valves.

The reactor block consists of two alumina units each containing 10 reactors. The blocks are heated with a heating unit comprising 6 heating patrons ($\Sigma P_i=1900W$) that are controlled by two PID-controllers in order to guarantee a homogenous temperature distribution. The reactor block is constructed in a way that each reactor is arranged with the same distance towards a heating patron. With the described design a maximum temperature deviation of $< \pm 1$ K was achieved in the reactor block. The reactors themselves are sweated to Cajon connections which seal up the system with a copper packing ring.

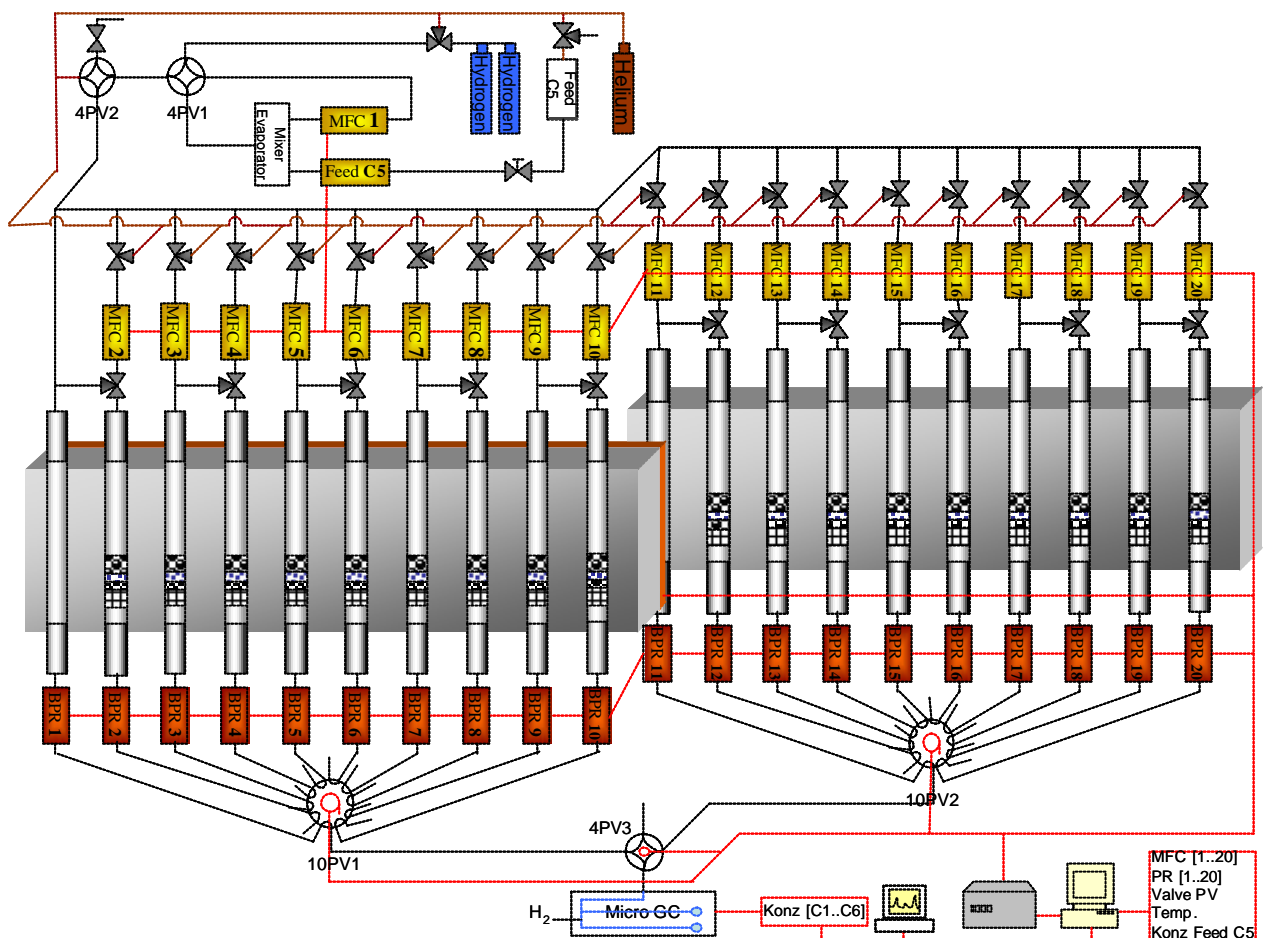


Figure 3: Setup scheme.

In Figure 4 a typical distribution of the conversion is given for the 20 reactors. A maximum absolute deviation of the average conversion ($X=24.3\%$) of $+3.2\%$ and -2.2% was measured. In Figure 5 the Gaussian function also known as the standard normal distribution is shown for the values from [3], where σ is the standard deviation given as the distance between the inflection points of equation 1.

$$P(x) = \frac{1}{s\sqrt{2p}} \cdot \exp\left[\frac{-x^2}{2s^2}\right] \quad (\text{equation 1})$$

The area below the Gaussian function gives the probability that a variable will assume for an interval $[-x, x]$. Therefore the maximum of the curve is given by the value that occurs with the highest probability and is defined as the average value. From the results of Figure 5 a confidential interval in which a variable occurs with the probability of 95% was calculated for a conversion between 22.2 and 26.5% which is equal to relative a deviation of 8.8%.

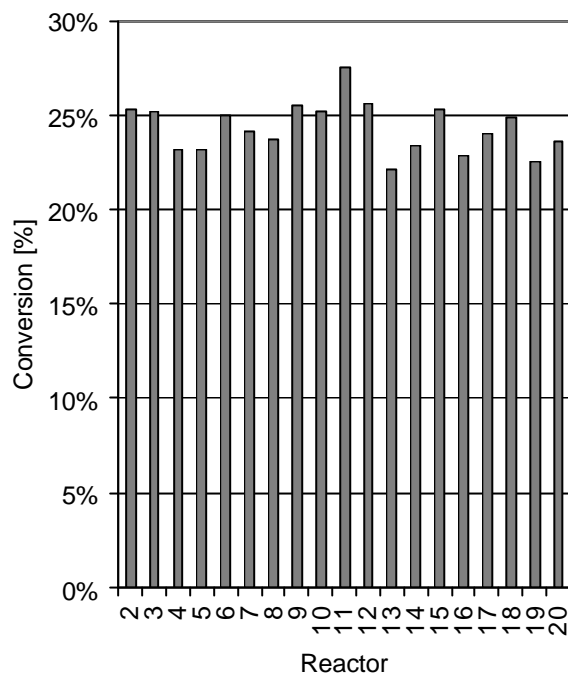


Figure 4: Typical distribution of measurements in reactor block.

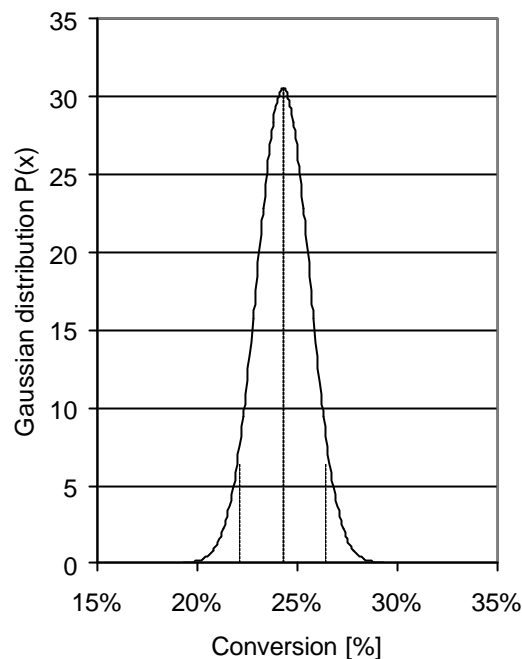


Figure 5: Gaussian distribution.

2.3 Temperature programmed desorption studies

Temperature programmed desorption (TPD) method is frequently used for the analysis of the number and strength of active sites. A 6-fold parallel TPD system was built for that purpose. Molecules adsorb onto the surface from the gas phase and desorb from the active sites by heating the sample in vacuum. The set-up consists of six quartz tubes heated uniformly by electrical ovens. The samples in the tubes are connected to a rotary pump and were activated at 350°C (rate of 10°C/min) for 1h at a residual pressure of 10^{-3} mbar. Ammonia is introduced into the sample holders through a dosing valve at 150°C and a pressure of 0.6 mbar for 1h after the activation program. Then, the system is outgassed at 150 °C for one hour, for removing physisorbed ammonia. In order to obtain the ammonia desorption profiles a linear temperature ramp of 10 °C/min was applied to the samples that were heated up to 800°C. During this ramp, desorption was monitored by a mass spectrometer (*Balzer QME 200*). The setup is controlled with the help of an HPVee program that allows to heat up the samples in sequence and leads the desorbed gas to the analytic unit through pneumatic triggered valves. Before the heating sequence the ammonia signal is monitored for 30 min in order to receive a constant baseline. In each set

of experiments in the 6-fold parallel system a reference sample with known acidity site density was measured to calibrate the response of the MS.

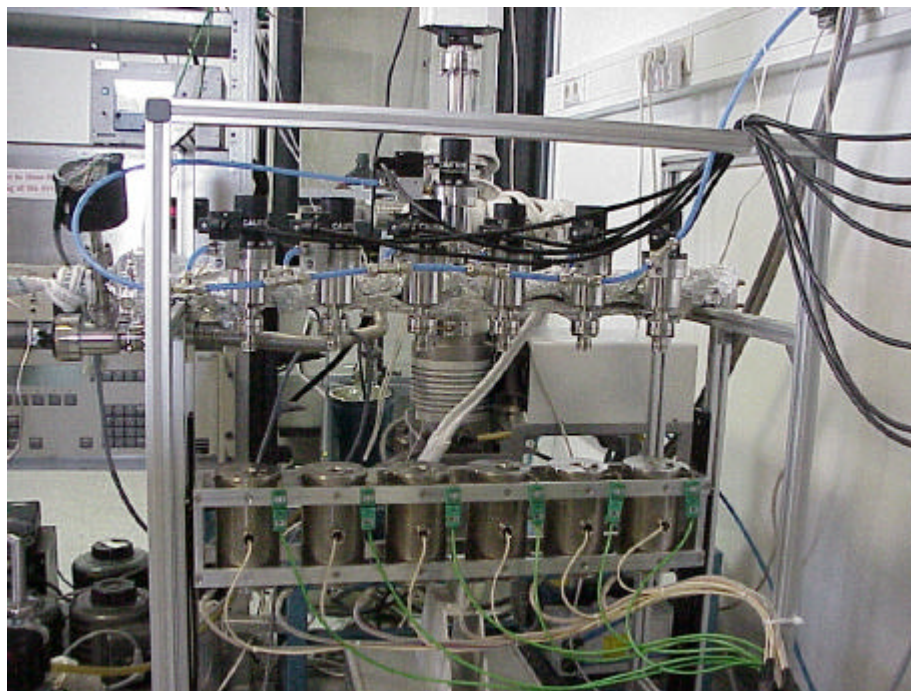


Figure 6: Setup for temperature programmed desorption studies.

Figure 7 shows a reproducibility test of the system. As reference sample 15 mg of H-MOR zeolite was used. After activation of the sample at 400°C, pyridine adsorption at 150°C was carried out as described above. The desorption profile was measured heating up the samples with a heating rate of 10°C/min until reaching 700°C. The area below the desorption peak is a proportional to the concentration of acid sites. The evaluation of the acidity of the samples showed a maximum deviation of 5.8% of the average acidity and an average deviation of 4.1%. The standard deviation for one run was calculated to be 0.055. Furthermore there was no significant temperature shift of the desorption profile before the first inflexion point, indicating that the temperature difference between the reactors is negligible. The maxima of the curves which is an indication of the strength of the acid sites is similar for all reactors except the one that contains the lowest ammonia uptake and shows a temperature shift of 10°C.

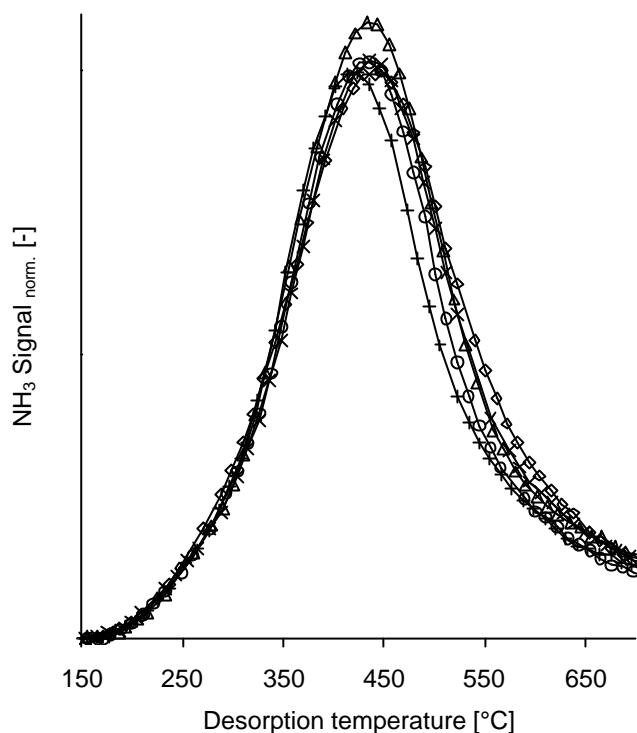


Figure 7: Reproducibility test of 6-fold TPD for reactor 1 (◻), reactor 2 (◄), reactor 3 (✕), reactor 4 (⊖), reactor 5 (⊕) and reactor 6 (◊).

2.4 Acknowledgements

The financial support by Bundesministerium für Bildung und Forschung Project (BMBF:03C0307D) is gratefully acknowledged. The authors would like to thank Xaver Hecht and Andreas Marx for technical support on the 20-fold parallel reactor system and the 6-fold TPD setup.

REFERENCES

- [1] W. Huybrechts, J. Mijoin, P. A. Jacobs, J. A. Martens, *Appl. Catal. A: Gen.* 243, 1 (2003).
- [2] A. Holzwarth, P. Denton, H. Zanthoff, C. Mirodatos, *Catal. Today* 67, 309 (2001).
- [3] Feller, W. *An Introduction to Probability Theory and Its Applications*, Vol. 1, 3rd ed. New York: Wiley, 1968.

Chapter 3

3 KINETIC STUDIES ON PENTANE HYDROISOMERIZATION OF Pt/H-BEA

3.1 Abstract

In the following chapter the acidic and metallic properties of a Pt loaded H-BEA samples are characterized. The role of hydrogen for catalyst activity and stability was investigated by deactivation experiments under hydrogen and helium atmosphere. Significantly different product selectivities were observed under hydrogen and helium atmosphere indicating that the role of Pt during the hydroisomerization reaction is to keep the concentration of olefins low in order to prevent oligomerization reaction. The influence of Pt on isomerization activity was studied varying the metal content. In further kinetic experiments the reaction enthalpy, reaction rates, reaction orders and activation energies were determined. A kinetic model was derived in order to determine the kinetic relevant partial step in the consecutive reaction mechanism.

3.2 Introduction

Metal loaded zeolites are widely used catalysts in oil reforming processes and can be used in particular for de/hydrogenation, cyclization, aromatization, hydrogenolysis and isomerization reactions. Reforming is a process in which hydrocarbon mixtures are converted into isomers containing mostly the same carbon number but having enhanced octane numbers. Catalysts with hydrogenating sites and protonic acid sites show high catalytic activity and stability [1]. For about 50 years, zeolite based catalysts have been used for the hydroisomerization reaction [2].

For alkane hydroisomerization a bifunctional model was introduced by Mills and Heinemann in the 1950s [3], while Weisz first described olefinic products as intermediates [4]. A detailed description of the isomerization mechanism is given in Chapter 1. In order to design and optimize catalysts, a detailed understanding of the reaction mechanism, kinetic and catalyst properties is of primary interest. The balance between the metallic and the acidic function, which determines the rate of the de/hydrogenation and C-C rearrangement, can generally be considered the determining parameter for activity, stability and selectivity. If the ratio between the metal and acid function is too low the dehydrogenation step is rate limiting. This leads to an enhanced probability of successive cracking and oligomerization reactions of the alkenes and finally to the formation of coke.

If however the ratio between the metal and acid sites is sufficient for the dehydrogenation step to be in equilibrium, the activity per acid site reaches a maximum and the rearrangement on the acid sites becomes limiting [1]. The bifunctional catalyst can then be considered as an ideal hydroisomerization catalyst as far as activity and stability [5] are concerned.

The role of alkene intermediates in the classical mechanism was questioned at low temperatures and high hydrogen pressures since the concentration of alkenes was estimated to be very small [6, 7]. One alternative reaction pathway over bifunctional catalysts has been suggested to be the direct activation of the alkane on the acidic sites, the key role of the metallic component being to prevent poisoning of the acid sites by hydrogenation of the olefinic intermediates [7]. Positive reaction orders in hydrogen for metal-free H-MOR at 270°C were observed during hydrocracking reactions for heavier alkanes (C₇) in case of desorption limitations [8]. The rate of desorption hence can be enhanced by hydrogen through a hydride transfer from molecular hydrogen, producing a high paraffin/olefin ratio. This is due to the interaction of the carbenium ion (or olefin) with hydrogen producing the corresponding paraffin and regenerating the initial Brønsted acid site. It was proposed that hydrogen can be activated on metal free samples and that hydride abstraction from hydrogen molecule by an adsorbed olefin is possible if the supply of hydrogen is large enough. Fujimoto studied the isomerization of *n*-pentane over Pt-SiO₂ / H-ZSM-5 hybrid catalyst and suggested that hydrogen spills over from Pt to the zeolite as H⁺ and H⁻ ions. The proton regenerates the Brønsted acid sites and the hydride reacts with the isomerized carbenium ion to form the product [9, 10, 11].

All mechanistic studies show that the kinetic behavior during the hydroisomerization reaction is strongly dependent on the material properties, the probe molecule and the operating conditions. For a better understanding of the bifunctional catalysts the following section describes in detail the key characteristics of a metal loaded zeolite BEA and explains the limiting properties of the material for the pentane hydroisomerization. With the help of a kinetic approach the rate limiting step for the pentane hydroisomerization on the materials is identified.

3.3 Experimental

3.3.1 Catalyst preparation

Zeolite BEA 25 (Si/Al=12.5) from Süd-Chemie AG was loaded with Pt at concentrations between 0.2 and 2.3 wt % by ion-exchange with aqueous $\text{Pt}(\text{NH}_3)_4(\text{OH})_2$ solution. A solution containing the appropriate amount of $\text{Pt}(\text{NH}_3)_4(\text{OH})_2$ and an amount of NH_4OH corresponding to the theoretical concentration of protons (competitive adsorption) in the sample was added drop wise to the slurry at 40°C in order to exchange the cations of the zeolite to obtain the metal loaded H^+ -form of the zeolite. After the ion exchange the solid was centrifuged, washed and freeze dried. The samples were calcined in air at 350°C for 16 h (heating rate $0.5^\circ\text{C}/\text{min}$) and finally reduced at 300°C in H_2 for 4 h. The samples are referred to as Pt/H-BEA.

3.3.2 Atomic adsorption spectroscopy (AAS)

The concentrations of aluminium, silicon and platinum were determined by Atomic absorption spectroscopy using a UNICAM 939 AA-Spectrometer. Typically 20-40 mg of the sample was dissolved in a boiling mixture containing 0.5 ml of hydrofluoric acid (48%) and 0.1 ml of nitrohydrochloric acid at the boiling point of the mixture (ca. 110°C).

3.3.3 Transition electron microscopy (TEM)

To study the metal particles a JEM-2010 JEOL microscope was used. The accelerating voltage was 120 keV (LaB6 electron source). The resolution of the microscope was 0.2 nm. The samples were suspended in ethanol by ultrasonic treatment. Drops of this dispersion were placed on a copper grid-supported film. Transmission electron micrographs were recorded at a magnification of 54000.

3.3.4 Hydrogen Chemisorption

The fraction of accessible Pt sites was determined by hydrogen chemisorption measurements. Although the number of hydrogen atoms adsorbed per platinum atom has been found to vary from less than 1 up to 2 [12], a H/Pt ratio of 1 was assumed [13]. Hydrogen chemisorption was performed using a Sorptomatic 1990 Series sorptometer (Porotec Sorptomatic 1990 Automated BET). Approximately 1g of catalyst was reduced in hydrogen at 350°C for 2h and subsequently evacuated. All isotherms were measured at

35°C. The amount of chemisorbed hydrogen was determined after removing physisorbed hydrogen from the sample by evacuation at 35°C. The hydrogen uptake on the sample was determined by extrapolating the linear part of the adsorption isotherm to zero pressure.

3.3.5 Temperature programmed desorption (TPD)

Temperature programmed desorption was performed in a 6-fold parallel TPD system. The catalysts were activated by heating in vacuum to 350°C (heating rate 10°C/min) and remaining at 350°C for 2 h. Ammonia was adsorbed at 150 °C with a partial pressure of 0.6 mbar for 1 h. Subsequently the samples were evacuated at 10^{-3} mbar for 2 h in order to remove physisorbed molecules. For the TPD experiments the 6 samples were (sequentially) heated from 150°C to 800°C with a rate of 10°C/min and the desorbing species were monitored by mass spectrometry (*Balzers QME 200*). In each set of experiments a reference sample with known concentration of acid sites was used for calibrating the MS signal.

3.3.6 IR spectroscopy

IR spectra were measured from 4000 to 1100 cm^{-1} at a resolution of 4 cm^{-1} using a Perkin Elmer 2000 spectrometer. For the adsorption of pyridine studies a self supporting wafer was pressed and activated at 350°C (increment 10 °C/min) for 90 min. After cooling to 150°C, the spectrum of the activated samples was recorded. Pyridine was adsorbed at 150°C with a partial pressure of 0.05 mbar for 30 min and the sample was subsequently evacuated until the IR spectra remained constant. To compare the spectra of the different samples all spectra were normalized by the intensity of the lattice vibration overtones of the zeolite between 1750 and 2100 cm^{-1} . Additionally, the weight of the wafers was used to determine the mass per surface area necessary for calculating the concentration of Brønsted and Lewis acid sites according to the method published by Emeis [14].

3.3.7 Kinetic studies

The catalytic activity was studied with a 20-fold parallel plug flow reactor system. The reactant gas flow and pressure of each reactor were controlled by individual digital mass flow controllers and back-pressure regulators. The liquid feed (pentane) was adjusted and mixed with hydrogen by a digitally controlled evaporator - mixer. For the analysis of the products a HP-MicroGC (GC M200) was used, capable of separating aliphatic C_1 to C_6

hydrocarbons (including their isomers) in less than 2 min. The total pressures, flow rates, temperatures and alkane concentrations were varied automatically. The data recorded was stored in a relational MS Access database.

3.4 Results and Discussion

3.4.1 Physical chemical properties of Pt/H-Beta

Transmission electron microscopy was used for determining the crystallite size of the support and platinum particle size. The primary crystallite size of the samples was small (30-100 nm) independent of the metal loading. For all samples metal clusters with a diameter above 5 nm were not observed. The particles were uniformly dispersed on the zeolite support for all samples see Figure 1 and Figure 2. The magnification given did not allow a quantitative determination of a representative platinum particle size distribution, however, it can be assumed that the particle size distribution is narrow since all particles observed possessed a diameter between 1 and 5 nm.

Table 1: Characterization data and activation energies for Pt/H-BEA samples.

Pt/H-BEA	0.2 wt% Pt	0.4 wt% Pt	1.0 wt% Pt	2.3 wt% Pt
Pt content (AAS) [wt%]	0.22	0.41	1.03	2.29
Total Acidity [mmol H ⁺ / g]	0.54	0.52	0.56	0.52
Ratio Brønsted / Lewis acid sites [-]	0.95	0.99	1.00	-
Metal dispersion [mol H / mol Pt]	0.84	0.73	0.52	0.60
Particle diameter [Å] ⁽²⁾	11	16	25	22
Apparent activation energy [kJ / mol] ⁽¹⁾	104	103	107	99

⁽¹⁾: determined for the hydroisomerization reaction.

⁽²⁾: determined through H₂ chemisorption assuming cubooctahedral shaped particles.

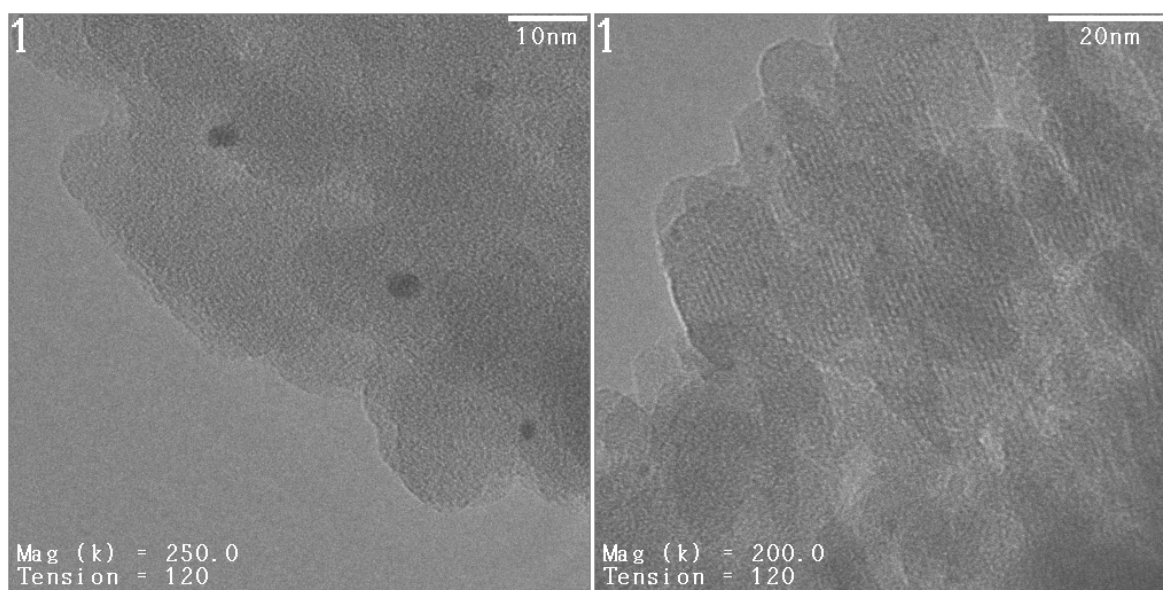


Figure 1: TEM of H-BEA 0.2 wt% Pt (left) and 0.4 wt% Pt (right).

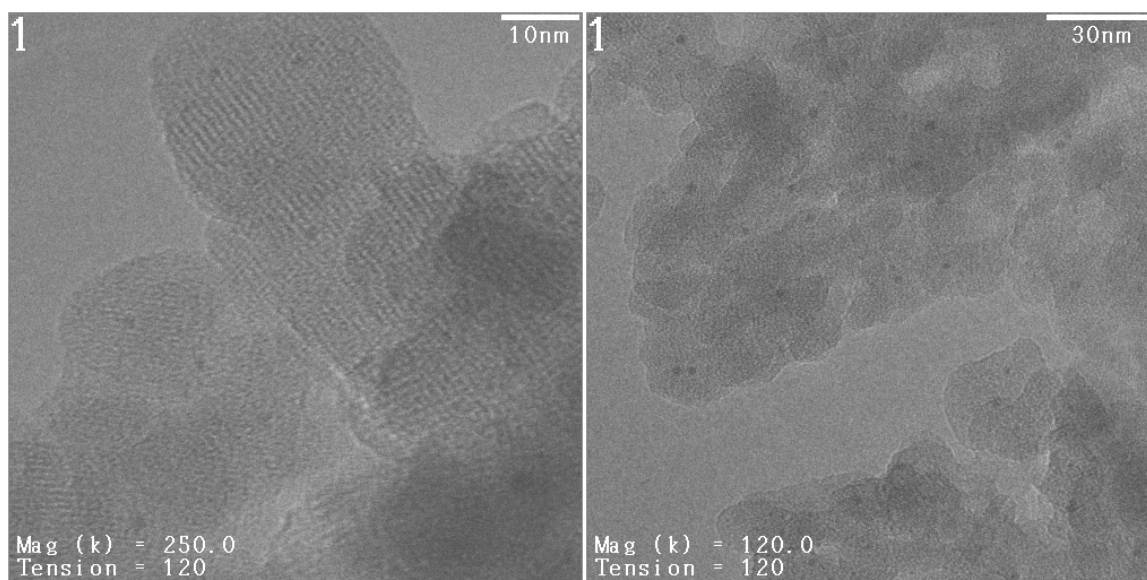


Figure 2: TEM of H-BEA with 1 wt% Pt with a magnification of 250k (left) and 120k (right).

The accessible metal surface area was determined by hydrogen chemisorption measurements (Figure 4). Normalizing the chemisorbed amount of hydrogen by the metal loading shows that the metal dispersion is decreasing with increasing metal content. Assuming a cubooctahedral shape for the platinum particle, it was possible to generate metal clusters with a computer program (CERIUS, [15]) and calculate the particle size for a given metal dispersion. The results of the metal dispersion and the particle sizes are presented in Table 1. The table shows that the particle sizes calculated from the results of

the hydrogen chemisorption measurements are in agreement with the particle sizes observed by TEM.

The activation energy of the isomerization reaction was determined at a total pressure of 4 bar and a WHSV of 30 h⁻¹ for conversion levels below 10% where a linear correlation between the logarithmic isomerization rate constant and the inverse temperature was observed. The apparent activation energies were similar for the different platinum content (99 – 107 kJ/mol) and are given in the summary of the characterization data in Table 1.

The total number of acid sites on the zeolite was determined by NH₃ TPD. The desorption profiles for the zeolites loaded with different metal contents show two characteristic maxima attributed to acid sites with different strength. Similar desorption profiles of ammonia on zeolite beta have been reported in [16]. The low temperature peak of zeolite beta corresponds to relatively weak acid properties (124-127 kJ/mol) compared to MFI or MOR structures [16]. The presence of strong Lewis acid sites, which were indicated by the high temperature peak of the ammonia-TPD, is attributed to synergetic effect of extra-framework alumina with framework Brønsted acid sites [17, 18]. The strength of the acid sites, which is indicated by the position of the maxima, did not vary significantly among the catalysts with the metal loading which is confirmed by the observation of similar apparent activation energies. The concentrations of acid sites are summarized in Table 1.

IR studies were carried out in order to investigate the structural properties of the zeolite samples with different metal loading. No distinct differences were observed in the region of the hydroxyl groups. Pyridine adsorption was carried out to determine the concentration of Brønsted and Lewis acid sites. The results obtained by the quantitative evaluation of the pyridine ring vibrations at 1544 cm⁻¹ (for pyridine on Brønsted sites) and 1455 cm⁻¹ (for pyridine on Lewis sites) are summarized Table 1.

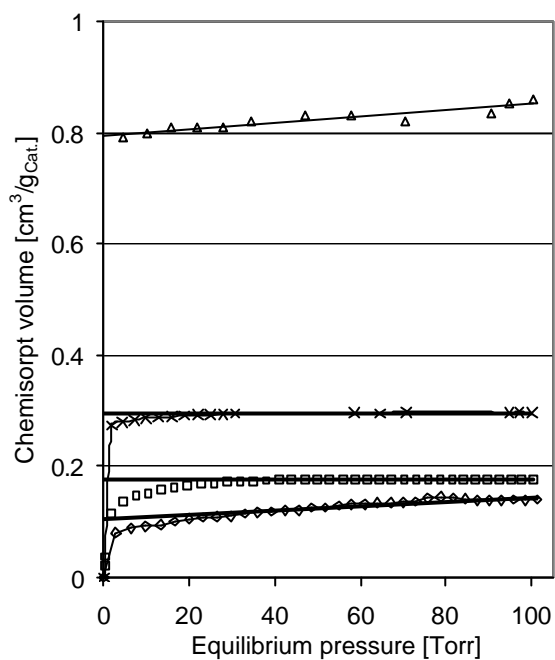


Figure 3: H₂-chemisorption for 0.2 wt% Pt (\diamond), 0.4 wt% Pt (\square), 1 wt% Pt (\times) and 2.3 wt% Pt (\triangle).

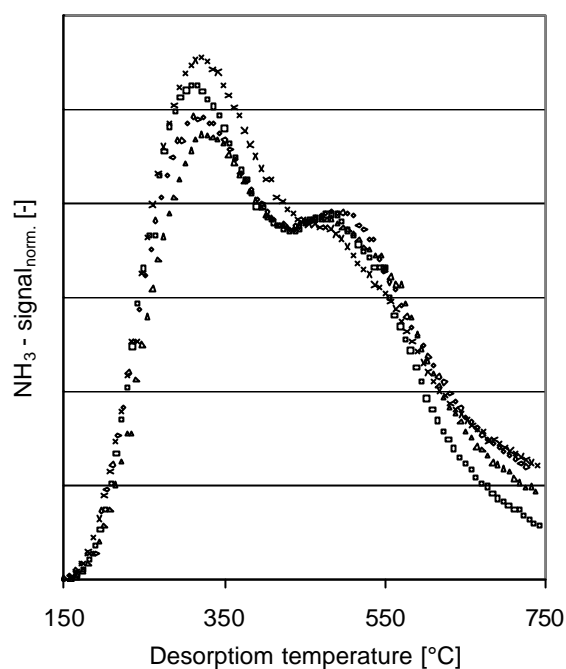


Figure 4: TPD profiles for 0.2 wt% Pt (\diamond), 0.4 wt% Pt (\square), 1 wt% Pt (\times) and 2.2 wt% Pt (\triangle).

3.4.2 Determination of the equilibrium constant

In order to determine the equilibrium constant for the pentane hydroisomerization reaction the ratio between *n*- and iso- pentane was measured for different flow rates and catalyst weights at a pressure of 4 bar and a temperature range of 230-350 °C (shown in Figure 5). The equilibrium constant was determined from data points corresponding to high conversion and low iso-pentane selectivity. According to the equation of van't Hoff the equilibrium constant *K* for an isochoric and isobaric system is related to the standard reaction enthalpy ΔH_R^0 as follows:

$$\frac{d(\ln K)}{dT} = \frac{\Delta H_R^0}{RT^2} \quad \text{equation 1}$$

Assuming that the standard reaction enthalpy ΔH_R^0 is independent of the temperature, equation 1 can be integrated leading to:

$$\ln K_T = \ln K_{T_0} - \frac{\Delta H_R^0}{R} \left(\frac{1}{T} - \frac{1}{T_0} \right) \quad \text{equation 2}$$

According to equation 2 the standard reaction enthalpy can be determined from the slope of a plot of $\ln K$ vs. T^{-1} . Figure 6 shows the linear correlation between the logarithmic adsorption constant and the inverse temperature. A value for ΔH_R^0 of -7 kJ/mol was determined for the standard reaction enthalpy.

Alkane hydroisomerization is an equilibrium limited reaction, in which branched paraffin isomers are generally favored by low temperatures. The determination of the reaction enthalpy showed that the reaction is slightly exothermic. Thus while the temperature dependence of the equilibrium position is marginal, significant changes in equilibrium positions can only be achieved by a severe enhancement of the strength of the acid sites. However the lower the applied temperature, the more beneficial equilibrium positions can be reached. In contrast to this, elevated temperatures are necessary to reach faster the equilibrium at a given WHSV.

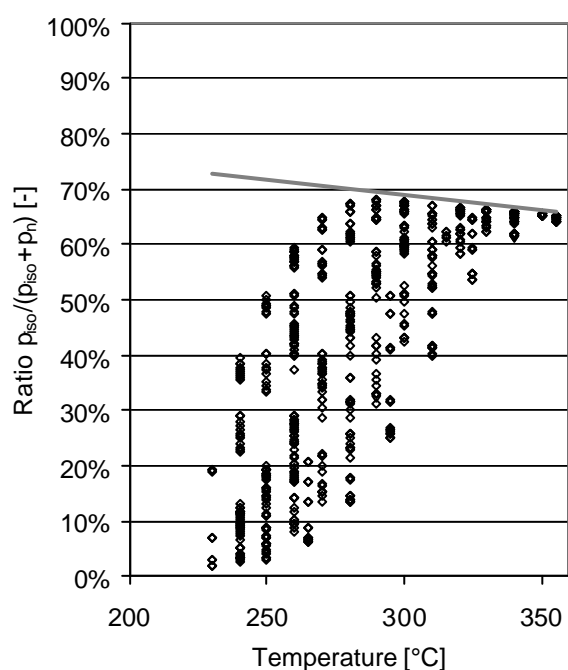


Figure 5: Approach towards the thermodynamic equilibrium.

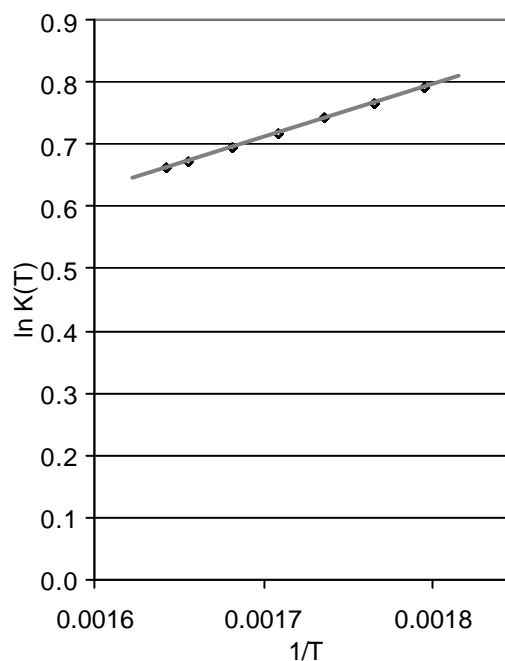


Figure 6: Determination of standard reaction enthalpy (van't Hoff).

3.4.3 Kinetic studies on isomerization stability and activity

In Figure 7 the role of platinum for catalyst stability was investigated comparing the isomerization reaction under helium and hydrogen atmosphere (290°C, WHSV=4 h⁻¹, 3 mol% feed stream and atmospheric pressure). Furthermore, the activity of a Pt free sample under hydrogen is included. The results show a rapid deactivation under helium atmosphere whereas the catalyst activity remained constant under hydrogen for the Pt/H-BEA catalyst. It is well known that platinum hydrogenates coke precursor and therefore prevents catalyst deactivation. Similarly the isomerization selectivity was reduced from 50% to 30% during the deactivation run under He atmosphere, while it remained constantly high at 93% when the reaction was carried out under hydrogen atmosphere. Graphitic species, C_xH_y polymers as well as PtC was observed on Pt black samples if exposed to hydrocarbons in the absence of hydrogen [19]. Hydrocarbon deposits on sulfated zirconia and strongly acidic zeolites resemble each other and are basically present as alkenic, allylic cations, cycloolefinic cations as well as aromatic compounds [20, 21]. Besides poisoning of the metal sites, coke deposits also block the acid sites of a zeolite. In [22] it was shown that the deactivation of a Pt-mordenite catalyst during pentane isomerization can be correlated to the formation of coke on the acid sites. Comparing the Pt/H-BEA sample under He atmosphere with the Pt free sample it is furthermore obvious that for the investigated reaction conditions Pt is also essential for the activation of the alkane. As n-pentane is a weak base the acid strength of the zeolite appears to be insufficient to directly protonate the alkane which points to a classical bifunctional mechanism. In addition it is interesting to note that initial isomerization rate for the Pt/H-BEA under helium atmosphere is higher than under hydrogen atmosphere. Similar results were obtained for the pentane isomerization on Pt/H-MOR in N₂ and H₂ atmosphere [23]. According to the bifunctional mechanism high hydrogen pressure shifts the de/hydrogenation equilibrium on the metal sites towards the alkane and therefore reduces the olefin concentration, which leads to a reduction of the isomerization rate. Furthermore, hydrogen can interact with a carbenium-ion leading to the formation of an unbranched paraffin and regenerating a Brønsted acid site. It is thus concluded that the expected reaction order for hydrogen of -1 reduces the initial isomerization activity under hydrogen atmosphere. Additionally a bimolecular reaction pathway can be involved under the lack of hydrogen which was shown to possess a lower activation energy and thus a higher activity [24]. Nevertheless hydrogen is essential to guarantee catalyst stability.

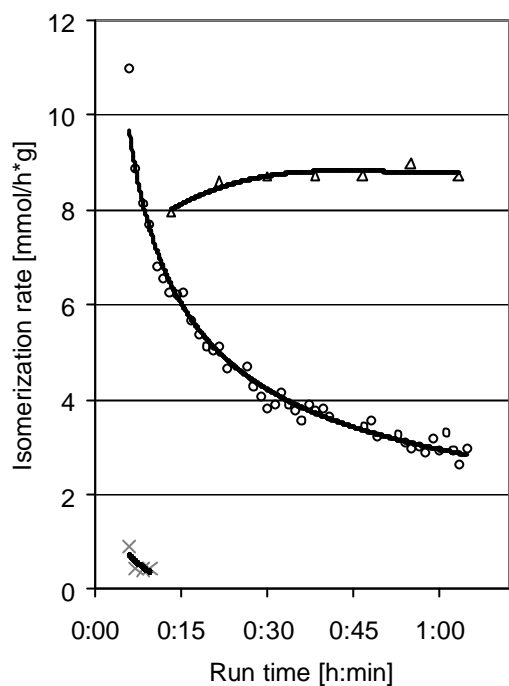


Figure 7: Catalyst deactivation for Pt/H-BEA with 0.4 wt% under hydrogen atmosphere (Δ) and under Helium atmosphere (\circ) and H-BEA (\times) under hydrogen atmosphere.

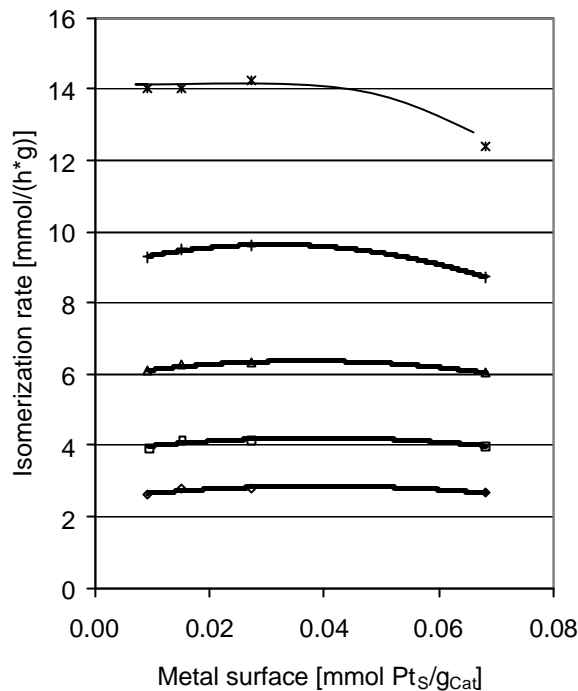


Figure 8: Isomerization rate for different Pt contents at a temperature of 250°C (\diamond), 257°C (\square), 264°C (Δ), 271°C ($+$) and 278°C (\star).

The influence of the accessible metal surface on the isomerization reaction was investigated at a total pressure of 11 bar and a WHSV of 15 h^{-1} under differential conditions at temperatures between 250 and 280°C (Figure 8). For the kinetic measurements external transport limitation was excluded experimentally. Figure 8 shows that the isomerization rate for low temperatures is not affected by the Pt content. At higher temperatures a decrease of the isomerization rate can be observed at high Pt loadings. This trend is due to an enhanced importance of the side reaction for the samples with high Pt loading. The consequent reduction of the pentane partial pressure available for the isomerization results in the reduction of the isomerization rate. The higher conversion level leads to a reduction of the pentane concentration in the feed which results in a falsification of the isomerization rate. This indicates that the metal function is balanced for a molar ratio of $\text{Pt}_{\text{surface}}/\text{H}^+ > 0.03$ and furthermore leads to the conclusion that the kinetically relevant step of the reaction occurs on the acid sites. The apparent activation energies presented in Table 1 did not differ severely for the different Pt-loadings, which confirms that these

catalysts share the same energy barrier and therefore there is no shift in the rate determining step with increasing Pt_{surface}/H^+ ratio.

3.4.4 Catalyst selectivity

In Figure 9 and Figure 10 the selectivity of the by products are shown for Pt/H-BEA with 0.4 wt%. Figure 9 shows the distribution of the side products for steady state conditions under hydrogen atmosphere (280°C, 4bar, WHSV 5-30 h⁻¹). The distribution of the formed side product was independent of the conversion level. Extrapolating the slope of the product distribution for the species C₁, C₂, C₃ and n-C₄ towards the point of origin of the diagram results in a positive initial slope indicating that these products originate from a primary side reaction. The initial slope for iso-butane was found to be zero, which indicates that iso-butane is formed in a secondary reaction. No larger molecules than pentane were observed among the side products.

Figure 10 shows the distribution of side products during the deactivation run under helium atmosphere presented in Figure 7. The distribution of the products was significantly different. No methane or ethane fragments had been observed. The major product formed in the beginning of the reaction was iso-butane. Higher contents of iso-hexane were detected in the course of the deactivation run while the product spectra did not show n-hexane. The high contents of iso-hexane and iso-butane appear to be cracking products resulting from multibranched C₁₀⁺ intermediates that are formed *via* a bimolecular mechanism. Formation of decan is likely as under the lack of hydrogen a high concentration of pentene molecules is expected, which potentially react with C₅ carbenium ion. Since after isomerization of the dimer cation (C₁₀⁺) the intermediate is composed of an electron donating tetra-butyl group and an electron withdrawing secondary or tertiary carbenium ion at the beta position, the predominant formation of iso-butane is expected [25]. The increasing content of iso-hexane in the course of the deactivation run is assigned to longer chain intermediates formed by successive oligomerization. The fact that only 90 to 95% of the carbon atoms feed into the reactor are detected in the product stream indicates significant formation of coke deposits which lead to catalyst deactivation. The results clearly show that hydrogen is necessary for the hydrogenation of olefins in order to prevent oligomerization reaction that leads to coke formation and catalyst deactivation.

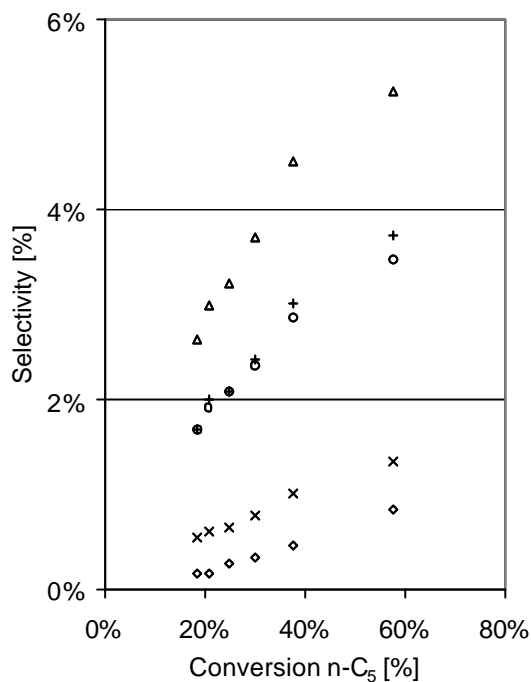


Figure 9: Product distribution for Pt/H-BEA (0.4 wt% Pt) under hydrogen atmosphere: C_1 (\times), C_2 (\circ), C_3 (Δ), $n-C_4$ ($+$) and $iso-C_4$ (\diamond).

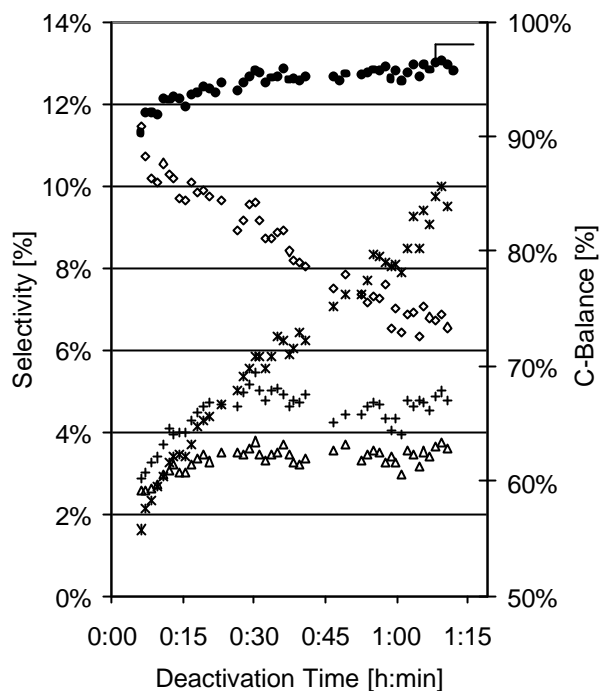


Figure 10: Product distribution for Pt/H-BEA under He atmosphere: (0.4 wt% Pt): C_3 (Δ), $n-C_4$ ($+$), $iso-C_4$ (\diamond), iso -hexanes (\ast) and C-Balance (\bullet).

3.4.5 Kinetic approach

Reaction orders can vary in a complex manner with reaction conditions although changes in reaction path do not occur since heterogeneous catalysis is highly non linear for active sites (shown in [26]). This means that even simple reaction mechanisms can lead to complicated macro-kinetics which display variable reaction order and activation enthalpies. Hence, instead of using power law rate and determining the apparent reaction orders for defined reaction conditions a kinetic approach is derived accounting for adsorption phenomena to study the partial pressure dependencies of the pentane isomerization reaction. For the approach the following assumptions are made:

- Langmuir-Hinshelwood mechanism
- Elementary reversible reactions
- Identical sites and constant number of sites under all reaction conditions
- No interaction between intermediates and each active site is covered by a single intermediate only

Assuming that transport limitations are absent the hydroisomerization reaction occurs according to the following bifunctional mechanism:

In the first step the reactants hydrogen and pentane are adsorbed on the metal surface. The pentane molecule dehydrogenates and diffuses to acid sites where a carbenium ion is formed. The carbenium ion rearranges on the acid sites, deprotonates and diffuses back to the metal sites where a subsequent hydrogenation occurs. Finally the products desorb from the surface into the gas phase.

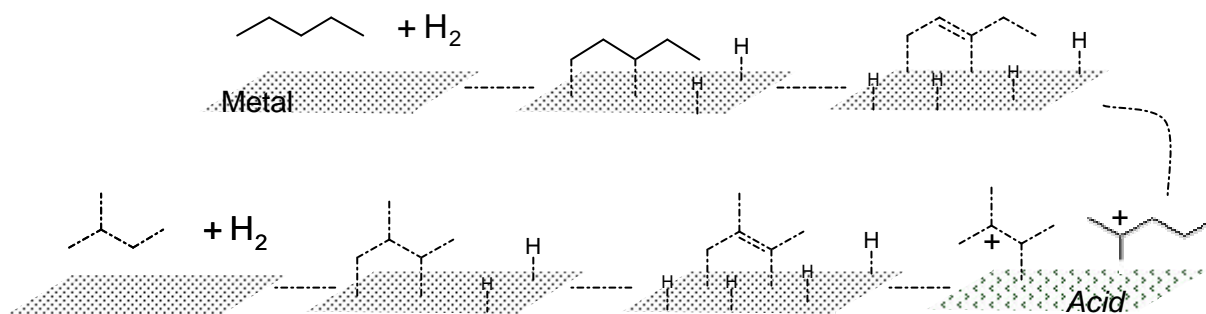
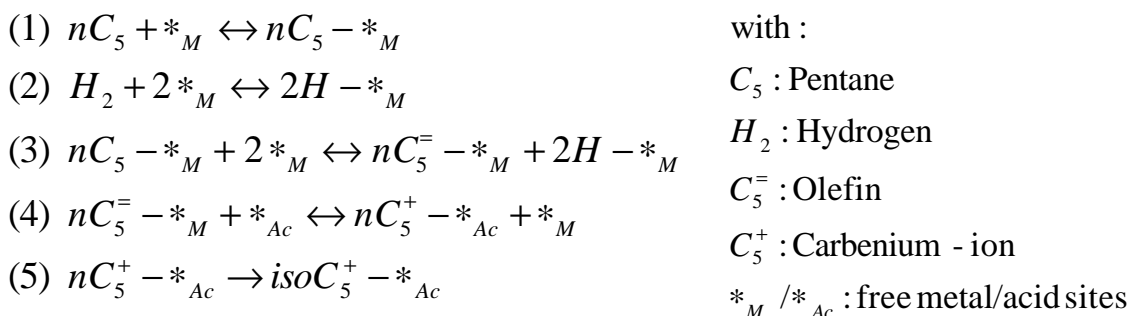


Figure 11: Scheme for the reaction mechanism.

Figure 7 shows that the platinum content does not influence the isomerization rate, therefore, it is assumed that the rate determining step of the reaction is the rearrangement of the carbenium-ion on the acid site (being the intrinsically slowest step in the reaction), while the dehydrogenation step on the metal sites can be assumed to be quasi equilibrated. In Figure 11 the individual reaction steps on the metal sites and acid sites are given, assuming that hydrogen adsorbs dissociatively on the metal sites. The rate equation will be derived assuming that the rearrangement of the n-carbenium ion on the acid site is the kinetically relevant step of the reaction. Pentane is a weak base and therefore the rate of formation of the carbenium ion should be rather low. However it can be assumed that the rate determining step is the skeletal isomerization rather than the formation of the carbenium ion. In fact the skeletal rearrangement involves the lengthening of a C-O bond and therefore is exposed to a higher activation energy which was confirmed by quantum mechanic calculations and kinetic model studies for hexane isomerization [27, 28].

Below the reaction equations and the corresponding rate equations normalized to the total amount of sites are given below.



$$\begin{aligned}
 (1) \quad r_1 &= k_1 \cdot p_{n-C5} \cdot \Theta_m - k_{-1} \cdot \Theta_{n-C5,m} \\
 (2) \quad r_2 &= k_2 \cdot p_{H_2} \cdot \Theta_m^2 - k_{-2} \cdot \Theta_{H,m}^2 \\
 (3) \quad r_3 &= k_3 \cdot \Theta_{n-C5,m} \cdot \Theta_m^2 - k_{-3} \cdot \Theta_{H,m}^2 \cdot \Theta_{n-C5,m} \\
 (4) \quad r_4 &= k_4 \cdot \Theta_{n-C5,m} \cdot \Theta_{AcH} - k_{-4} \cdot \Theta_{n-C5^+,Ac} \cdot \Theta_m \\
 (5) \quad r_5 &= k_5 \cdot \Theta_{n-C5^+,Ac} - k_{-5} \cdot \Theta_{iso-C5^+,Ac} \Leftrightarrow (\text{RDS})^*
 \end{aligned}$$

with:

p_{n-C5} : partial pressure n - pentane	k_x : rate constant forward reaction
p_{H_2} : partial pressure hydrogen	k_{-x} : rate constant backward reaction
Θ_m : fraction of free metalsites	$K_x = \frac{k_x}{k_{-x}}$
$\Theta_{n-C5,m}$: fraction n - pentane on metalsite	Θ_{AcH} : fraction free acid sites
$\Theta_{n-C5,m}^{\ominus}$: fraction n - pentene on metalsite	$\Theta_{n-C5^+,Ac}$: fraction n - carbenium ion on acid site
$\Theta_{H,m}$: fraction hydrogen atom on metal site	$\Theta_{iso-C5^+,Ac}$: fraction iso - carbenium ion on acid site

*: (rate determinant step)

The simplified equations for the acid site (6) and metal site (7) balance can be derived, where it is assumed that the most abundant species on the acid sites are the carbenium ions. The metal sites are occupied by n-pentane, hydrogen atoms and olefins.

$$\begin{aligned}
 (6) \quad 1 &= \Theta_{AcH} + \Theta_{n-C5^+,Ac} \\
 (7) \quad 1 &= \Theta_m + \Theta_{n-C5,m} + \Theta_{H,m} + \Theta_{n-C5,m}^{\ominus}
 \end{aligned}$$

If reaction (4) is in equilibrium the acid site balance (6) can be transformed according to (8)

$$(8) 1 = \Theta_{AcH} + \frac{K_4 \cdot \Theta_{n-C_5^+}}{\Theta_m} \cdot \Theta_{AcH}$$

Similar if reactions (1), (2) and (3) are equilibrated the metal site balance (7) can be transformed to (9).

$$(9) 1 = \Theta_m + K_1 p_{n-C_5} \Theta_m + \sqrt{K_2 p_{H_2}} \Theta_m + \frac{K_3 K_1 p_{n-C_5}}{K_2 p_{H_2}} \Theta_m$$

The fraction of n-carbenium ions on the acid sites can be calculated from the balance of the acid sites (8) using the fraction of olefin on the metal sites from (3) as shown in (10)

$$(10) \Theta_{n-C_5^+,Ac} = (1 - \Theta_{AcH}) = 1 - \frac{1}{1 + \frac{K_4 \cdot \Theta_{n-C_5^+}}{\Theta_m}} = \frac{\frac{K_1 K_3 K_4 p_{n-C_5}}{K_2 p_{H_2}}}{1 + \frac{K_1 K_3 K_4 p_{n-C_5}}{K_2 p_{H_2}}}$$

Correlation (10) can be used to solve (5) deriving the final rate equation. Note that the equilibrium rate constants are summarized according to equation 3.

$$K^* = \frac{K_1 K_3 K_4}{K_2} \quad \text{equation 3}$$

Finally, the overall rate of the reaction normalized to the number of acid sites can be derived as the final reduced rate expression describing the dependence of the hydroisomerization rate on the pentane and hydrogen partial pressure for the forward reaction (equation 4).

$$TOF = \frac{k_{rkt} \cdot K^* \cdot p_{n-C_5}}{1 + K^* \cdot p_{n-C_5}} \bigg/ p_{H_2} \quad \text{equation 4}$$

Figure 12 shows the isomerization rates obtained for a temperature of 280°C. The pentane and hydrogen partial pressure was varied in the range of 0.1 – 0.6 bar for pentane and 6 – 28 bar for hydrogen. The projection of the isomerization rate into the pentane partial pressure plane shows a linear dependency and a reaction order for pentane of approximately n=1. In Figure 13 the kinetic rate equation (equation 4) was fitted for low conversion levels and for the different pentane and hydrogen partial pressure by varying the rate constant k and the product of the adsorption constant K* using a ‘Generalized

Reduced Gradient” (GRG2) nonlinear optimization code. The correlation of the measured and simulated rate fits with a value for the Pearson product moment correlation coefficient of $R^2 = 0.988$. The standard deviation of the difference between the measured and the simulated values was determined to be a value of 0.33. The result for the rate constant and the product of the adsorption constants are listed in Table 2.

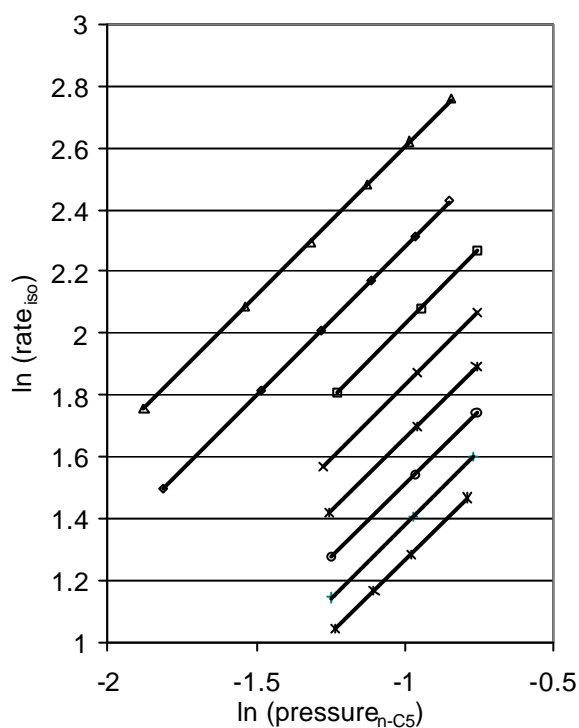


Figure 12: Bilogarithmic plot of the iso-pentane formation vs. the n-pentane partial pressure for Pt/H-BEA (0.2 wt% Pt) at 280°C and various total pressures between 5-25 bar.

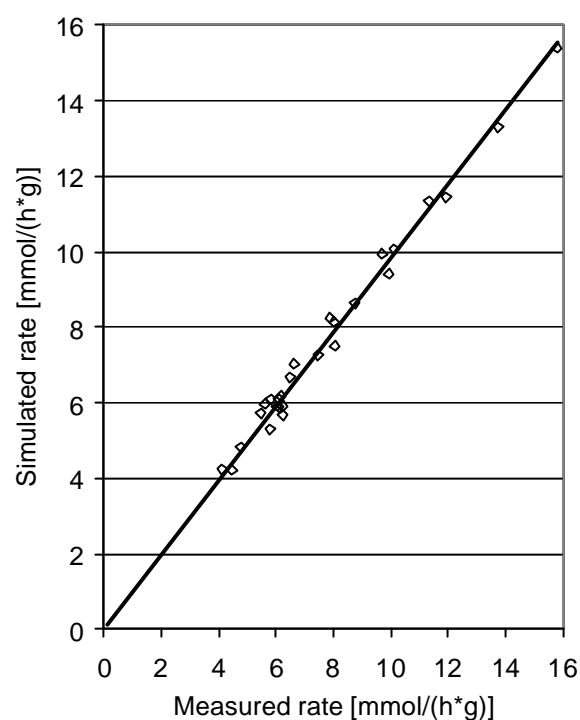


Figure 13: Difference between simulated rate determined by kinetic approach and measured rate of Pt/H-BEA (0.2 wt% Pt) at 280°C and various total pressures between 5-25 bar.

Table 2: Summary kinetic fit at 280°C.

k_{iso}	K^*	Formal order C_5	Formal order H_2	R^2	Standard deviation
$3.53 \cdot 10^4$ mol/(h* mol H ⁺)	0.03	+1	-1	0.988	0.33

In Figure 13 it was shown that the derived rate equation can be fitted simultaneously over a wide range of pentane and hydrogen partial pressures with a standard deviation of

0.33. Only two variables were used for the adjustment of the reduced kinetic expression that is the rate constant and a composite adsorption constant. The formal reaction order was determined to be +1 for n-pentane and -1 for hydrogen. Hence, a linear enhancement of the isomerization rate with increasing pentane partial pressure and a hyperbolic decrease of the isomerization rate with increasing hydrogen partial pressure was observed. The above results strongly indicate that the isomerization mechanism proceeds through a bifunctional pathway which is limited by the acidic properties of the zeolite.

In [29] a reaction order on H-BEA (1.6wt%-Pt) for the alkane of +0.7 and hydrogen of -0.3 was observed for the hexane hydroisomerization under atmospheric pressure. In addition an apparent activation energy of 113 kJ/mol ($220^{\circ}\text{C} < T < 280^{\circ}\text{C}$) was measured. Pentane isomerization on MOR zeolite (0.4 wt%-Pt) at 30 bar total pressure resulted in a reaction order for the alkane of +0.3 and hydrogen -0.8, while an apparent activation energy of 147 kJ/mol ($180^{\circ}\text{C} < T < 220^{\circ}\text{C}$) was determined [30]. In [31] pentane hydroisomerization on H-BEA (0.5wt%-Pt) led to a reaction order for the alkane of 0.5 and hydrogen of -1 and an apparent activation energy of 124 kJ/mol ($250^{\circ}\text{C} < T < 300^{\circ}\text{C}$) under atmospheric pressure. In general the differences in the observed reaction orders are explained by a different coverage of the reactants dependent on the reaction conditions. Indeed using power law rate equation a reduction of the apparent reaction order of pentane was observed for the Pt/H-BEA samples with increasing total pressure which is due to the fact that the adsorption isotherms level off at high coverages. The apparent activation energies were measured for the catalysts with different Pt-contents in the range between 100-110 kJ/mol ($260^{\circ}\text{C} < T < 310^{\circ}\text{C}$). The difference in the apparent activation energy possibly resulted from the different adsorption enthalpy since the experimentally determined activation energy consists of the sum of the true activation energy and the adsorption enthalpy. Hence a change in the latter due to a different support affects the apparent activation energy. Additionally higher temperature and low pentane partial pressures can lead to a minor surface coverage which corresponds to a higher degree of strong adsorption sites occupied and therefore a higher adsorption energy is observed. A reduced apparent activation energy due to the occurrence of pore diffusion limitations or single file diffusion can be excluded since a linear correlation in the Arrhenius plot was observed over a wide temperature range and single file diffusion restrictions or pore mouth catalysis appears to be unlikely in the three dimensional channel system of the BEA structure for the pentane isomerization.

A bifunctional pathway of the alkane hydroisomerization reaction at temperatures below 300°C was observed by a number of authors *e.g.* [32, 33, 34]. We therefore conclude that for the investigated reaction conditions pentane isomerization over Pt-loaded H-BEA with a $\frac{Pt_S}{H_{BAS}^+}$ ratio > 0.03 succeeds via classical bifunctional pathway. The catalyst is considered to be “well balanced” meaning that the activity of the (de)hydrogenation step is equilibrated and that the alkene concentration is maintained evenly dispersed throughout the catalyst [35].

3.5 Conclusions

H-BEA samples with different platinum loadings between 0.2 and 2.3 wt% possess similar concentration and strength of acid sites. It was shown that isomerization takes place *via* a classical bifunctional mechanism in which hydrogen has a negative effect on the isomerization rate with a reaction order of $n_{H_2} = -1$ and n-pentane enhances the rate according to a reaction order of $n_{C_5} = +1$. The isomerization activity is independent of the metal loading. This leads to the conclusion that the dehydrogenation step is equilibrated and that the kinetic relevant step of the reaction takes place on the acid sites. No deactivation phenomena were observed for all Pt containing samples. The reaction enthalpy was calculated as -7 kJ/mol while an apparent activation energy of about 105 kJ/mol was determined. Furthermore it was shown that hydrogen is essential for catalyst stability in order to keep the concentration of olefins low. Under helium atmosphere oligomerization reaction occurred primarily resulting in the formation of iso-butane and iso-hexanes. It is thus concluded that the metal sites are essential for the activation of the alkane and in order to keep the concentration of olefins low to prevent the occurrence of oligomerization reaction.

3.6 Acknowledgements

The financial support by Bundesministerium für Bildung und Forschung Project (BMBF:03C0307D) is gratefully acknowledged. The authors would like to thank Xaver Hecht for H₂-chemisorption, Martin Neukam for the AAS and Florencia Williams for the TEM measurements.

REFERENCES

- [1] M. Guisnet, *Polish J. Chem.*, 77 637-656 (2003).
- [2] H.W. Kouwenhoven, W.C. van Ziyll Langhout, *Chem. Eng. Progr.* 67, 65 (1971).
- [3] G.A. Mills, H.Heinemann, T.H. Millikan, A.G. Oblad, *Ind. Eng. Chem.* 45, 134 (1953).
- [4] P.B. Weisz, *Adv. Catal.* 13, 137 (1962).
- [5] M. Guisnet, F. Alvarez, G. Giannetto, G. Perot, *Catal. Today* 1, 415 (1987).
- [6] E. Iglesia, S.L. Soled, G.M. Kramer, *J. Catal.* 144, 238 (1993).
- [7] H.Y. Chu, M.P. Rosynek, J.H. Lunsford, *J. Catal.* 178, 352 (1998).
- [8] J. Meusinger, A. Corma, *J. Catal.* 152, 189 (1997).
- [9] A. Zhang, I. Nakamura, K. Aimoto, K. Fujimoto, *Ind. Eng. Chem. Res.* 34, 1074 (1995).
- [10] A. Zhang, I. Nakamura, K. Fujimoto, *J. Catal.* 168, 328 (1997).
- [11] T. Kusakari, K. Tomishige, K. Fujimoto, *Appl. Catal. A: Gen.* 224, 219 (2002).
- [12] J. de Graaf, A.J. van Dillen, K.P. de Jong, D.C. Koningsberer, *J. Catal.* 203, 307 (2001).
- [13] P.H. Lewis, *J. Catal.* 11, 162 (1968).
- [14] C.A. Emeis, *J. Catal.* 141, 347 (1993).
- [15] Cerius2 program suite (Accelrys Inc, 2001).
- [16] Y. Miyamoto, N. Katada, M. Niwa, *Micro. Meso. Mat.* 40, 271 (2000).
- [17] A. Corma, A. Martinez, C. Martinez, *Appl. Catal. A: Gen.* 132, 169 (1996).
- [18] F. Lonyi, J.H. Lunsford, *J. Catal.* 136, 566 (1992).
- [19] N.M. Rodriguez, P.E. Anderson, A. Wootsch, U. Wild, R. Schlögl, Z. Paal, *J. Catal.* 197, 365 (2001).
- [20] F. Babou, G. Coudurier, J.A. Vedin, *J. Catal.* 152, 341 (1995).
- [21] K.B. Fogash, Z. Hong, J.M. Kobe, J.A. Dumestic, *Appl. Catal. A: Gen.* 172, 107 (1998).
- [22] C. Lenoir, F. Rohr, M. Stöcker, P. Ruiz, *C.R. Chimie* in press (2005).
- [23] N. Essayem, Y. Ben Taarit, C. Feche, P.Y. Gayraud, G. Sapaly, C. Naccache, *J. Catal.* 219, 97 (2003).
- [24] H. Matsushashi, H. Shibata, H. Nakamura, K. Arata, *Appl. Catal. A: Gen.* 187, 99 (1999).
- [25] T. Wakayama, H. Matsushashi, *J. Mol. Catal. A: Chem.* 239,32 (2005).
- [26] H. Lynggaard, A. Andreasen, C. Stegelmann, P. Stoltze, *Prog. Surf. Sci.* 77, 71 (2004).
- [27] A.M. Rigby, G.J. Kramer, R.A. van Santen. *J. Catal.* 170, 1 (1997).

-
- [28] G. Yaluris, J.E. Aparicio, L.M. Madon, J.A. Dumesic, *J. Catal.* 153, 54 (1995).
- [29] A. van de Runstraat, J.A. Kamp, P.J. Stobbelaar, J. van Grondedella, S. Krijnen, R.A. van Santen, *J. Catal.* 171, 77 (1997).
- [30] A. Hollo, J. Hancsok, D. Kallo, *Appl. Catal. A: Gen.* 229, 93 (2002).
- [31] T. Matsuda, K. Watanabe, H. Sakagami, N. Takahashi, *Appl. Catal. A: Gen.* 6397, 1 (2002).
- [32] R. Ravishankar, S. Sivansanker, *Appl. Catal. A: Gen.* 142, 47 (1996).
- [33] J.M. Grau, J.M. Parera, *Appl. Catal. A: Gen.* 106, 27 (1993).
- [34] F. Alvarez, F.R. Ribeiro, G. Perot, C. Thomazeau, M. Guisnet, *J. Catal.* 162, 179 (1996).
- [35] T.L.M. Maesen, S. Calero, M. Schenk, B. Smit, *J. Catal.* 221, 241 (2004).

Chapter 4

4 IMPROVING BIFUNCTIONAL ZEOLITES FOR THE ALKANE ISOMERIZATION VIA GAS PHASE SULFATION: EFFECT OF TEMPERATURE DURING SULFATION

4.1 Abstract

Pt containing H-BEA zeolites were functionalized with sulfate anions *via* H₂S chemisorption followed by oxidation. The treatment generates sulfate groups and Brønsted acidic sites, modifies the supported metal particles and leads to higher activity and selectivity for pentane hydroisomerization. The strength and the accessibility of the acid sites present in the parent material were not affected by this procedure. The concentration of Brønsted acidic sites and the catalytic activity for light alkane isomerization varied sympathetically. The parallel increase of the isomerization selectivity indicates that either the residence time of the alkoxy intermediates decreases for the modified samples (suppressing undesired cracking reactions on the acid sites) or that the selective decoration of the Pt particles with sulfur reduces hydrogenolysis on the metal particles.

4.2 Introduction

Iso-Pentanes and hexanes are important components of high octane motor fuels, which are produced to a significant extent *via* hydroisomerization of the n-alkanes. Mechanistically, hydroisomerization occurs in three steps. In the first step, the alkane is dehydrogenated. The generated alkene adsorbs on a Brønsted acid site forming an alkoxy group (a carbenium ion in the transition state), which isomerizes and eventually desorbs. In the third step, the iso-olefin is hydrogenated to the iso-alkane. Catalysts are, therefore, bifunctional with a metal (Pt, Pd) catalyzing the hydrogenation/dehydrogenation step and an acidic function for the formation and isomerization of the alkoxy group/carbenium-ion. The metal component also helps to reduce catalyst deactivation by hydrogenating coke precursors.

As the reaction proceeds *via* carbenium ions, other Brønsted acid catalyzed reactions such as oligomerization and cracking compete with isomerization [1, 2]. In addition, side reactions on the metal such as hydrogenolysis of the alkane to smaller alkanes may reduce the selectivity of the overall hydroisomerization reaction [3, 4]. Eventually, the isomer yield is limited by the thermodynamic equilibrium between the iso- and n-isomers. Because

branched alkanes are thermodynamically the more favored the lower the reaction temperature is the reaction temperature should be as low as possible. Therefore, catalysts active at low temperatures, such as heteropolyacids, sulfated or tungstated zirconia and Pt on chlorinated Al_2O_3 have been explored [5, 6, 7]. Pt containing catalysts based on zeolites operate at somewhat higher temperatures (and thus limit the maximum yield achievable), but have the advantage to be less sensitive towards water and oxygenates. Currently, most industrial catalysts for isomerization of pentane and hexane are based on Pt/H-MOR as catalytically active component, but new materials based on sulfated oxides have been commercially introduced [8, 9].

Whether hydrogenation/dehydrogenation or the acid catalyzed conversion is rate determining depends upon the concentration of the catalytic functions in the catalyst. At a low concentrations of accessible metal atoms, their abundance determines the concentration of olefins and, hence, the catalytic activity. With a sufficient concentration of available metal surface atoms the hydrogenation/dehydrogenation is equilibrated. Under such conditions, the rate determining step is the isomerization of the alkoxy groups/ carbenium ions. Thus, the concentration and strength of Brønsted acid sites determines the activity of the catalyst by controlling the concentration and lifetime of the alkoxy groups and the relative ratio of carbon-carbon bond cleavage versus isomerization [10]. The main focus for catalyst development lies on the modification of the acidic and textural properties of the catalysts. Examples for tailoring for that approach include the dealumination of zeolites or the partial ion exchange with divalent cations such as Zn^{2+} [11, 12].

In that context anion modification seems promising as reports suggest that modification with $(\text{NH}_4)_2\text{SO}_4$ has a positive effect on acidity and catalytic activity [13] of zeolites. The modification appears to involve formation of aluminum sulfate species [13]. In this context it is interesting to note also that sulfur oxide species appear to promote the activity for metal catalyzed reactions [14, 15, 16, 17]. With that in mind we have modified Pt containing zeolite by treatment with H_2S and subsequent oxidation and characterized the acid-base and catalytic properties of the new zeolite based bifunctional catalysts. The procedure ensures the generation of sulfur species close to the metal particles throughout the zeolite material and the subtle control of the overall and local concentration of the sulfate species formed in the new material.

4.3 Experimental

4.3.1 Catalyst preparation

Zeolite Beta with a Si/Al ratio of 12.5 (H-BEA 25) was received from Süd-Chemie AG and was loaded with 1 wt % Pt by ion-exchange with aqueous $\text{Pt}(\text{NH}_3)_4(\text{OH})_2$ solution. A solution containing the appropriate amount of $\text{Pt}(\text{NH}_3)_4(\text{OH})_2$ and an amount of NH_4OH corresponding to the theoretical amount of protons (competitive adsorption) in the sample was added dropwise to the slurry at 40°C. After the ion exchange the solid was centrifuged, washed and freeze dried. The samples were calcined in air 350°C for 16 h (heating rate 0.5°C/min) and finally reduced at 300°C in H_2 for 4 h. The metal loading after the preparation was determined using atomic absorption spectroscopy (AAS).

Pt-loaded ASA catalyst with a Si/Al ratio of 9.5 was synthesized using a mixture of acetic acid with $\text{AlCl}_3 \cdot 6\text{H}_2\text{O}$ (pH=1.5) and sodium silicate solution (water glass, Merck) with NH_4OH (pH = 12). The solution was washed several times with ammonium acetate in order to eliminate Na^+ cations from the acidic support and finally calcined at 675°C. Pt was impregnated using $\text{Pt}(\text{NH}_3)_4(\text{OH})_2$ and subsequently calcined at 300°C for 5 hours and reduced with H_2 at 350°C for 2 hours. Subsequently, this sample is tagged as the parent sample (Pt/BEA).

For the sulfation procedure the samples were heated in He atmosphere from room temperature to the sulfation temperature with a heating rate of 7.5°C/min. Directly after reaching the target temperature the sulfation procedure was initiated by passing a mixture containing 1.8 vol.% H_2S in H_2 over the Pt loaded zeolite at 350°C, 450°C or 550°C for 2h at a WHSV of 2 [$\text{g}(\text{H}_2\text{S})/(\text{g}_{\text{cat}}\cdot\text{h})$]. Subsequently, the material was oxidized in air for 2 h at a WHSV of 2 [$\text{g}(\text{O}_2)/(\text{g}_{\text{cat}}\cdot\text{h})$]. The catalysts are named Pt/BEA S350, Pt/BEA S450 and Pt/BEA S550, respectively. Before characterization and the kinetic tests the samples were reduced in hydrogen for 90 min at 350°C (heating rate 5°C/min).

4.3.2 Hydrogen chemisorption

Hydrogen chemisorption was performed using a Sorptomatic 1990 Series instrument. About 1g of catalyst was reduced in hydrogen at 350°C for 2h and subsequently evacuated. All adsorption isotherms were measured at 35°C. The amount of chemisorbed hydrogen was determined after removing physisorbed hydrogen by evacuation at 35°C from the

sample and determining that fraction quantitatively by repeating the exposure and measuring the uptake. The isotherm of chemisorbed hydrogen has been determined by subtracting the second isotherm (containing only physisorbed H₂) from that measured in the first experiment (containing chemisorbed and physisorbed H₂). The monolayer coverage of hydrogen adsorbed has been determined by extrapolating the linear part of the adsorption isotherm to zero pressure. The fraction of metal surface atoms has been calculated by assuming the adsorption of one hydrogen atom per Pt surface atom.

4.3.3 X-ray absorption spectroscopy (XAS)

The structural and chemical properties were investigated by X-ray absorption spectroscopy (XAS) measured on beamline X1 at Hasylab, DESY, Hamburg. The storage ring DORIS III operates with a positron energy of 4.5 GeV and a current between 85 and 51 mA. X-ray absorption spectra were recorded at the Pt-L_{III}-edge (11564 eV) in transmission mode, using a stepwise moving Si (111) monochromator. The intensity of incident and transmitted X-rays were recorded using ionization chambers. The monochromator was detuned to 60 % of the maximum intensity to avoid contributions of high harmonics in the X-ray beam. The samples were pressed into self-supporting wafers and placed in the sample holder equipped with a heating and cooling system. Activation and reduction of the samples was carried out in hydrogen for 2h at a temperature of 350°C. The spectra were measured at liquid nitrogen temperature.

For EXAFS analysis the oscillations were extracted from the background using a second order polynomial function and after weighting with k^2 the oscillations were Fourier transformed in the range between 3 and 13 Å⁻¹. The local environment of the Pt atoms was determined from the analysis of the EXAFS in k-space applying phase-shift and amplitude functions for Pt-Pt and Pt-S calculated assuming multiple scattering processes (FEFF Version 8.10 [18]) using the program Viper [19].

4.3.4 Ion-Chromatography

The amount of sulfate species present on the samples was determined by liquid ion-chromatography (Metrohm 690) using an anion column IC SUPER-SEP with phthalic acid (2.5mmol/l) and 5% acetonitrile as eluents. For the determination of the sulfate content 20mg of catalyst was dissolved in 100 ml sodium hydroxide (0.01 mol/l).

4.3.5 N₂ adsorption

The specific surface areas and pore volumes were determined by physisorption of nitrogen using a Sorptomatic 1990 Series instrument. About 500 mg of the sample was heated to 350°C and evacuated for 1h before nitrogen adsorption was carried out at a temperature of -196°C. The specific surface area was calculated according to the Brunauer-Emmett-Teller (BET) method. The pore volume was determined using the t-plot method.

4.3.6 Temperature programmed desorption (TPD)

Temperature programmed desorption was performed in a home built 6-fold parallel TPD system. The catalysts were activated by heating in vacuum to 350°C (rate of 10°C/min) for 2 h. Ammonia was adsorbed at 150 °C with a partial pressure of 0.6 mbar for 1 h and subsequently the samples were evacuated at 10⁻³ mbar for 2 h in order to remove physisorbed molecules. For the TPD experiments the 6 samples were (sequentially) heated from 150°C to 800°C with a rate of 10°C/min and the species desorbing were monitored by mass spectrometry (*Balzers QME 200*). In each set of experiments a reference sample with known concentration of acid sites was used to calibrate the MS signal.

4.3.7 IR spectroscopy

IR spectra after adsorption of pyridine were measured from 3800 to 1100 cm⁻¹ at a resolution of 4 cm⁻¹ using a Perkin Elmer 2000 spectrometer and a heatable high vacuum IR cell described previously [20]. A self supporting wafer was activated by heating in vacuum with an increment 10 °C/min to 350°C and keeping it at that temperature for 60 min. After cooling the sample to 150°C the spectrum of the activated zeolite was recorded. Pyridine was adsorbed at 150°C with a partial pressure of 0.05 mbar for 30 min and the sample was subsequently evacuated at that temperature until IR spectra recorded in intervals of 10 minutes did not vary from each other. To compare the spectra of the different samples all spectra were normalized by the intensity of the lattice vibration overtones of the zeolite between 1750 and 2100 cm⁻¹. Alternatively, the weight of the wafers was used to determine the mass per surface area necessary for calculating the concentration of Brønsted and Lewis acid sites according to the method published by Emeis [21].

In situ IR measurements during sulfur treatment and C₅ isomerization were carried out using a flow cell equipped with ZnS windows and a resistance heated furnace for the sample holder. For *in situ* IR experiments the samples were pressed into self supported wafers (ca. 2 mg) and activated for 90 min at 350°C in hydrogen. For H₂S and oxidation treatment a flow of 20 ml/min was used.

4.3.8 Temperature programmed reduction studies

Temperature programmed reduction (TPR) studies were performed in a flow reactor system heated with a cylindrical, ceramic oven equipped with 3x 1000W of thermal output from Horst GmbH. The gases evolved during TPR were monitored by a mass spectrometer (*Balzers QME 200*). For activation the samples were heated in He atmosphere from room temperature to 375°C with a heating rate of 5°C/min. This temperature was held for 90 min.

4.3.9 Kinetic studies

The catalytic activity was studied with a 20-fold parallel plug flow reactor system. The reactant gas flow and pressure of each reactor was controlled by individual digital mass flow controllers and back-pressure regulators. The liquid feed was adjusted and mixed with hydrogen by a digitally controlled evaporator - mixer. For the analysis of the products a HP-MicroGC (GC M200) was used, capable to separate aliphatic C₁ to C₆ hydrocarbons (including their isomers) in less than 2 min. The total pressures, flow rates, temperatures and alkane concentrations were varied automatically. For the kinetic experiments external diffusion limitations were experimentally excluded and the activity was determined under differential reaction conditions. All data recorded were stored in a relational MS Access database.

The isomerization activity will be presented as the rate constant k_{iso} for the formation of iso-C₅, which was calculated according the equation given below, where $n-C_5^{Feed}$ and $n-C_5^{exit}$ signify the concentration of n-pentane in the feed and at the exit of the reactor respectively.

$$k_{iso} = \frac{\text{rate formation iso-C}_5}{\text{concentration n-C}_5^{Feed}} = \frac{Flow \cdot \ln\left(\frac{n-C_5^{Feed}}{n-C_5^{exit}}\right) \cdot S_{iso-C_5}}{m_{Cat}}$$

4.4 Results

4.4.1 Preparation procedure and sulfation loading

In principle, sulfate ions could be introduced *via* several approaches into a zeolite, including direct impregnation with ammonium sulfate, the sorption of SO₃ (including the oxidative sorption of SO₂) and the sorption of H₂S or an organic sulfide with subsequent oxidation. We have opted for the latter route, because it assures the most subtle method to introduce sulfates and to modify the zeolite acidity without inducing damage to the structure or the generation of high local concentrations of sulfates. The method applied used the equilibration with H₂S in hydrogen at several temperatures in order to assure the equilibration of the metal particles with sulfur at the accessible Pt surface and its subsequent oxidation to SO₃, which was trapped by the aluminum oxide nanoclusters in the zeolite pores.

Table 1: Concentration of acid sites, sulfate concentration, fraction of Pt surface atoms and specific surface area of Pt/BEA after sulfur treatment at different temperatures.

Sample	Brønsted acid sites [mmol/g]	Lewis acid sites [mmol/g]	SO ₄ ²⁻ content [mmol/g]	SO ₄ ²⁻ / Pt [mol/mol]	Surface Pt atoms [H/Pt]	N ₂ - volume [cm ³ /g]
Pt/H-BEA	0.28	0.28	-		0.52	110
Pt/BEA S350	0.39	0.29	0.44	8.7	0.11	102
Pt/BEA S450	0.32	0.27	0.14	2.6	0.06	105
Pt/BEA S550	0.24	0.21	0.06	1.2	<0.01	95

With increasing temperature of the equilibration with H₂S, the overall retention of sulfur in the material decreased (see Table 1). As the retention of sulfur originally occurs *via* the formation of Pt sulfide species the results indicate that the most sulfur is retained at the lowest reaction temperature in line with the decreasing stability of Pt sulfide with increasing temperature. While the content of sulfate species was in the same order of magnitude than the concentration of acid sites for a sulfation temperature at 350°C, it was strongly reduced applying higher temperatures (see Table 1). The maximum amount of sulfur deposited in one step is estimated by using the concentration of sulfur bound as PtS to be 0.05 mmol per gram zeolite for a single preparation step. It is interesting to note that this is about the concentration that is retained at the highest reaction temperature (see Table

1). As the amount of sulfur retained decreased with increasing temperature, the results suggest that at 350 °C either more than one sulfur atom was retained per accessible Pt atom or that H₂S was adsorbed not only on Pt, but also on the zeolite acid sites similar to what has been observed for H₂S adsorption on H-ZSM5 [22]. The fact that at the highest equilibration and oxidation temperature the concentration sulfate retained was equal to the concentration of Pt suggests that at least a part of the more weakly bound H₂S was oxidized in the procedure.

4.4.2 Characterization of metal particles

As the various treatments and the use of the catalyst in a strongly reducing atmosphere could lead to marked modification of the metal particles great care was taken to understand the size of the particles, their oxidation or electronic state and concentration accessible Pt atoms.

Hydrogen chemisorption was used to assess the concentration of accessible metal atoms. The results are summarized in Table 1. For the parent Pt/BEA with 1wt% Pt the H/Pt ratio was determined to be 0.5. The concentration of accessible Pt atom that adsorbed hydrogen was severely reduced after the sulfur treatment with the decrease being more pronounced with increasing S-treatment temperature. For the sample Pt/BEA S550 the concentration of accessible Pt dropped below the detection limit.

X-ray absorption spectroscopy was applied to explore the electronic and structural features of the Pt particles [23]. The XANES of Pt/BEA before and after sulfur treatment are compared with that of a Pt foil in Figure 1 a. For the untreated catalyst the intensity of the peak above the absorption edge (white line) was smaller compared to the Pt foil. The sulfur treatment at 350°C led to an increase of the intensity of the white line compared to that of parent Pt/BEA. For the samples Pt/BEA S450 and Pt/BEA S550 the intensity of the white line further increased. The additional peak at 17 eV above the Pt L_{III} edge (assigned to multiple scattering contributions) increased in intensity with increasing temperature of the sulfur treatment. For the parent sample and the sample Pt/BEA S350 only a small peak was observed, while for the samples Pt/BEA S450 and Pt/BEA S550 a well defined peak at 17 eV above the Pt L_{III} edge developed. This peak is attributed to be part of the EXAFS oscillations and hence its increase suggests an increase in the particle size.

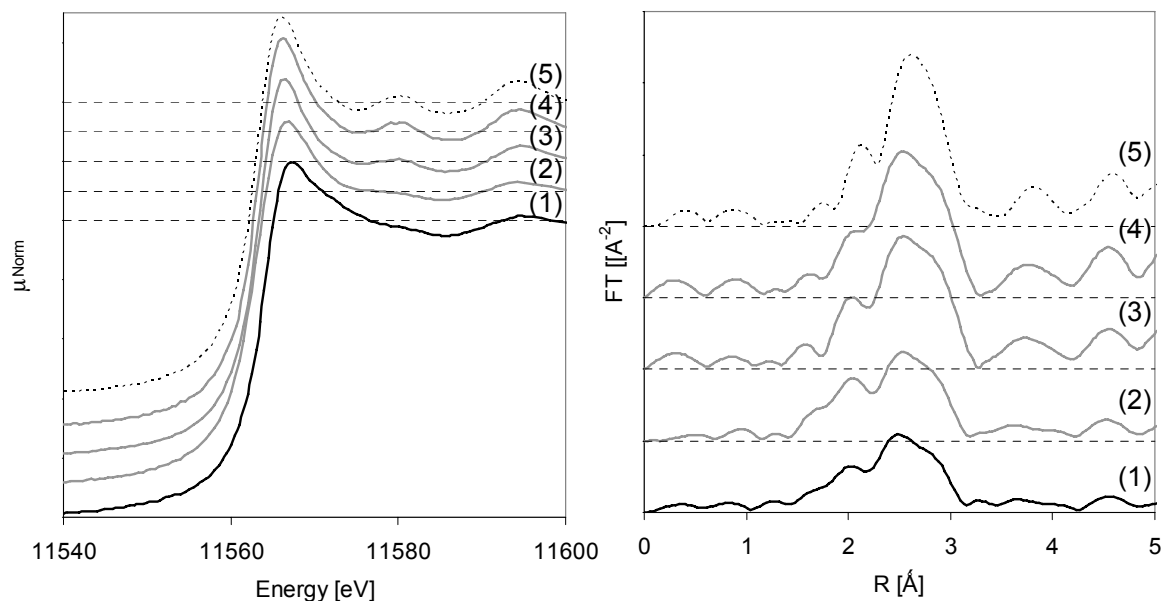


Figure 1: (a) XANES and (b) Fourier transformed EXAFS (k^2 -weighted) for Pt/BEA (—) (1), H₂S and air treated (—) Pt/BEA S350 (2), Pt/BEA S450 (3), Pt/BEA S550 (4) and Pt-foil (.....) (5).

Table 2: Results of the analysis of the EXAFS for Pt/BEA before after sulfur treatment.

Sample	shell	Number of neighbors ¹	Distance [Å] ²	DW factor ³	E ₀ correction [eV] ⁴
Pt/BEA	Pt-Pt	8.3	2.74	$6.4 \cdot 10^{-3}$	8.4
Pt/BEA S350	Pt-Pt	8.3	2.75	$6.1 \cdot 10^{-3}$	8.3
	Pt-S	0.98	2.29	$5.2 \cdot 10^{-2}$	8.8
Pt/BEA S450	Pt-Pt	10.1	2.76	$4.2 \cdot 10^{-3}$	9.4
	Pt-S	0.91	2.25	$1.6 \cdot 10^{-2}$	3.9
Pt/BEA S550	Pt-Pt	11.3	2.76	$5.0 \cdot 10^{-3}$	8.9

¹: coordination number of the absorber-backscatter pair

²: average absorber-backscatter distance

³: Debye -Waller factor

⁴: inner potential correlation

The radial distribution functions of Pt for Pt/BEA catalysts before and after sulfur treatment are compared in Figure 1 b and the results of the analysis of the EXAFS are summarized in Table 2. The parent material shows Pt-Pt contributions of the first (approximately 2.7 Å) and minor contribution of the second coordination shell

(approximately 3.9 Å). The sample Pt/BEA S350 showed the same contributions for Pt-Pt scattering and additional Pt-S contributions around 2 Å, which indicates that a direct bond between the Pt and sulfur was formed. The Pt-Pt contributions in the first (~ 2.7 Å) and second coordination shell (~ 3.9 Å) increased for the samples Pt/BEA S450 and Pt/BEA S550 indicating growth of the Pt particles, while the Pt-S contribution was more pronounced the lower the temperature during sulfur treatment.

4.4.3 Characterization of zeolite and sulfate compound

The TPD of NH_3 from Pt/BEA after sulfur treatment at different temperatures and that of the parent catalyst are compiled in Figure 2. Two overlapping peaks for NH_3 desorption were observed indicating the presence of two sorption states of ammonia. For the parent material, the peaks were found at 350°C and at 550°C. The maximum at lower temperature did not vary significantly with the treatments while that at higher temperature shifted to 480°C indicating that the strength of the interaction of the acid sites decreased after sulfation. For the sample sulfated at 350°C the amount of ammonia desorbed was markedly higher than for the parent sample. For the sample Pt/BEA S450 it was higher than the parent, but lower than the sample Pt/BEA S350. For the sample Pt/BEA S550 the concentration of ammonia adsorbed was lower than for the parent sample.

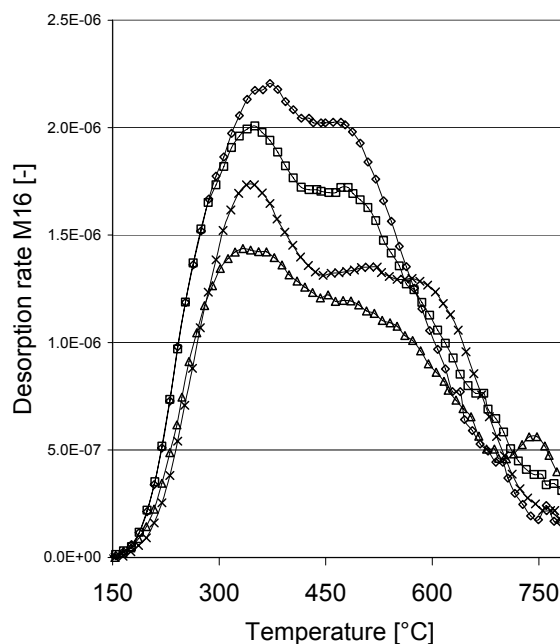


Figure 2: NH_3 -TPD of Pt/BEA (— \times —), Pt/BEA S350 (— \diamond —), Pt/BEA S450 (— \square —) and Pt/BEA S550 (— \triangle —).

The XRD of the zeolite samples did not show any variations of the zeolite crystallinity after the sulfur treatment, i.e., the materials were identified as polymorph BEA without changes in the intensity or location of the diffraction peaks induced by the treatments. Additional peaks were also not observed indicating that, if formed, other phases were either X-ray amorphous or below the detection limit.

The IR spectra of Pt/BEA and of the sulfur treated samples before and after pyridine adsorption are shown in Figure 3. For the catalyst Pt/BEA S350 the intensity of the band at 3608 cm^{-1} (strong Brønsted acid sites) increased by 15% compared with the parent material. For the sample Pt/BEA S450 the intensity was approximately identical and for the sample Pt/BEA S450 the intensity of the band at 3608 cm^{-1} was reduced compared with the parent material. The formation of additional silanol groups at (3733 cm^{-1}), assigned to SiOH groups at defects, was observed with the samples treated at 450 and 550 °C. Pyridine adsorption led to the disappearance of the bands at 3608 and 3785 cm^{-1} , assigned to Brønsted acidic hydroxyl and AlOH groups, respectively and to decrease in intensity of the silanol groups at 3743 cm^{-1} indicating that all hydroxyl groups were accessible for pyridine and that the sulfur treatment did not cause pore blocking.

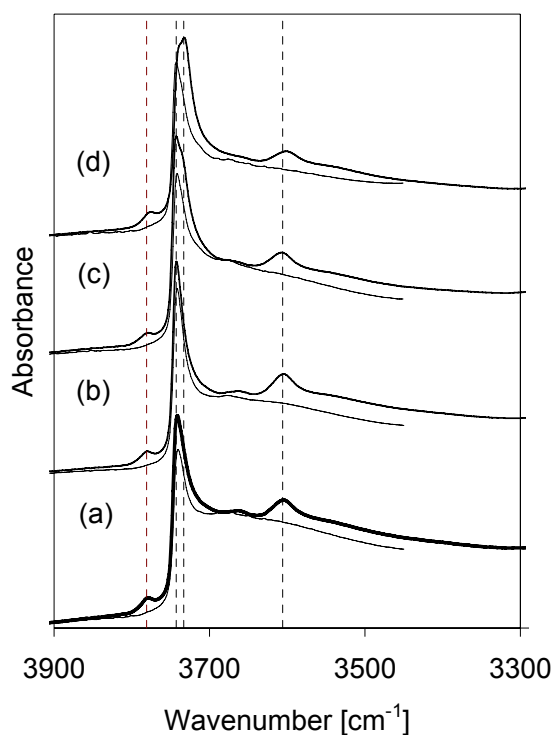


Figure 3: IR spectra (normalized lattice vibration between 1750 and 2100 cm^{-1}) of activated Pt/BEA (a) (—), H_2S and air treated (—) Pt/BEA S350 (b), Pt/BEA S450 (c) Pt/BEA S550 (d) and after pyridine adsorption (— ·).

The IR spectra before and after pyridine adsorption of the parent Pt/BEA material and the samples after sulfur treatment at different temperatures are shown in Figure 4. The typical bands of pyridine ring vibrations (1544 cm^{-1} for pyridine on Brønsted sites, 1490 cm^{-1} for pyridine interacting with Brønsted and Lewis sites and 1455 cm^{-1} for pyridine on Lewis sites) were observed for all materials. The quantitative evaluation of the pyridine ring vibrations showed that the concentrations of pyridinium ions and of Lewis acid coordinated pyridine varied considerably (see Table 2). Sulfur treatment at low temperatures led to higher concentrations of Brønsted acid sites, while the concentration of Lewis acid sites remained constant. With increasing treatment temperature the concentration of Brønsted and Lewis acid sites decreased. Pt/BEA S450 showed a reduced Brønsted and Lewis acid sites concentration. Also the concentration of sulfate on the samples decreased with increasing sulfur treatment temperature (as measured using ion chromatography). The band observed at 1385 cm^{-1} , assigned to surface sulfate species [24], [25] decreases with increasing sulfur treatment temperature and was not observed for the parent material. It should be noted that the concentration of sulfate on the sample is in the same order of magnitude than the concentration of acid sites for the sample sulfated at low temperatures, while at a sulfation temperature of 550°C the concentration of sulfate species is reduced by a factor of almost 10. When comparing these variations in the concentrations of sulfates and Brønsted and Lewis acid sites, it is evident that sulfate groups deposited may influence but not generate the majority of the acid sites.

The differences in the IR spectra before and after adsorption of pyridine on Pt/BEA S350 are compared in more detail in Figure 5. After adsorption of pyridine the band at 1385 cm^{-1} , assigned to the stretching frequency of a covalent S=O bond, is reduced and a new band at 1335 cm^{-1} , assigned to the S=O stretching vibration perturbed by pyridine, was observed. This indicates that the basic molecule interacted (directly or indirectly) with the sulfate group similar to what has been observed for the sulfate groups of sulfated zirconia [26.]

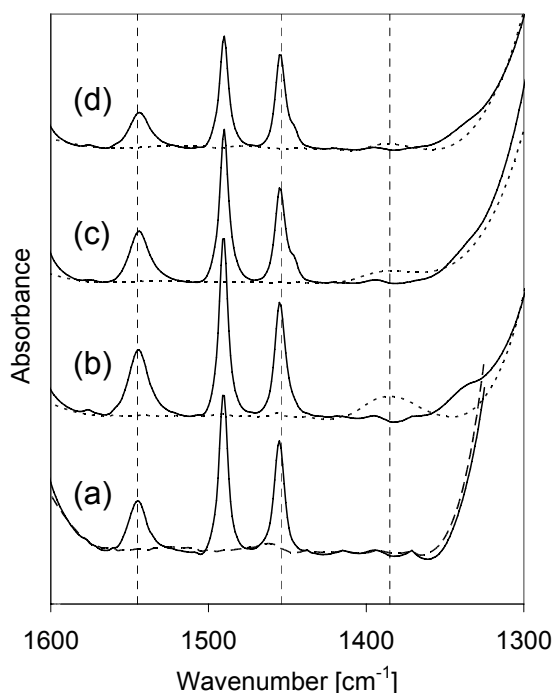


Figure 4: IR spectra of: (—) activated Pt/H-BEA (a), Pt/BEA S350 (b), Pt/BEA S450 (c), Pt/BEA S550 (d) and after pyridine adsorption (---).

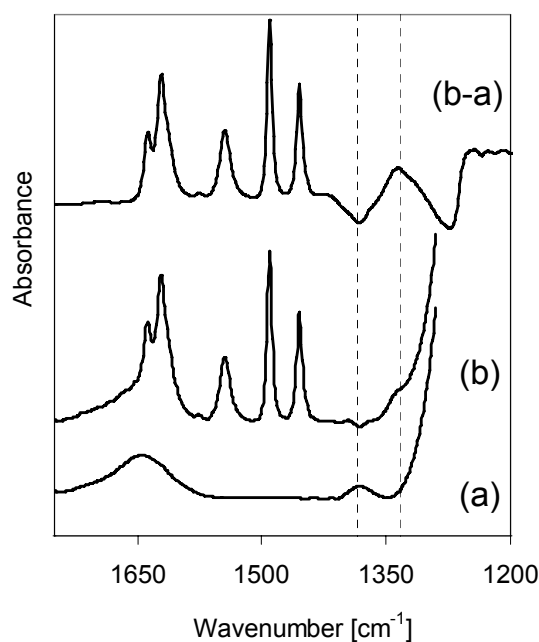


Figure 5: IR spectra of activated Pt/BEA S350 (a), after adsorption of pyridine (b) and difference spectra (b-a).

4.4.4 Nature and reactivity of sulfate species under reaction conditions

The *in situ* IR measurements of the Pt/H-BEA catalyst at 350°C during H₂S treatment and oxidation are shown in Figure 6. During H₂S treatment in hydrogen atmosphere bands at 1445 and 1330 cm⁻¹ were observed, while during oxidation in air an intense band at 1385 cm⁻¹ was formed. In accordance with [27] and [28] the band at 1330 cm⁻¹ is attributed to SO₂ physisorbed on alumina. The band at 1145 cm⁻¹, which should also appear with physisorbed SO₂ was masked by strong bands of the zeolite lattice vibrations. Note that a band around 1400 cm⁻¹ was assigned to strongly bound sulfate species on magnesium-alumina spinels [29] and on MgO [28] exposed to SO₂/O₂. The small band at 1445 cm⁻¹ appears in the region of organic sulfates or molecular sulfuric acid [25].

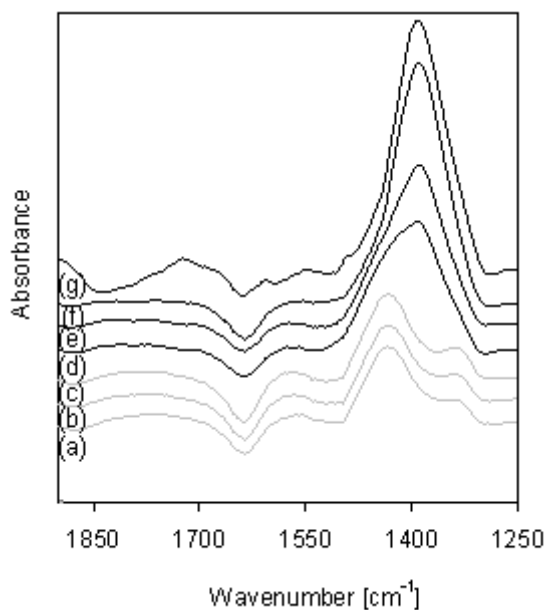


Figure 6: Difference *in situ* IR spectra during H_2S treatment (—) after (a) 1min, (b) 6min, (c) 90min and oxidation (—) (d) 1min, (e) 2min, (f) 40 min, (g) 60 min.

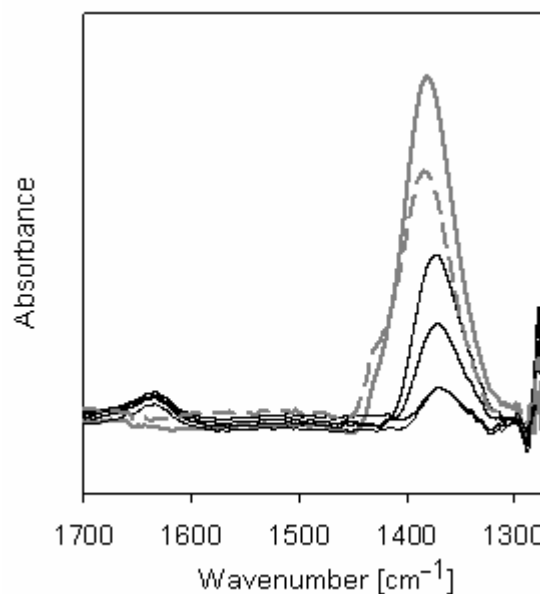


Figure 7: Differences in the IR spectra after oxidation of H_2S treated sample (—); during hydroisomerization reaction (—) and after reactivation in Helium at 400°C (---).

To explore the presence of sulfates species under reaction conditions the changes in intensity of the S=O band (1385 cm^{-1}) were followed *in situ* on a sulfur treated Pt/BEA catalyst during hydroisomerization of 3 mol% pentane in hydrogen at 300°C and 1 bar total pressure (see Figure 7). The presence of hydrogen and pentane led to an immediate reduction of the intensity of the sulfate band at 1385 cm^{-1} , which reached a constant level after 2 h time on stream. In addition to the reduction of the band at 1385 cm^{-1} the formation of water was observed by the presence of the $\delta(\text{OH})$ band at 1641 cm^{-1} during hydroisomerization. Under reaction conditions the intensity of the band at 1385 cm^{-1} decreased strongly, however, after heating the sample to 400°C in He for 2 h approximately 80% of the intensity compared to the sulfur treated sample before the reactions was regained. The hydroxyl groups at higher wavenumbers (3608 cm^{-1}) were not influenced during the hydroisomerization reaction.

In order to analyze the stability of the sulfate species on the surface of the catalysts, temperature programmed reduction measurements were carried out for the Pt/BEA S350. The sample was activated in He at 350°C for 90 min before the TPR to remove all physisorbed water. During the reduction in H_2 the sample was heated up to a temperature of 1000°C with an increment of 7.5 K/min . The H_2S signal during the TPR is shown in Figure

8. At temperatures above 380°C H₂S started to desorb and reached a maximum at a temperature of 440°C. At a temperature of 440°C the formation of water was observed which results from the decomposition of the sulfate species. This indicates that the sulfur species were stable under reaction condition applied for the isomerization reaction.

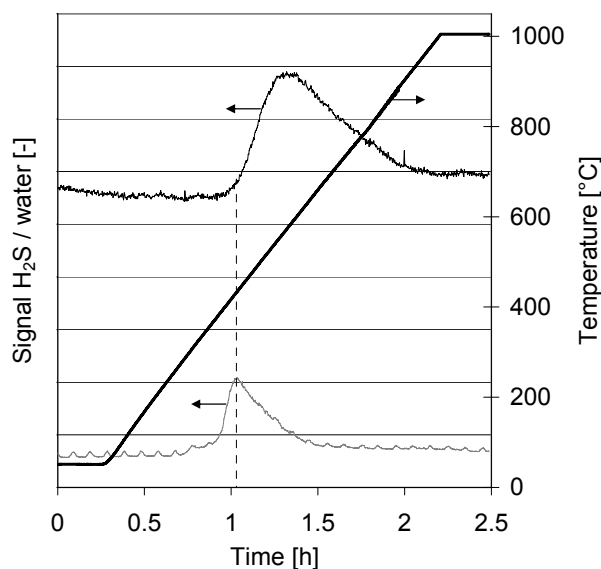


Figure 8: Temperature programmed reduction of Pt/BEA S350 (water (—) and H₂S Signal (—)).

4.4.5 Hydroisomerization of pentane

The catalytic activity of the parent Pt/BEA and the samples sulfated at different temperatures is represented for a total pressure of 4 bar, a WHSV of 30 h⁻¹, in a temperature range between 260 and 350°C in Figure 9 in the form of an Arrhenius plot. In general a higher isomerization rate was observed with decreasing sulfation temperature. The comparison of the activities of the parent and modified catalysts in the kinetic regime (linear part at low temperatures) shows the positive effect of the milder treatments (Pt/BEA S350, Pt/BEA S450). Increasing the sulfation temperature to 550°C on the other hand leads to a reduction of the isomerization rate compared to the parent material. The apparent activation energies varied between 102 and 110 kJ/mol. The very subtle variations in the apparent energy of activation and the larger variation of the composed preexponential factor suggest that the main effect of the sulfate treatment resulted in a variation of the concentration of the (Brønsted) acid sites. This is nicely illustrated in the linear correlation between the concentration of Brønsted acid sites and the isomerization activity as shown in Figure 10. The lower activity than expected acidity for Pt/BEA S550 is attributed the very

low concentration of accessible Pt atoms in this sample. For this catalyst the concentration of metal sites is so low that the concentration of available metal sites influences or controls the catalytic activity. The direct correlation indicates that, as expected, the reaction of intermediately formed olefins on the Brønsted acid sites controls the kinetics of the reaction, i.e., that normalized to Brønsted acid sites the parent and Pt/BEA S350, Pt/BEA S450 have the same catalytic activity. The lower than expected activity for Pt/BEA S550 is attributed to the very low concentration of accessible Pt atoms in this sample. For this catalyst the concentration of accessible Pt atoms is so low that it influences or controls the catalytic activity.

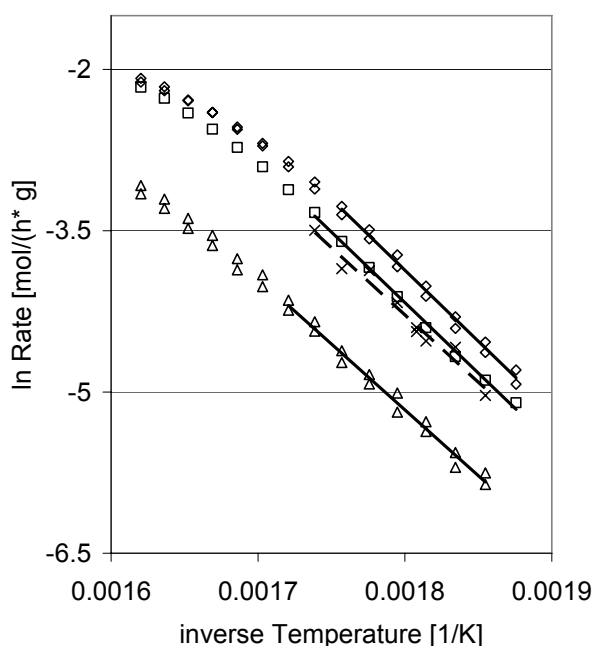


Figure 9: Isomerization activity between of Pt/BEA (—×—), Pt/BEA S350 (—◇—), Pt/BEA S450 (—□—) and Pt/BEA S550 (—△—).

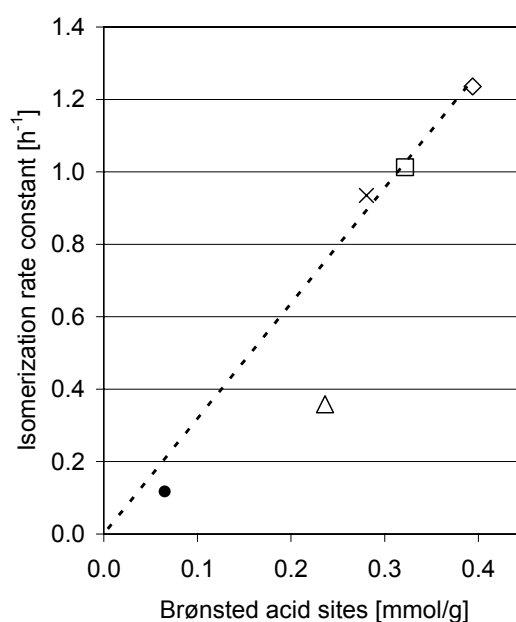


Figure 10: Correlation of Brønsted acidity and isomerization activity for Pt/BEA S350 (—◇—), Pt/BEA S450 (—□—), Pt/BEA S550 (—△—) and Pt-ASA (●).

Table 3: Apparent activation energy for Pt/BEA and H₂S/air treated samples.

Sample	Apparent activation energy [kJ/mol]
Pt/H-BEA	104
Pt/BEA S350	110
Pt/BEA S450	109
Pt/BEA S550	102

The iso-pentane selectivity at various conversion levels (the WHSV was varied between 5 and 30 h⁻¹) at a temperature of 300°C and a total pressure of 4 bar (H₂/C₅ ≈ 30) is shown in Figure 11. The thermodynamic equilibrium between n- and iso-pentane at 300°C, which is the upper limit for the selectivity achievable, is included in the graph. The iso-pentane selectivity of the untreated catalyst decreased sympathetically with increasing conversion, while after the sulfation the selectivity reached almost 100%, independently of the conversion level until the thermodynamic equilibrium was reached.

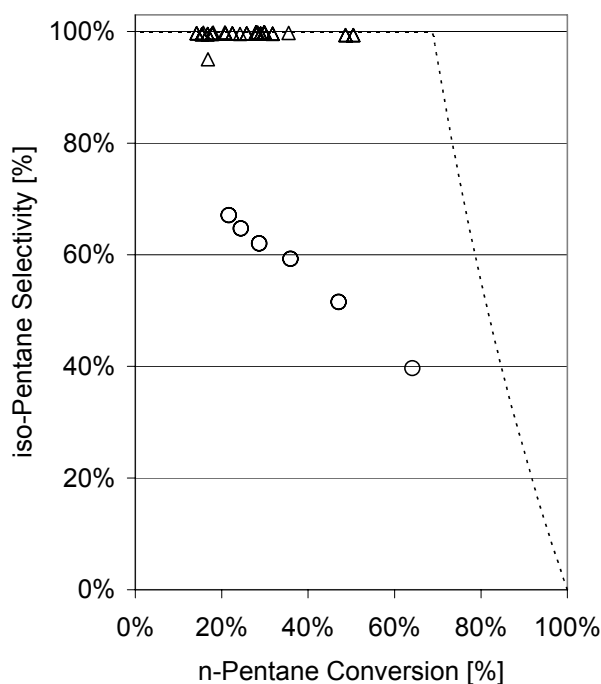


Figure 11: Selectivity to iso-pentane for Pt/BEA at 300°C (○) and Pt/BEA S350 (△); equilibrium for 300°C (- - - -).

The main side reaction for the parent material under the conditions studied was C-C bond cleavage (Figure 12). Products from oligomerization (i.e. hydrocarbons > C₅) were only observed in negligible concentrations. A symmetric distribution of C₂ and C₃ and C₁ and C₄ alkanes was observed independently of the conversion level. The concentration of the primary products ethane/propane and methane/butane were found to be nearly equal. At higher temperatures the concentration of C₁ increased as a result of a more enhanced activity for secondary C-C bond breaking reactions. The sulfation treatment did not influence the product distribution of the cracking/hydrogenolysis reactions. Only low concentrations of iso-butane were found resulting from a consecutive reaction (the zero initial slope at zero conversion). Figure 13 shows the logarithmic rate of the formation of

the side products *versus* the inverse reaction temperature. In the low temperature region a linear relationship of the rate of formation of side products and the inverse temperature was observed. At higher temperatures and, thus, closer to the equilibrium concentrations, the formation of n- and iso-butane decreased due to consecutive reactions. The apparent activation energies measured below 300°C (linear region) are given in Figure 13. Ethane and propane show similar apparent activation energies (about 110 kJ/mol) indicating that both products are formed in parallel. The apparent energies of activation of methane and n-butane are higher suggesting a different pathway of formation or a different sorption state of the precursor.

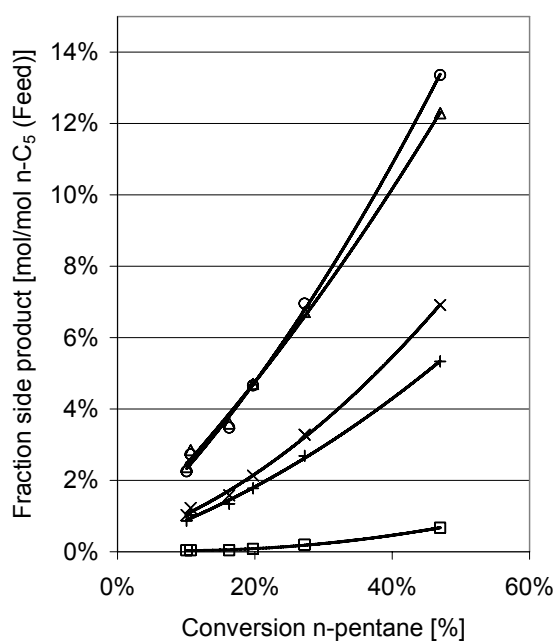


Figure 12: Product distribution for Pt/BEA Methane (X), Ethane (O), Propane (Δ), iso-Butane (□) and n-Butane (+) at 280°C.

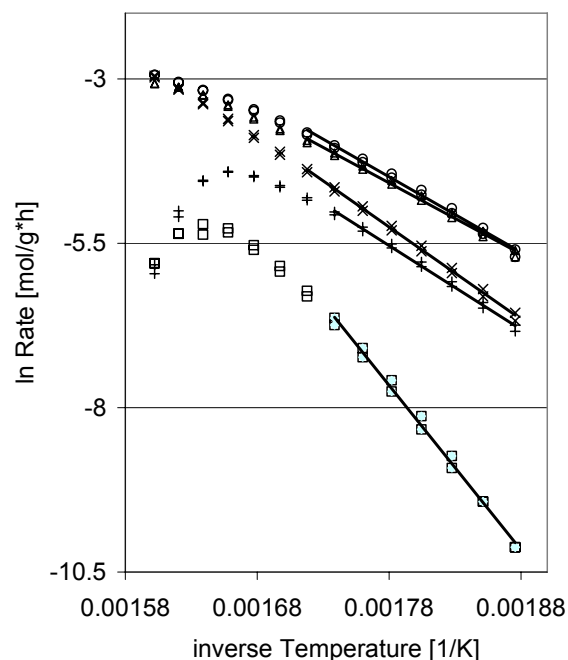


Figure 13: Arrhenius Plot for Pt/BEA: Methane ($E_A=138$ kJ/mol) (X), Ethane ($E_A=113$ kJ/mol) (O), Propane ($E_A=106$ kJ/mol) (Δ), iso-Butane ($E_A=250$ kJ/mol) (□) and n-Butane ($E_A=125$ kJ/mol) (+).

To explore the kinetics of the side reactions on a catalyst with very low concentration of acid sites n-pentane conversion was carried out on a Pt-loaded silica alumina catalyst with 0.8 wt% platinum. The low concentration of acid sites (0.065 mmol H^+ /g) induced only a low activity for acid catalyzed isomerization and cracking reactions. The product distribution (see Figure 14) showed only a low concentration of iso-pentane indicating that the acid catalyzed isomerization hardly occurred with the

space velocity used. This suggests that with this catalyst lighter alkanes are formed primarily from metal catalyzed reactions.

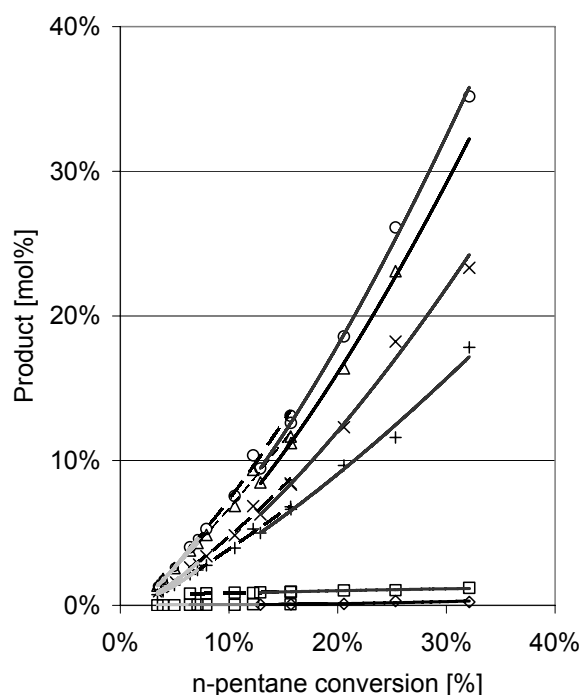


Figure 14: Product distribution for Pt-ASA: Methane (X), Ethane (O), Propane (Δ), iso-Butane (\diamond), n-Butane (+) and iso-Pentane (\square); at 280°C (—), 300°C (— —) and 320°C (— · —).

The experiment was carried out at 280°C, 300°C and 320°C in order to cover a wide conversion range with a weight hourly space velocities 5 and 15 h⁻¹. Figure 14 shows that the temperature did not severely affect the product distribution indicating that all products had approximately the same apparent energy of activation. Ethane and propane as well as methane and n-butane evolved in parallel and with identical molar concentrations. Iso-butane was observed only to a negligible extent. The product distribution for these lighter resembles that of Pt/BEA shown in Figure 12, with the exception of the same apparent energy of activation for all light alkanes. It is also noteworthy to mention that the perfect linear dependence between product yields and overall conversion suggests that the transformation of products does not play a significant role.

4.5 Discussion

4.5.1 Influence of sulfur treatment on metal properties

Hydrogen chemisorption and XAS measurements at the Pt_{LIII} edge were used to explore the effects of the sulfation on Pt. For the parent Pt/BEA hydrogen chemisorption a dispersion of approximately 50% was estimated. Assuming spherical Pt particles, this suggests an average particle size of *ca.* 25 Å. However, the first shell coordination number ($N_{\text{Pt-Pt}}=8.3$) suggests an average particle size of *ca.* 15 Å and in consequence that approximately 70% of the Pt atoms are exposed [23, 30]. Previously, a similar difference between the fraction of surface atoms measured by H₂ chemisorption and EXAFS has been assigned to a restricted access of H₂ the Pt particles within the pores of the zeolite [31].

Treatment with H₂S and subsequent oxidation results in a severe decrease of the fraction of metal surface atoms able to chemisorb H₂ at all treatment temperatures. Both the EXAFS coordination number and the intensity of the peak at 17 eV above the Pt L_{III} edge suggest that the size of the metal particles remains unaffected after sulfation at 350°C (Pt/BEA S350). However, the higher coordination numbers for Pt-Pt determined from the EXAFS analysis and the more pronounced peak at 17 eV above the Pt L_{III} edge indicate sintering of the metal particles during treatment at 450°C and 550°C. Thus, we conclude that the treatment with H₂S and the subsequent oxidation leads to blocking of a significant fraction of the surface atoms by sulfur. In addition to this, the Pt particles sinter to an increasing extent as the treatment temperature is raised to 450°C and 550 °C.

It should be noted that the increase of the peak above the absorption edge (white line) with increasing severity of the treatment could result from particle size effects or from changes in the electron density on the metal. As the highest intensity of the white line was observed for the Pt foil (largest particle size) and the whiteline intensities varied in parallel to the particle size, we tentatively attribute the intensity changes to particle size effects. Note that the similar particle size in the parent and Pt/BEA S350 allows us to conclude that a small increase in the whiteline after sulfur treatment is due to a slight degree of electron withdrawal from the Pt particles.

EXAFS of Pt/BEA S350 shows the presence of Pt-S contributions. Using a metal dispersion of 50% for the sample Pt/BEA S350 and the average number of Pt-S direct

neighbors $N_{\text{Pt-S}}=0.98$, we conclude that every Pt surface atom is in direct contact with two sulfur atoms. In combination with the low impact of this high sulfur concentration on this catalyst, we speculate that the sulfur on the surface is at least partially oxidized. This in turn suggests that the sintering observed for Pt/BEA S450 and Pt/BEA S550 is caused by the increased mobility of the sulfur (oxide) decorated Pt particles [32, 33]. The lower intensity of the Pt-S contribution in the EXAFS of Pt/BEA S550 is attributed to the generally lower concentration of sulfur retained and the reduced fraction of exposed metals.

4.5.2 Impact of the sulfur treatment on the acidic properties

The acid base properties of the parent Pt/BEA varied drastically with the H₂S and oxidation treatment applied. Using NH₃ TPD the concentration and strength of acid sites is seen to first increase compared to the parent Pt/BEA (Pt/BEA S350, Pt/BEA S450) and then to decrease (Pt/BEA S550) (see Figure 2). However, the decrease of the strongly held NH₃ (desorbing at higher temperatures) and the increase of the concentration of the more weakly held NH₃ (desorbing at lower temperature) suggests that the sulfation reduced the concentration of the strongest acid sites and increased the sites of weak and moderate acid strength.

In situ IR spectroscopy shows that a new band at 1385 cm⁻¹, which is the stronger the lower the sulfation temperature was. It is assigned to asymmetric stretching frequency of S=O in surface sulfate species [25, 24]. The downward shift of the bands of the S=O stretching vibration of these sulfate groups after adsorption of pyridine suggests that the sulfates interact directly or indirectly with pyridine and all accessible to this base (see Figure 4 and 5).

The ring vibration of adsorbed pyridine indicate the presence of strong Brønsted acid sites as well as Lewis acids associated with accessible Al³⁺ cations in all materials studied. The higher concentration of Brønsted acid sites in Pt/BEA S350, Pt/BEA S450 compared to the parent sample detected in this way suggests a direct and marked impact of the sulfation treatment, while the concentration of Lewis acid bound pyridine hardly varied.

In principal, the increase in the concentration of Brønsted acid sites could be caused by two effects. (i) The formation of new Brønsted acidic OH groups affiliated with sulfate groups or (ii) the removal of cationic alumina species from ion exchange sites (forming sulfates), making zeolite SiOHAl groups accessible. As the zeolite OH groups of BEA are

well defined, the comparison between the intensity of the OH groups and the concentration measured according to the intensity of the pyridinium ion vibration can help to differentiate between these two options. In Figure 15 the intensity of the band at 3608 cm^{-1} is compared to the intensity of the band of the pyridine ring vibrations at 1545 cm^{-1} using a relative extinction coefficient (for $\nu=3608\text{ cm}^{-1}$) and the method described in [21] (for $\nu=1545\text{ cm}^{-1}$). One notes a clear correlation for all three sulfate treated samples between the intensity of the band for the OH groups and the band of the pyridinium ions. The parent sample has the same intensity of the bridging OH band than that of Pt/BEA S450, but the concentration of pyridinium ions is higher with the latter. This suggests that at least for this sample sulfation Brønsted acid sites must exist that are not part of the zeolite OH groups. On the other hand, the concentration of zeolite OH groups increases (as judged by the OH band at 3608 cm^{-1}) compared to the parent sample for Pt/BEA S350 indicating that the treatment has removed some of the anionic aluminum oxide clusters that compensate for the charge of Al-O tetrahedra in the parent material. Thus, we conclude that the sulfate treatment has two effects under optimal preparation conditions, i.e., it creates new acidic OH groups in the zeolite by removing oxide clusters blocking acid sites and it creates new OH groups affiliated with sulfate that are not readily directly detected, because of hydrogen bonding [34]. Extrapolating the trend line observed with the sulfur treated samples it appears to be parallel to the trend line known for the correlation of bridging hydroxy groups in zeolites and the concentration of adsorbed base molecules. This suggests that a constant concentration of Brønsted acidic SO_4 groups are formed in this material which generates approximately 0.5 mmol/g Brønsted acid sites independent of the treatment.

At higher sulfation temperatures (Pt/BEA S550) additional silanol groups at 3733 cm^{-1} , assigned to SiOH groups at defects, and the severe reduction of the band at 3608 cm^{-1} indicate the partial destruction of the zeolite framework. At this point it is interesting to note that sulfuric acid is thermodynamically only stable up to a temperature of 350°C . Thus, the enhancement of bridging hydroxyl groups by leaching of extra-framework alumina species from the ion exchanged sites with *in situ* formed (mobile) surface sulfates is more likely at a sulfation temperature of 350°C .

The fact that sulfate species possess strong Brønsted acidity and thus enhance the concentration of acid sites can be explained by the conversion of $(\text{AlO})_3\text{S}=\text{O}$ groups to Brønsted acidic $(\text{AlO})_2\text{SOO}^-\text{H}^+$ groups in the presence of water or OH groups [24]. The S-OH groups are usually strongly hydrogen-bonded to the surface lead generating very broad

OH bands [34]. The disappearance of the S=O vibration during the hydroisomerization reaction and the fact that it can be regained by heating the sample in He, confirms that the sulfate species were converted to ionic species rather than reduced to sulfides. In addition the formation of water was observed while the S=O band at 1390 cm^{-1} disappeared.

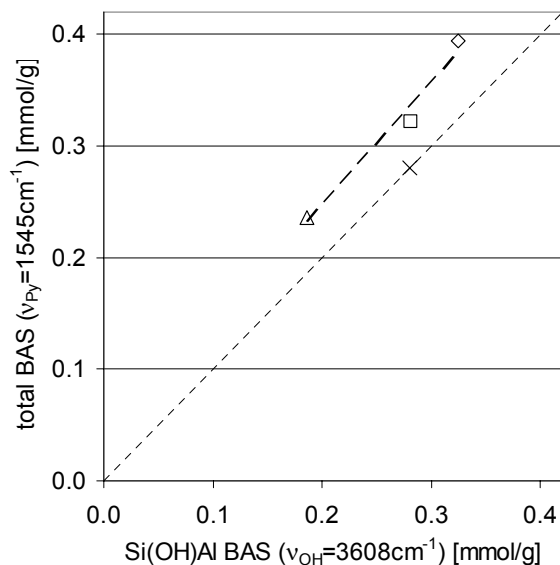


Figure 15: Comparison of Brønsted acidity with the Brønsted acidity of Si(OH)Al groups and Pt/BEA (—×—), Pt/BEA S350 (—◇—), Pt/BEA S450 (—□—) and Pt/BEA S550 (—△—).

4.5.3 Catalytic properties

Pentane hydroisomerization mechanism proceeds on bifunctional Pt loaded zeolites via a mechanism consisting of a dehydrogenation step on the metal sites, followed by an isomerization step *via* carbenium-ions on the acid sites and a final hydrogenation step on the metallic sites [35, 36]. The activity and selectivity of bifunctional catalyst, therefore, depends on the ratio between metal sites and acidic sites, which determines the concentration of olefins and carbenium-ions on the catalyst surface.

The linear region in the Arrhenius plots at temperatures below 300°C (shown in Figure 9) reveal the absence of pore diffusion limitations in the three dimensional pores of the BEA zeolite under the reaction conditions studied. For the catalysts Pt/BEA S350 and Pt/BEA S450 an enhanced hydroisomerization activity was observed, while for Pt/BEA S550 the activity decreased. The linear correlation of the Brønsted acid site concentration and the activity for the parent and catalysts treated at 350°C and 450°C (Pt/BEA S350 and

Pt/BEA S450) suggests that the rate determining step of the reaction over these materials is the rearrangement of the carbenium ion on the acid site (Figure 10). The deviation observed for the catalyst Pt/BEA S550 indicates a shift in the rate determining step towards the dehydrogenation step on the metal sites resulting from the excessive reduction of metal surface due to the sintering at the elevated temperatures. Therefore, the activity of this catalyst was only about half of that one would expect for a catalyst with a corresponding acidity. The small changes in the apparent activation energies for the catalyst before and after sulfur treatment are in agreement with the similar strength of the acid sites observed during ammonia TPD.

Besides the enhanced activity of the catalysts after sulfur treatment, a significant improvement of the selectivity to iso-pentane, i.e., a reduction of the formation of light alkanes, was observed. The reaction to these latter products can be caused by metal catalyzed hydrogenolysis or hydrocracking involving also acid catalysis. The product distribution as function of the conversion of Pt/BEA was symmetric with respect to the concentrations of C₂ and C₃ as well as for C₁ and C₄ fragments. The products were similar to those observed with Pt/ASA. This support is only weakly acidic (0.065mmol H⁺/g) and did not show significant activity for the pentane isomerization reaction (Figure 12).

Two possible reaction routes can lead to light alkanes, bifunctional hydrocracking and metal catalyzed hydrogenolysis. (i) In the first case, the side reaction occurs on the acid sites and the function of the metal compound is to dehydrogenate pentane and to hydrogenate the olefins formed from the acid catalyzed cracking of the olefins. The selectivity enhancement after sulfation could be explained with a reduction of the strength of the Brønsted acid sites as evidenced by TPD of ammonia. The weaker Brønsted acid sites retain the alkenes less and lead so to a lower fraction of cracked molecules. While a shift from cracking to isomerization is well established, the changes in the distribution of acid sites are rather subtle and it is difficult to accept, but not ruled out, that such a subtle change (only a fraction of the sites are changed in strength) can lead to a so pronounced modification of the catalytic properties (ii) Hydrogenolysis, the second possible pathway to light alkanes, takes place only on the metal. The reduction of the available metal surface atoms would lead to the severe reduction of the rate of this structure sensitive reaction. In Chapter 3 it was argued that the side reaction originates from a metal catalyzed hydrogenolysis reaction since Pt possessed a direct influence on isomerization selectivity at which high metal loadings led to a reduced isomerization selectivity. The activity of the

side reaction furthermore showed a dependency on particle size which is characteristic for the structure sensitive hydrogenolysis reaction in the given particle size range. In addition the product distribution and catalytic behavior of the zeolite Beta based catalysts resembles that of the Pt loaded amorphous silica alumina, which was not able to perform acid catalyzed cracking reaction. It is argued that hydrogenolysis requires larger ensembles of metal atoms or the presence of highly uncoordinated metal atoms, as the reaction involves dehydrogenated intermediates with multiple bonds to the metal particle [37]. Both, larger free ensembles of Pt atoms and highly reactive and exposed metal atoms, would be reduced dramatically by the presence of sulfur on the metal.

In contrast de/hydrogenation is less demanding with respect to the number, arrangement and reactivity of metal surface atoms and, so, it is conceivable that the sulfur treatment blocks the sites required for hydrogenolysis while leaving a sufficiently high concentration of Pt sites to maintain the hydrogenation/dehydrogenation equilibrium on the bifunctional catalysts. Note that in the case of Pt/BEA S550 this concentration is so low that hydrogenation/dehydrogenation is concluded to be not in equilibrium.

4.6 Conclusions

The sequential treatment with H₂S and air severely modifies the acidic and metallic properties of the bifunctional catalyst based on Pt containing zeolite BEA. It was shown that it is possible to enhance the Brønsted acidity of the sample at low sulfation temperatures. The enhancement of Brønsted acid sites is attributed to the removal of cationic alumina species blocking ion exchange sites and to the formation of additional Brønsted acidic sulfate species. If the procedure is carried out at 550 °C the concentration of Brønsted acid sites is reduced by dealumination.

The presence of sulfur species reduces the available metal surface atoms compared with the parent material. While for all samples sulfur is seen to exist on the surface, its oxidation state seems to depend strongly on the atmosphere, i.e., in reducing atmosphere most likely sulfide species are formed. For Pt/BEA S350 and Pt/BEA S450 the reduction of available Pt surface atoms by decoration of the Pt particles with sulfur atoms is concluded to be the dominating effect. In contrast, for Pt/BEA S550, sulfation causes a lower available metal surface area primarily due to sintering of the Pt particles.

The isomerization activity is significantly enhanced for materials treated with H₂S/air up to 450 °C. For the parent material and these new catalysts the isomerization activity is directly correlated with the concentration of Brønsted acid sites indicating that the carbenium ion chemistry is rate determining. With Pt/BEA S550 the concentration of metal sites remaining was insufficient to equilibrate the hydrogenation/dehydrogenation step causing the overall rate decreased. The selectivity of the sulfur treated catalyst is dramatically increased to values of near 100 % isomerization. While we cannot completely exclude the modification of the Brønsted acid sites to be responsible, we currently think that the modification of the metal particles by sulfur species eliminates the hydrogenolysis of alkanes observed with the parent sample.

Thus, the described approach offers a promising new route to tailor zeolite based bifunctional catalysts and to rejuvenate deactivated catalyst. The experimental conditions should be as mild as possible in order to maintain the structural integrity of both catalyst components.

Acknowledgements

The financial support by Bundesministerium für Bildung und Forschung Project (BMBF:03C0307D) is gratefully acknowledged. The XAFS experiments were carried out at HASYLAB, DESY, Hamburg, Germany and supported by the TMR-Contract ERBFMGECT950059 of the European Community. The authors would like to thank Xaver Hecht for H₂-chemisorption measurements and technical support on the 20-fold parallel reactor system and Hendrik Dathe for stimulating discussion on XAS and the nature of sulfate species.

REFERENCES

- [1] M. Guisnet, N.S. Gnep, *Appl. Catal A: Gen.* 146, 33 (1996).
- [2] A. Corma, J. Planelles, J. Sanchez-Marin, F. Thomas, *J. Catal.* 93, 30 (1985).
- [3] H.-C. Wu, L.-J. Leu, C. Naccage, K.-J. Chao, *J. Mol. Catal A: Chem.* 127, 1143 (1997).

-
- [4] S. Kuba, P. Lukinskas, R.K. Grasselli, B.C. Gates, H. Mnötzinger, *J. Catal.* 216, 353 (2003)
- [5] N. Essayem, Y.B. Taârit, C. Feche, P.Y. Gayraud, G. Sapaly, C. Naccache, *J. Catal.* 219, 97 (2003).
- [6] S. Kuba, P. Lukinskas, R.K. Grasselli, B.C. Gates, H. Knözinger, *J. Catal.* 216, 353 (2002).
- [7] Y. Ono, *Catal. Today* 81, 3 (2003).
- [8] US Patent: 5,157,199 (1992).
- [9] US Patent: 6,107,235 (2000).
- [10] K.-J. Chao H.-C. Wu, L.-J. Leu, *Appl. Catal. A: Gen.* 143, 223 (1996).
- [11] M.A. Saberi, R. Le Van Mao, M. Martin, A.W.H. Mak, *Appl. Catal. A Gen.* 214, 229 (2001).
- [12] M.A. Saberi, R. Le Van Mao, *Appl. Catal. A: Gen.* 242, 139 (2003).
- [13] T. Lei, J.S. Xu, Z. Gao, *Mater. Chem. Phys.* 60, 177 (1999).
- [14] C.P. Hubbard, K. Otto, H.S. Gandhi, K.Y.S. Ng, *J. Catal.* 144, 484 (1993).
- [15] A.F. Lee, K. Wilson, R.M. Lambert, C.P. Hubbard, R.G. Hurley, R.W. McCabe, H.S. Gandhi, *J. Catal.* 184, 491 (1999).
- [16] R. Burch, E. Haplin, M. Hayes, K. Ruth, J.A. Sullivan, *Appl. Catal. B: Enviro.* 19, 199 (1998).
- [17] J.M. Jones, V.A. Dupont, R. Brydson, D.J. Fullerton, N.S. Nasri, A.B. Ross, A.V.K. Westwood, *Catal. Today* 81, 589 (2003).
- [18] A.L. Ankudinov, J.J. Rehr, *Phys. Rev. B* 62, 2437 (2000).
- [19] K.V. Klementiev, VIPER for Windows, freeware: <http://www.desy.de/~klmn/viper.html>.
K.V. Klementiev, *J. Phys. D: Appl. Phys.* 34, 209 (2001).
- [20] J.A. Lercher, Ch. Gründling, G. Eder-Mirth, *Catal. Today* 27, 353(1996).
- [21] C.A. Emeis, *J. Catal.* 141, 347 (1993).
- [22] C.L. Garcia, J.A. Lercher, *J. Phys. Chem.* 96, 2230 (1992).
- [23] A. Jentys, *Phys. Chem. Chem. Phys.* 1, 4059 (1999).
- [24] O. Saur, M. Bensitel, A.B. Mohammed Saad, J.C. Lavalley, C.P. Tripp, B.A. Morrow, *J. Catal.* 99, 104 (1986).
- [25] T. Yamaguchi, T. Jin, K. Tanabe, *J. Phys. Chem.* 90, 3148 (1986).
- [26] X. Li, K. Nagaoka, J.A. Lercher, *J. Catal.* 227, 130 (2004).
- [27] M.A. Babaeva, A.A. Tsyganenko, *Kinet. Catal. Vol* 25, 787 (1985).
- [28] M.B. Mitchell, V. N. Sheinker, *J. Phys. Chem.* 100, 7550(1996).
- [29] J.A. Wang, L.F. Chen, R. Limas-Ballesteros, A. Montoya, J.M. Dominguez, *J. Mol. Catal. A: Chem.* 194, 181 (2003).
- [30] J. de Graaf, A.J. van Dillen, K.P. de Jong, D.C. Koningsberger, *J. Catal.* 203, 307 (2001).

- [31] S. Feast, M. Englisch, A. Jentys, J.A. Lercher, *Appl. Catal. A Gen.* 174, 155 (1998).
- [32] J.-R. Chang, S.-L.- Chang, T.-B. Lin, *J. Catal.* 169, 338 (1997).
- [33] J.-R.Chang, S.-L.- Chang, *J. Catal.* 176, 42 (1998).
- [34] X. Li, K. Nagaoka, J.A. Lercher, *J. Catal.* 227, 130 (2004).
- [35] P.B. Weisz, *Adv. Catal.* 13, 137 (1962).
- [36] F.J.M.M de Gauw, J. Grondelle, R.A. van Santen, *J. Catal.* 206, 295 (2002).
- [37] E. H. van Broekhoven, V. Ponec, *J. Mol. Catal.* 25, 109 (1984).

Chapter 5

5 PREPARING IMPROVED BIFUNCTIONAL ZEOLITE BASED CATALYSTS BY SULFATE MODIFICATION: THE ROLE OF Pt CONTENT AND THE PREPARATION CONDITIONS

5.1 Abstract

The surface chemistry and the physicochemical properties of Pt-HBEA modified by sulfation *via* H₂S sorption and calcination in air is described. The treatment with H₂S causes partial dealumination of the zeolite framework and the formation of anionic alumina species resulting in the partial exchange of the bridging hydroxyl groups of the zeolite. Subsequent calcination leads to formation of aluminum sulfate clusters and the formation of Brønsted acidic sulfate species. The nature of the sulfur species during H₂S treatment and oxidation characterized by *in situ* sulfur K-edge XAS, ion chromatography and temperature programmed oxidation. Pt catalyzes the formation of SO₃ acting as the sulfation agent. The high concentration of Brønsted acid sites in the modified materials leads to high rates of pentane isomerization. In parallel, partial poisoning of Pt particles by sulfur increases the selectivity for isomerization by suppressing alkane hydrogenolysis.

5.2 Introduction

Bifunctional catalysts containing acid-base and metal sites show high reactivity, selectivity, and stability for alkane conversion reactions [1]. One of the most prominent applications for such bifunctional catalysts is the hydroisomerization of n-paraffins. It is widely accepted that it consists of three major individual reaction steps. In the first, the alkane is dehydrogenated to the alkene on the metal [2]. The alkene adsorbs on Brønsted acid sites forming an alkoxy group (i.e., a carbenium ion in the transition state), which isomerizes and eventually desorbs. In the third step, the isoolefin is hydrogenated to the isoalkane on the metal. The balance between the metallic and the acidic function determines which of the reactions, hydrogenation/dehydrogenation or C-C rearrangement, is rate determining and controls activity, stability, and selectivity [1, 3, 4, 5, 6].

Contacting such bifunctional catalysts with H₂S or sulfur oxides can severely change the catalytic behavior [7]. Depending on the oxidation state of sulfur, the interaction of the sulfur containing molecules occurs with acid-base or with metallic sites. In general,

molecules with nucleophilic sulfur tend to influence the metallic sites [8] and affect the hydroisomerization activity and selectivity negatively [9]. However, it has also been observed that H₂S interacts with Brønsted and Lewis acidic sites in zeolites such as HZSM-5 or HY [10, 11]. Molecules containing electrophilic sulfur and the sulfate groups formed from them enhance the catalytic acid base related catalytic activity of many oxides. Examples include sulfate promoted oxides such as sulfated zirconia, Fe₂O₃, Al₂O₃ or TiO₂ [12, 13, 14]. Also for zeolites, the introduction of sulfate groups by deposition of (NH₄)₂SO₄ on H-MOR [15] or the *in situ* generation of sulfate groups from electrophilic sulfur species deposited [16] increases the concentration of acid sites. This increase in activity was ascribed to nanoclusters involving SO₄²⁻ and extra-framework alumina. It is interesting to note that small amounts of SO₂ also promote metal catalyzed reactions [17, 18, 19, 20].

In this chapter, we wish to report on a systematic study for a modification strategy based on H₂S deposition and subsequent oxidation [17] shown previously to be highly promising. Specifically, we explore the role of the metal to acid site ratio and the role of Pt during the sulfation process.

5.3 Experimental

5.3.1 Catalyst preparation

Zeolite Beta with a Si/Al ratio of 12.5 was obtained from Süd-Chemie AG and loaded with Pt by ion-exchange in aqueous Pt(NH₃)₄(OH)₂. A solution containing Pt(NH₃)₄(OH)₂ and NH₄OH corresponding to the theoretical amount of protons was added dropwise to a slurry of the zeolite in water at 40°C. After the ion exchange, the solid was separated from the liquid by centrifugation, washed, and freeze-dried. The samples were calcined in air at 350°C for 16 h (increasing to that temperature with a rate of 0.5°C/min) and finally reduced at 300°C in flowing H₂ for 4 h. The metal loading after the preparation was determined by atomic absorption spectroscopy (AAS). Samples with a metal loading between 0.2 and 2.3 wt. % were prepared in that way and the samples are named Pt-BEA(x), with x indicating the metal loading.

For sulfation, the samples were heated in flowing He from ambient to the desired sulfation temperature with a rate of 7.5°C·min⁻¹. After reaching it a mixture containing 1.8 vol.% H₂S in H₂ was passed over the Pt containing zeolite. Subsequently, the material was

oxidized in air at a WHSV of 2 [g(O₂)/(g_{cat}·h)] and finally reduced in H₂ for 90 min by increasing the temperature from ambient to 350°C with a heating rate 5°C/min. The samples are referred to as Pt-BEA-S for the sample treated with H₂S and Pt-BEA-SA for the subsequent oxidized ones.

Two different series of sulfated samples were prepared. In the first series a catalyst containing 0.2 wt. % Pt was treated with H₂S at 300°C for 3h and was subsequently oxidized between 0 and 5 h. The samples are referred to as Pt-BEA(0.2)S for the H₂S treated sample and Pt-BEA(0.2)SA(y) for the subsequently oxidized samples (y indicating the oxidation time in hours). For the second series of catalysts, the metal content was varied between 0.2 and 2.2 wt. % while the sulfation procedure was the same for all catalysts, i.e., 3h in H₂S and subsequently 3h in air both at 350°C. These samples are referred to as Pt- (x) SA. Two different series of sulfated samples were prepared. In the first series a catalyst containing 0.2 wt. % Pt was treated with H₂S at 300°C for 3h and was subsequently oxidized between 0 and 5 h. The samples are referred to as Pt-BEA(0.2)S for the H₂S treated sample and Pt-BEA(0.2)SA(y) for the subsequently oxidized samples (y indicating the oxidation time in hours). For the second series of catalysts, the metal content was varied between 0.2 and 2.2 wt. % while the sulfation procedure was the same for all catalysts, i.e., 3h in H₂S and subsequently 3h in air both at 350°C. These samples are referred to as Pt-BEA(x)SA.

Table 1: Catalyst preparation.

Sample name	Pt loading (x) [wt.%]	S treatment	Oxidation (y)
Pt-BEA(x)	0.2, 0.4, 0.6, 1.0, 2.2	-	-
Pt-BEA(0.2)S	0.2	3h (H ₂ S)	-
Pt-BEA(0.2)SA(y)	0.2	3h (H ₂ S)	0.5h, 1h, 2h, 3h, 5h
Pt-BEA(x)SA	0.2, 0.4, 0.6, 1.0, 2.2	3h (H ₂ S)	3h

5.3.2 ²⁷Al magic angle spinning nuclear magnetic resonance spectroscopy (MAS-NMR)

²⁷Al MAS NMR spectra were measured on a *Bruker MSL 300* NMR spectrometer at a field strength of 7.5 T and a spinning frequency of 15 kHz at a frequency of 78.202 MHz with 1.0 μs excitation pulses and recycle times of 0.1 s. 1 M aqueous solution of Al(NO₃)₃

was ($\delta = 0$ ppm) used for calibration of the chemical shifts. The samples were pressed into 4 mm ZrO_2 rotors without activation.

5.3.3 Ion-Chromatography

The total amount of sulfur and the amount of sulfate species on the samples were determined by liquid ion-chromatography (Metrohm 690) using an anion column IC SUPER-SEP with phthalic acid (2.5 mmol/l) and 5% acetonitrile as eluant. For the determination of the sulfate content, 20 mg of powdered catalysts are suspended in 100 ml NaOH (0.01 mol/l). The samples were stirred at 50°C for about 12h. Subsequently the liquid and the solid were separated by filtration. For determining the total amount of sulfur the liquid was oxidized with hydrogen peroxide before the analysis.

5.3.4 Hydrogen chemisorption

Hydrogen chemisorption was performed using a Sorptomatic 1990 Series instrument. About 1g of catalyst was reduced in hydrogen at 350°C for 2h and subsequently evacuated. All adsorption isotherms were measured at 35°C. The amount of chemisorbed hydrogen was determined after removing physisorbed hydrogen by evacuation at 35°C from the sample and determining that fraction quantitatively by repeating the exposure and measuring the uptake. The isotherm of chemisorbed hydrogen has been determined by subtracting the second isotherm (attributed physisorbing H_2) from that measured in the first experiment (chemisorbed and physisorbed H_2). The monolayer coverage of hydrogen adsorbed has been determined by extrapolating the linear part of the isotherm of chemisorbed hydrogen to zero pressure. The fraction of metal surface atoms has been calculated by assuming one hydrogen atom adsorbed per Pt surface atom.

5.3.5 Temperature programmed oxidation studies

Temperature programmed reduction (TPR) studies were performed in a flow reactor system heated with a cylindrical, ceramic oven equipped with 3x 1000W of thermal output from Horst GmbH. The gases evolved during TPR were monitored by a mass spectrometer (*Balzers QME 200*). Approximately 50mg of the samples were heated with a rate of 10 K/min in a mixture of 10 % oxygen in helium with a total flow rate of 30 ml/min.

5.3.6 X-ray absorption spectroscopy (XAS)

X-ray absorption spectroscopy (XAS) was measured at the Angstroemquelle Karlsruhe (ANKA). Spectra were recorded at the S K-edge (2.5 GeV) with an electron current between 100 and 200mA in fluorescence mode, using a stepwise moving Si (111) monochromator. The (monochromatic) flux rate on the sample was about $2 \cdot 10^{11}$ photons/s. Contributions of higher order reflections were minimized by detuning the second crystal of the monochromator to 60% of the maximum intensity. Harmonic rejection was provided by a grazing incidence pre-mirror, which acted as a high-energy filter. For the *in situ* measurements the sample were placed inside a reaction chamber sealed against vacuum with a 7.5 μm Kapton window to measure the fluorescence of the sample exposed to the X-ray beam. The outside of the cell was evacuated to minimize the scattering of the gas phase. The measurements in fluorescence mode at the S $K_{\alpha 1}$ and $K_{\alpha 2}$ emission lines were performed using a Keitek Si-drift Detector with an area of 10 mm^2 . The reference samples were measured in transmission mode using ionization chambers (filled with 60 mbar air) in front of and behind the sample. For energy calibration, the maximum of the first resonance (“white line”) in the spectrum of ZnSO_4 was set to 2481.4 eV.

The samples were prepared as self-supporting wafers (about 1 mg/cm^2) and reduced in hydrogen for 2h at a temperature of 350°C. Subsequently, the sample was treated with 1.8 vol% H_2S in hydrogen for 1h inside the XAS cell. Details of the experimental setup are described in ref. [21]. The first spectrum was recorded after flushing the sample in He. The H_2S treated catalyst was oxidized with air for 1h before the second spectrum was recorded. To remove scattering contributions and normalize the spectra to the amount of material exposed to the X-ray beam a linear background was fitted to the pre-edge region (2460 – 2473 eV) and the post-edge region (2506 – 2535 eV). $\text{Al}_2(\text{SO}_4)_3 \cdot 18\text{H}_2\text{O}$ pressed onto Kapton tape was used as a reference (measured in transmission) mode at room temperature at 80 mbar total pressure.

5.3.7 IR spectroscopy

I R spectra of the adsorption of pyridine were measured with a Perkin Elmer 2000 spectrometer in a vacuum cell described previously [22]. All spectra were recorded in the range between 4000 and 1100 cm^{-1} at a resolution of 4 cm^{-1} . Self-supporting wafers (1.5 mg/cm^2) were pressed and activated at 350°C (increment 10 K/min) for 90 min. After

cooling the cell to 150°C the spectrum (60 scans) of the activated sample was recorded. Pyridine was adsorbed at 150°C with a partial pressure of 0.05 mbar for 30 min and subsequently evacuated until the spectra remained constant. In order to compare the spectra of the different samples all spectra were normalized by the intensity of the overtones of the structural vibrations of the zeolite between 1750 and 2100 cm^{-1} . Additionally, the weight of the wafers was measured in order to determine the wafer mass per surface area necessary for calculating the amount of Brønsted and Lewis acid sites according to the method published by Emeis [23].

CO adsorption was carried out in a cell identical to that described above using a Bruker ISF88 spectrometer. Self-supporting wafers of 2 mg/cm^2 were pressed from the samples and reduced in 0.1 mbar of hydrogen at a temperature of 350°C for 2 h. Subsequently, the sample was outgassed for 1 h at 350 °C in vacuum. CO adsorption was carried out at a temperature of 40 °C and pressures of 0.05, 0.5, and 1 mbar.

In situ IR measurements during sulfur treatment were carried out using a flow cell equipped with ZnS windows and a resistance heated furnace for the sample holder. For *in situ* IR experiments the samples were pressed into self-supported wafers (1.5 mg/cm^2) and activated for 90 min at 350°C in hydrogen. For H₂S and oxidation treatment a flow of 30 ml/min was used. SO₃ treatment was performed by bypassing He with a flow of 30 ml/min over a SO₃ cylinder.

5.3.8 Catalytic test reactions

The catalytic activity was studied with a 20-fold parallel reactor system. Each plug flow reactor was controlled by an individual digital mass flow and pressure controller. The flow and composition of the reactant (pentane in H₂) was adjusted with a digital controlled evaporator mixer. The products were analyzed with a HP-MicroGC (GC M200), capable of separating the C₁ to C₆ components (including their isomers) in less than 2 min. With the complete computer control of the reaction system it was possible to vary the total pressure, flow rate, temperature and alkane concentration automatically. All data recorded was stored in an MS Access database.

5.4 Results

5.4.1 Physiochemical characterization

The effect of the sulfation process on the concentration of extra framework alumina of 0.2 wt.% Pt BEA was studied using ^{27}Al MAS NMR. The spectra of the parent Pt-BEA(0.2), of the sample treated with H_2S and of two samples with different oxidation times are compared in Figure 1. All spectra show a resonance at 54 ppm, which is assigned to Al at tetrahedral sites in the framework. The broad resonance at approximately 0 ppm is attributed to Al in octahedral coordination generated by dealumination of the zeolite framework. The observation of two peaks at 0 ppm and -8 ppm indicates that octahedral aluminum is present in two different environments. The sharp peak at *ca.* 0 ppm is affiliated with octahedral aluminum species connected to the framework [24], while the second peak having a significantly higher line width indicates a distortion of the surrounding area. Penta-coordinated Al between 30 and 50 ppm was not detected.

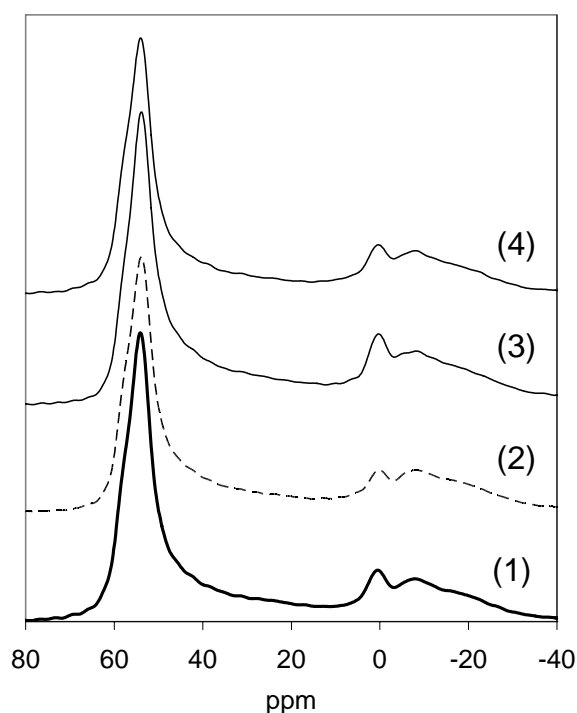


Figure 1: MAS ^{27}Al NMR for parent Pt-BEA(0.2) (—) (1), Pt-BEA(0.2)S (---) (2), Pt-BEA(0.2)SA(0.5) (— —) (3) and Pt-BEA(0.2)SA(5) (— · —) (4).

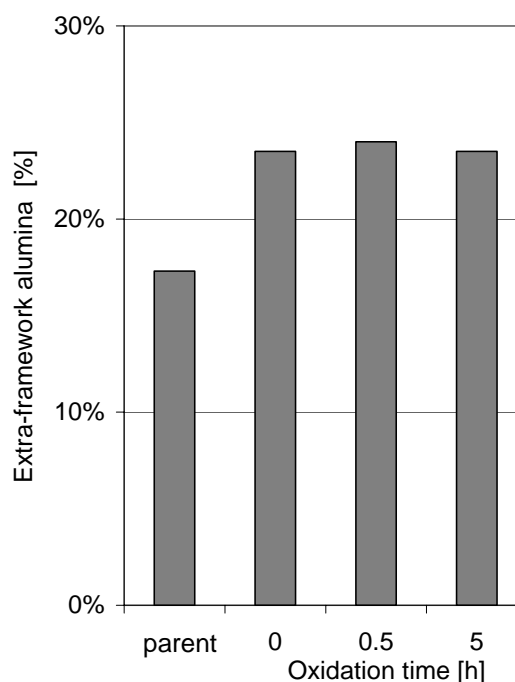


Figure 2: Content of extra-framework alumina for parent Pt-BEA(0.2), Pt-BEA(0.2)S and Pt-BEA(0.2)SA(0.5) and Pt-BEA(0.2)SA(5).

The percentage of octahedral sites determined from the integral intensity of the low field resonance and the sum of the two high field resonances is shown in Figure 2. H₂S treatment (without oxidation) led to a partial dealumination of the zeolite framework, while the subsequent oxidation of the samples with air did further increase the concentration of extra-framework Al species.

The nature of the sulfur species was studied by XANES at the S K-edge using the edge position to identify the oxidation state of the sulfur species present. The XANES region of the Pt-BEA catalysts treated with H₂S followed by oxidation and that of Al₂(SO₄)₃ as a reference are compared in Figure 3. The graph shows the presence of two types of sulfur species. For Pt-BEA(0.2)S two small peaks at 2471.5 keV and 2481.5 keV were observed, attributed to sulfur in the -2 and +6 oxidation state, respectively [25], [26]. After oxidation the peak at 2471.5 keV disappeared, while the intensity of the peak at 2481.5 keV increased significantly. Note that the intensity of the transition at the sulfur K-edge strongly increased with the oxidation state of S, therefore the intensities of the peaks above the edge cannot be directly related to the concentrations of the S²⁻ and the S⁶⁺ species [26].

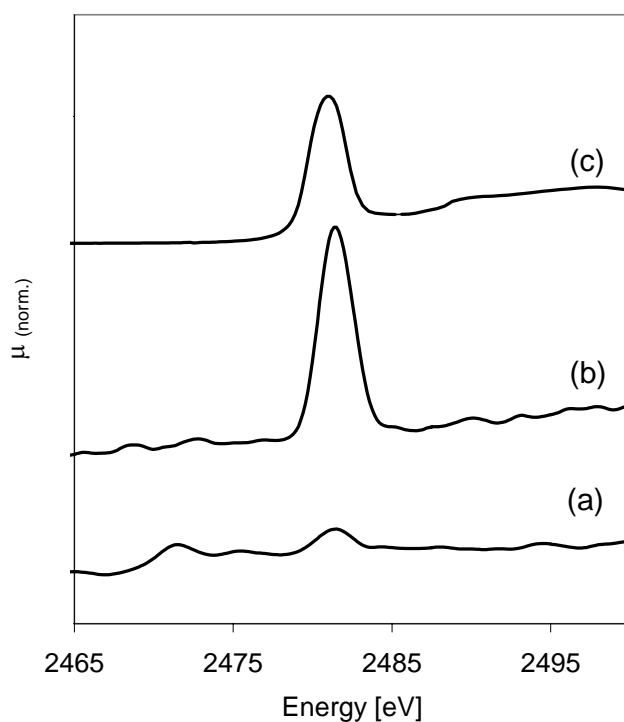


Figure 3: XANES of Pt-BEA treated with H₂S (a) followed by subsequent oxidation (b) and Al₂(SO₄)₃ (c).

The impact of oxidation on the nature of sulfur species was investigated for Pt-BEA(0.2)S and Pt-BEA(0.2)SA samples using liquid ion-chromatography to analyze the concentration of sulfur species after leaching from the catalysts. Figure 4 shows the total concentration of sulfur present and the concentration of sulfates present. The total amount of sulfur on the sample is decreased with increasing oxidation time, while the sulfate concentration increased. The XAS measurements suggest that the difference between the concentrations of all sulfur present and that of sulfate is due to sulfide species. Thus, sulfide formed during the H₂S exposure is converted to sulfates in the presence of oxygen. For a long oxidation time the total concentration of sulfur on the catalysts approaches the concentration of sulfate species indicating that a minor concentration of sulfide species remains even after calcination.

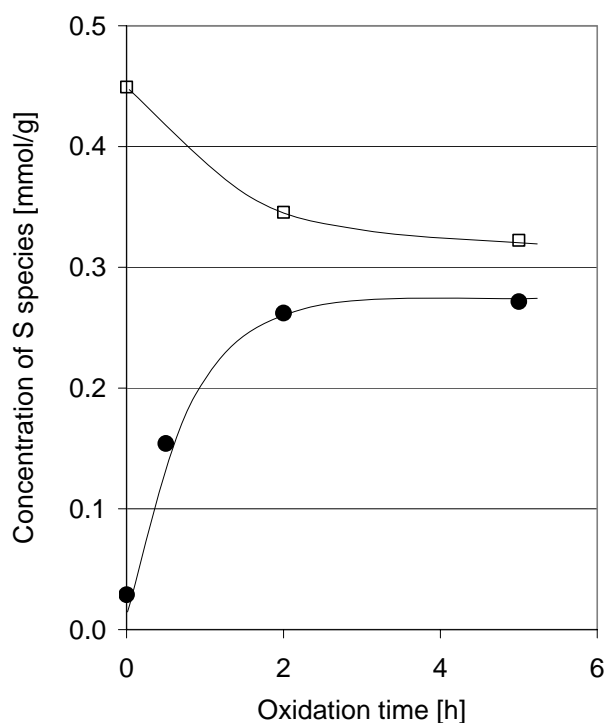


Figure 4: Concentration of sulfate species before (●) and after treatment with H₂O₂ (◻).

Figure 5 shows the TPO of Pt-BEA(0.2)S, Pt-BEA(0.2)SA(1) and Pt-BEA(0.2)SA(5). For the H₂S treated sample the formation of SO₂ was detected at approximately 250°C indicating the oxidation of adsorbed H₂S on the sample. The evolution of a second, smaller peak was observed at *ca.* 850°C, which is assigned to decomposing sulfate species. For Pt-BEA(0.2)SA(1) only a small peak was observed at 250 °C, while Pt-

BEA(0.2)SA(5) showed a broad maximum between 750 °C and 1000 °C. Note that in general SO_x evolved with the studied samples in two overlapping peaks with the high temperature peak being the more pronounced the longer the oxidation time is. The decomposition of $\text{Al}_2(\text{SO}_4)_3$ (added in Figure 5) shows a maximum at ca. 850°C, i.e., at the same temperature as the low temperature maxima for the Pt-BEA(0.2)S and Pt-BEA(0.2)SA samples.

It should be mentioned that ref. [27] reports two types of surface sulfate species on pure alumina. The one more stable at low surface coverages is attributed to a type with only one free S = O group. The second group was less stable and was attributed to a SO_3 group linked to an Al-O pair site or to an oligomer species such as S_2O_7 (see **Error! Reference source not found.**). These results agree qualitatively with the results of ref. [28] that alumina sulfate decomposed from 360 °C to 950°C, with a maximum between 880 °C and 950 °C to SO_x and Al_2O_3 .

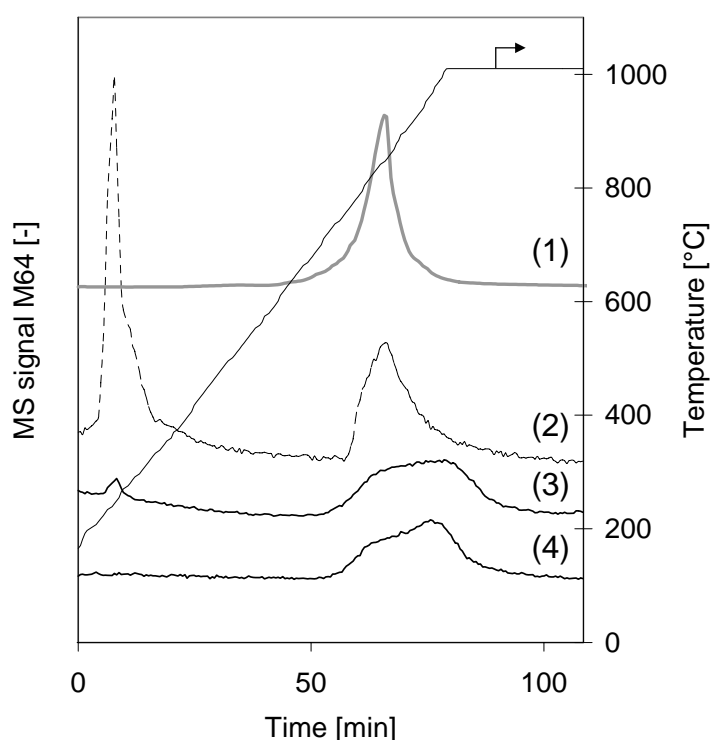


Figure 5: Temperature Programmed Oxidation for $\text{Al}_2(\text{SO}_4)_3$ (—) (1), Pt-BEA(0.2)S (---) (2) and Pt-BEA(0.2)SA(1) (—) (3) and Pt-BEA(0.2)SA(5) (—) (4).

5.4.2 Characterization of metallic properties

The Pt particles were studied by CO adsorption on Pt-BEA(0.2), Pt-BEA(0.2)S and BEA(0.2)SA(0.5), Pt-BEA(0.2)SA(2) and Pt-BEA(0.2)SA(5), respectively. The parent material showed an intense band at 2085 cm^{-1} , which is assigned to CO linearly adsorbed on Pt. H_2S treatment of the catalyst (Pt-BEA(0.2)S) led to the disappearance of that band. After oxidizing the H_2S treated samples (Pt-BEA(0.2)SA), linearly adsorbed CO was observed again (Figure 6), but the intensity of the band was only 50 % compared that observed with the untreated catalyst. With these samples a new band was observed at 2230 cm^{-1} , which is assigned to CO molecules adsorbed at coordinatively unsaturated Al^{3+} cations [22]. Bands at 2230 and 2186 cm^{-1} were also observed on MOR [29] and ZSM5 [30] and were attributed to adsorbed CO on non-framework Al^{3+} sites with high Lewis acid strength. With increasing oxidation time, the band at 2230 cm^{-1} increased in intensity, while the band at 2085 cm^{-1} was not affected (see Figure 6). A small shift of the wavenumber of adsorbed CO (2085 cm^{-1} to 2092 cm^{-1}) was observed from Pt-BEA(0.2) to Pt-BEA(0.2)SA. This shift points to a lower electron density on the metal particles being in contact with the sulfur species. During the sorption of CO on Pt the (occupied) 5σ orbital of CO overlaps with the $5d_{z^2}$ orbitals of Pt, while the occupied d_{xy} -orbitals of Pt lead to a backdonation of electrons into the non-bonding π -orbitals of CO, which lowers the C-O stretching frequency. Thus, on electron-rich particles a lower wavenumber of the C-O stretching vibration is expected, while for electron deficient particles a higher frequency is observed.

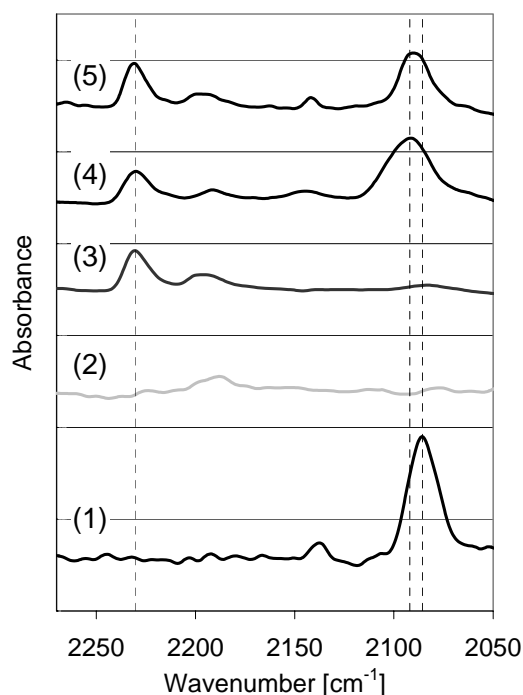


Figure 6: Adsorption of 1 mbar CO at 300 K on (1) Pt-BEA(0.2), (2) Pt-BEA(0.2)S, (3) Pt-BEA(0.2)SA(0.5), (4) Pt-BEA(0.2)SA(2) and (5) Pt-BEA(0.2)SA(5).

5.4.3 Characterization of acidic properties

The concentration of acid sites was evaluated by TPD of NH_3 compiled in Figure 7. Two overlapping maxima for NH_3 desorption at 330°C and about 520°C were observed for all samples indicating the presence of two desorption states of ammonia, presumably on acid sites differing in nature and/or strength. Conventionally the peak around 300°C is attributed to desorption from Brønsted acid sites, while the peak around 500°C is attributed to desorption from Lewis acid sites. Treatment with H_2S led to a reduction of the intensities of both peaks and to a tailing at high desorption temperatures compared to the parent material. After oxidation the intensity of the low temperature peak was enhanced, while the intensity of the high temperature peak was equal to or slightly lower than that of the parent material. The tailing at high temperatures is tentatively attributed to aluminum attached to defect sites possessing strong Lewis acidity generated by dealumination [31]. It is important to note that the total concentration of ammonia desorbed from the samples was higher after oxidation compared to the parent sample.

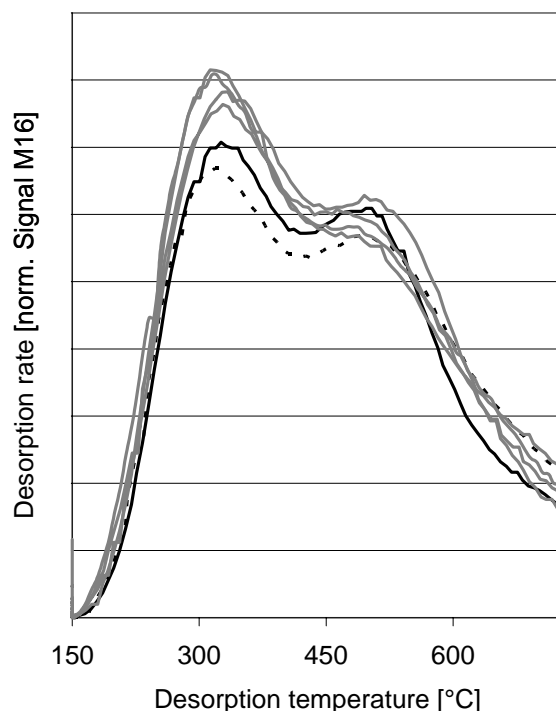


Figure 7: NH_3 -TPD profiles for Pt-BEA(0.2) (—), Pt-BEA(0.2)S (- - -) and Pt-BEA(0.2)SA(y) (.....).

The parent Pt-BEA(0.2) zeolite, Pt-BEA(0.2)S and Pt-BEA(0.2)SA were also characterized by IR spectra of *in situ* adsorbed pyridine. The difference spectra before and after pyridine adsorption are shown in Figure 8. For Pt-BEA(0.2) intense bands at 3733 and 3743 cm^{-1} were observed, attributed to silanol groups on the outer surface and at defects inside the pores. The weak band at 3608 cm^{-1} is assigned to bridging hydroxy groups (Brønsted acid sites). The band at 3785 cm^{-1} is assigned to terminal hydroxy groups on non-framework AlOOH species [32], while bands in the range between 3660 - 3680 cm^{-1} corresponding to aluminum extra framework species or partially hydrolyzed alumina species were not observed. Pyridine adsorption leads to a complete coverage of the bridging hydroxy groups at 3608 cm^{-1} and to a partial coverage of the silanol groups. Pt-BEA(0.2)S had a lower intensity of the accessible hydroxy groups, while the subsequent oxidation enhanced the intensity of the band at 3608 cm^{-1} compared with the Pt-BEA(0.2)S. However, compared to Pt-BEA(0.2) the intensity of the bridging hydroxy groups decreased about 25% for Pt-BEA(0.2)S and about 10% for Pt-BEA(0.2)SA. This is speculated to be caused by partial dealumination and the parallel blocking of acid sites by cationic alumina species. Additionally, one notes a pronounced reduction of the intensity of the silanol groups after the treatments described.

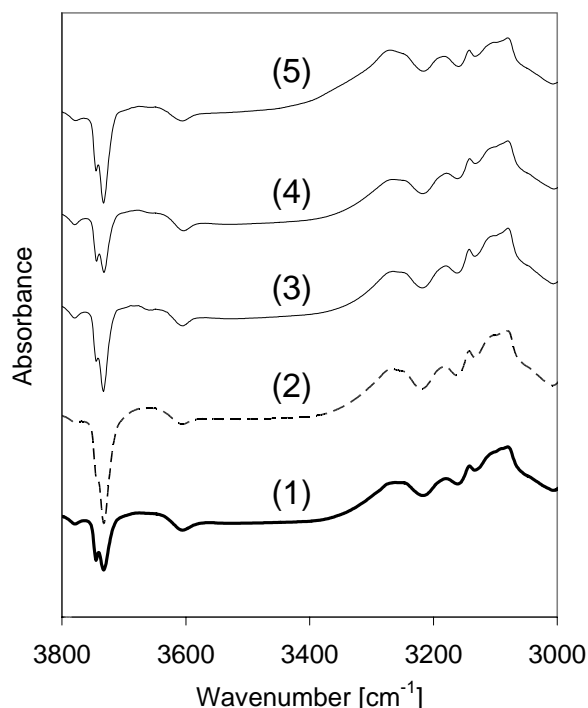


Figure 8: Difference spectra after pyridine adsorption for (1) Pt-BEA(0.2) (—), (2) Pt-BEA(0.2)S (---) and (3) Pt-BEA(0.2)SA(0.5) (—), (4) Pt-BEA(0.2)SA(2), (5) Pt-BEA(0.2)SA(5).

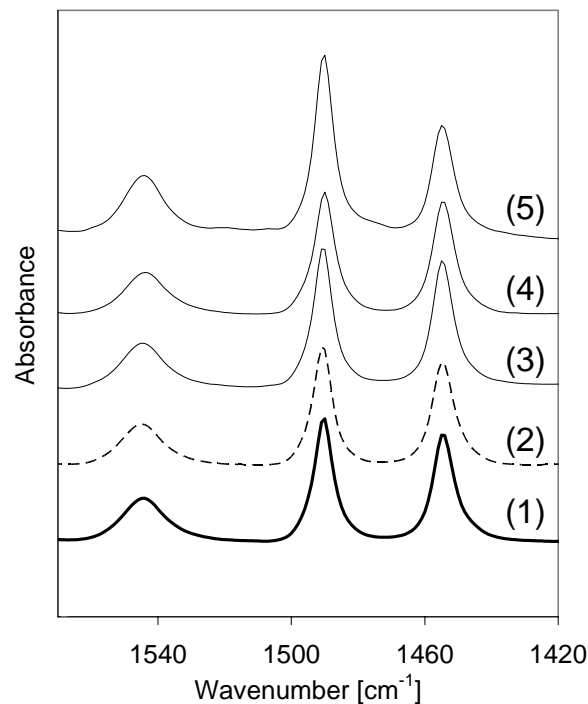


Figure 9: Difference spectra after pyridine adsorption for (1) Pt-BEA(0.2) (—), (2) Pt-BEA(0.2)S (---) and (3) Pt-BEA(0.2)SA(0.5) (—), (4) Pt-BEA(0.2)SA(2), (5) Pt-BEA(0.2)SA(5).

Table 2: Summary of characterization data of Pt-BEA(0.2)S and Pt-BEA(0.2)SA.

Sample	Brønsted acid sites [mmol/g]	Lewis acid sites [mmol/g]	Sulfate conc. [mmol/g]	Sulfide conc. [mmol/g]	Fraction of extra-framework Al [%]
Pt-BEA(0.2)	0.27	0.28	-	-	17.3%
Pt-BEA(0.2)S	0.25	0.29	0.029	0.421	23.5%
Pt-BEA(0.2)SA(0.5)	0.28	0.30	0.154	-	24.0%
Pt-BEA(0.2)SA(2)	0.29	0.30	0.262	0.088	-
Pt-BEA(0.2)SA(5h)	0.31	0.29	0.272	0.048	23.5%

The typical bands of pyridine ring vibrations (1544 cm^{-1} for pyridine sorbed on Brønsted acid sites and 1455 cm^{-1} for pyridine sorbed on Lewis acid sites) were observed. The quantitative evaluation of the adsorption structures is compiled in Table 2. The treatment with H_2S caused a reduction of the Brønsted acid site concentration. However,

it increased again after the subsequent oxidation of the samples. The concentration of Lewis acid sites was slightly enhanced after H₂S exposure; the subsequent oxidation of the H₂S treated samples did not affect it.

5.4.4 Influence of metal loading during sulfation process on acidic properties

Figure 10 shows the IR spectra of the sulfated samples with different metal loadings between 0.2 and 2.3 wt.% before and after pyridine adsorption. The quantitative evaluation of the pyridine ring vibrations showed that the concentration of Brønsted acid sites increases with the metal content, while the concentration of Lewis acid site remained approximately constant. Additionally, the band at 1385 cm⁻¹, assigned to the stretching frequency of a covalent S=O bond [33, 12], is more pronounced with higher metal loadings. After adsorption of pyridine, the band at 1385 cm⁻¹ shifted to 1335 cm⁻¹.

To study the influence of platinum on the sulfation, a Pt-free H-BEA sample and Pt-BEA(1.0) were treated with H₂S (in H₂) and air in an IR flow cell. The changes in the IR spectra during *in situ* H₂S treatment and after oxidation are shown in Figure 11. After H₂S treatment the spectra for the Pt loaded zeolite showed a band at 1445 cm⁻¹ and a smaller band at 1330 cm⁻¹, while during oxidation in air an intense band at 1385 cm⁻¹ was observed. It was not possible to detect bands below 1300 cm⁻¹ as the lattice vibrations of the zeolite lead to a complete absorption in this energy range. In [34, 35] a band at 1330 was assigned to SO₂ physisorbed on alumina. The small band at 1445 cm⁻¹ appears in the region of organic sulfates or molecular sulfuric acid [13]. For the Pt free sample it was not possible to observe any changes in the spectra during H₂S treatment. During oxidation the characteristic sulfate band at 1385 cm⁻¹ arises similar to the Pt loaded sample but with a significantly lower intensity. The IR spectra of the Pt-free H-BEA sample treated with SO₃ in He for 2 and 90 showed directly after starting the SO₃ treatment a band at the same position as for the Pt free H-BEA after H₂S/air treatment. In the course of the SO₃ treatment the intensity of the band at 1380 cm⁻¹ increased further and a new band appeared at around 1420 cm⁻¹, which is tentatively assigned to sulfuric acid [13] formed in the presence of sulfur trioxide and water (originating from the zeolite).

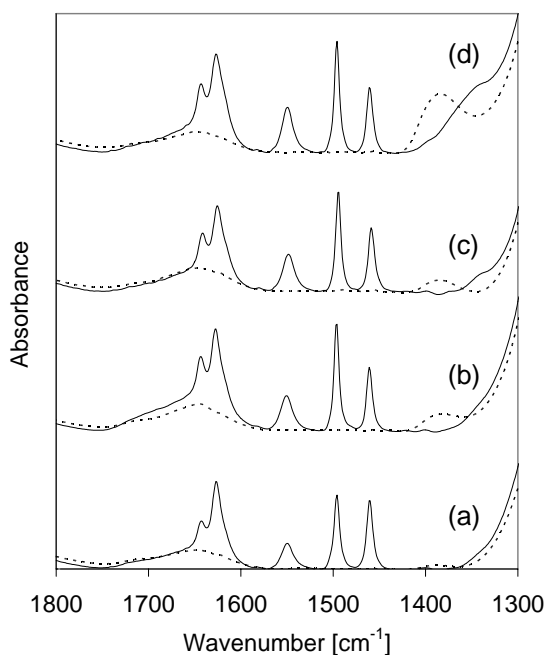


Figure 10: IR spectra before (---) and after pyridine adsorption (—) for (a) Pt-BEA(0.2)SA, (b) Pt-BEA(0.4)SA, (c) Pt-BEA(1.0)SA and (d) Pt-BEA(2.3)SA.

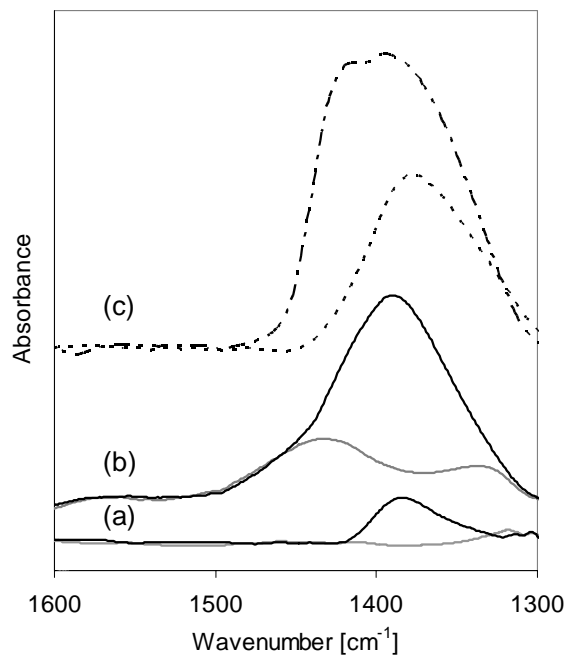


Figure 11: *In situ* IR during H₂S treatment (—) and during oxidation (—) for Pt free H-BEA (a), Pt-BEA(1.0) (b) and SO₃ treatment for Pt free H-BEA after 2 min (-.-.-) and 90 min (- - -).

The concentration of acid and metal sites of the zeolite samples before and after sulfation for different metal contents is summarized in Table 3. The accessible number of Pt surface atoms of the Pt-BEA samples was found to decrease with increasing metal loading. After sulfation a significant reduction of the metal surface was observed.

Table 3: Characterization data for the Pt-BEA(x) and Pt-BEA(x)SA samples.

Sample	Pt content (AAS) [wt.%]	Brønsted acid sites [mmol/g]	Lewis acid sites [mmol/g]	Ratio BAS/LAS [mol/mol]	Accessible Pt _{surface} [mol/mol]	E _{app} ¹⁾ [kJ/mol]
Pt-BEA (0.2)	0.22	0.27	0.28	0.94	0.84	103
Pt-BEA (0.4)	0.41	0.26	0.26	0.99	0.73	107
Pt-BEA (1.0)	1.03	0.28	0.28	1.00	0.52	108

Pt-BEA (2.3)	2.29	0.23	0.29	0.80	0.60	102
Pt-BEA (0.2)SA	0.22	0.28	0.30	0.91	-	89
Pt-BEA (0.4)SA	0.41	0.36	0.26	1.36	-	105
Pt-BEA (1.0)SA	1.03	0.39	0.29	1.35	0.10	109
Pt-BEA (2.3)SA	2.29	0.47	0.30	1.53	0.04	113

¹⁾: apparent activation energy for n-pentane isomerization

5.5 Kinetic experiments

5.5.1 neo-pentane hydrogenolysis

The hydrogenolysis of neo-pentane was used as test reaction to follow the catalytic activity of the metal particles for low metal contents. Under the reaction conditions neo-pentane conversion is only catalyzed by the metal sites. The neo-pentane conversion using a mixture of 2 mol% neo-pentane in hydrogen at a temperature of 350°C at atmospheric pressure is shown in Figure 12 for the parent Pt-BEA(0.2) catalyst and the samples treated with H₂S followed by subsequent oxidation.

After the treatment with H₂S the hydrogenolysis activity severely decreases, while after the oxidation of the catalysts with air the activity increases, however, the initial activity of the parent catalysts was not reached. Methane and iso-butane were detected as main products, the formation of a significant amount of ethane and propane occurred as a consecutive reaction at higher conversion levels only. Isomerization reactions of neo-pentane to iso and n-pentane were not observed. The apparent activation energies were determined in the temperature range between 350 and 400°C and are summarized in Table 3.

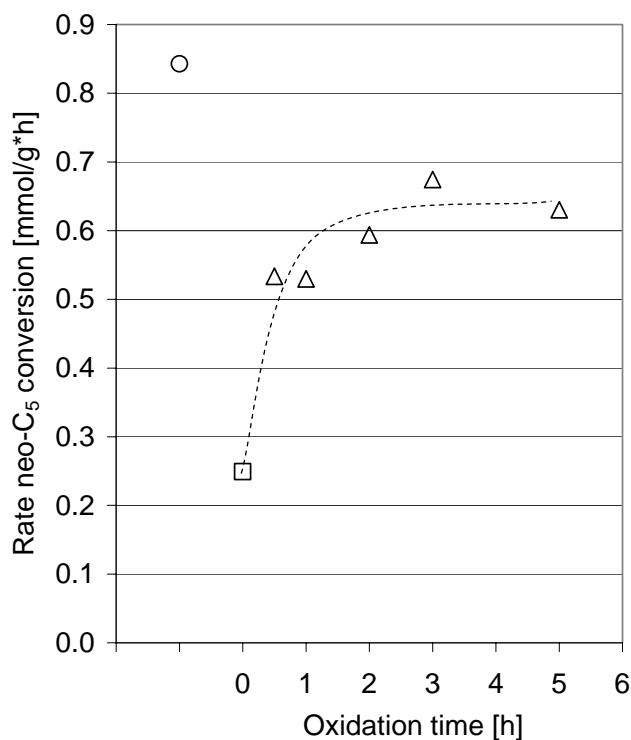


Figure 12: Neo-pentane conversion for Pt-BEA(0.2) (O); Pt-BEA(0.2)S (□) and Pt-BEA(0.2)SA(y) (Δ).

5.5.2 n-pentane hydroisomerization

The catalytic activity of the catalyst was investigated for the pentane hydroisomerization reaction at a total pressure of 4 bar, a WHSV of 30 [g_(feed)/g_(catalyst) h] and a temperature of 290°C. For the kinetic investigations the occurrence of transport limitations had been experimentally excluded. The isomerization rate for the parent Pt-BEA(0.2) material, the sample treated with H₂S and the samples treated with H₂S and air for different oxidation times is compared in Figure 13. The parent material was measured twice to show the reproducibility of two independent experiments in the 20-fold reactor system. Similar to the neo-pentane hydrogenolysis, H₂S treatment of the parent Pt-BEA(0.2) led to a significant reduction of catalytic activity. However, after subsequent oxidation of the H₂S treated sample the activity for the pentane hydroisomerization reaction exceeds the isomerization activity of the parent material.

Table 4 : Summary of kinetic data.

Sample	E _A : n-pentane isomerization [kJ/mol]	E _A : neo-pentane hydrogenolysis [kJ/mol]
--------	--	---

Pt-BEA(0.2)	103	114
Pt-BEA(0.2)S	107	-
Pt-BEA(0.2)SA(0.5)	83	159
Pt-BEA(0.2)SA(1)	89	165
Pt-BEA(0.2)SA(2)	91	149
Pt-BEA(0.2)SA(5)	91	150

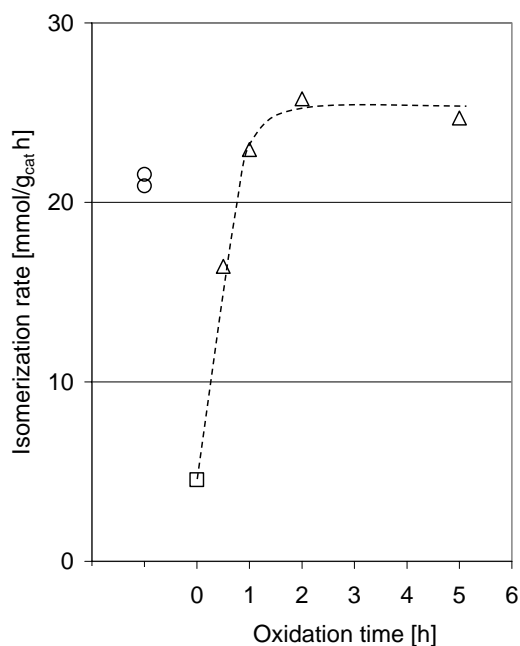


Figure 13: Isomerization activity for Pt-BEA(0.2) (○), Pt-BEA(0.2)S (□) and Pt-BEA(0.2)SA(y) (Δ) at 290°C.

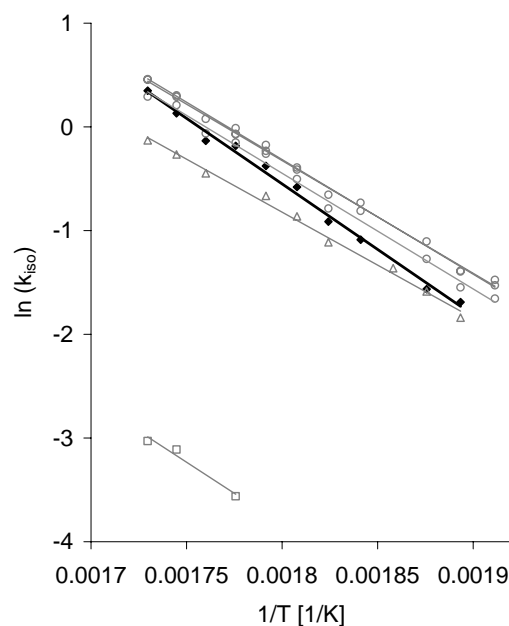


Figure 14: Isomerization activity for Pt-BEA (0.2) (◆) (—), Pt-BEA(0.2)S (□) (—), Pt-BEA(0.2)SA(0.5) (—) (Δ) and Pt-BEA(0.2)SA(1-5) (—) (○).

The data range for the determination of the apparent activation energies (temperature range 250 to 340°C, total pressure of 4 bar) is shown in Figure 14, the apparent activation energies are summarized in Table 4. The oxidized samples Pt-BEA(0.2)SA showed a lower apparent activation energy. Only minor changes in the apparent activation energies were observed. However a significant difference in the pre-exponential factors indicate that the concentration of active sites changes for the sulfated samples.

The influence of the metal loading on the isomerization activity is shown in Figure 15 for the catalysts before and after H₂S treatment and oxidation at p=4 bar, WHSV=30 h⁻¹

and $T=290^{\circ}\text{C}$. It is interesting to note that at metal contents above 0.2 wt.% an influence of the Pt loading on the isomerization activity for the Pt-BEA catalysts was not observed, while the isomerization selectivity was significantly reduced with increasing metal content as shown later. Note that the reduction of the activity for the untreated catalyst with a metal loading of 2.2 wt.% is due to a lower acidity of the sample. According to the classical reaction mechanism [2] the constant rate with increasing Pt content indicates that the dehydrogenation step is equilibrated, while the acid catalyzed C-C bond rearrangement is the rate determining step. The increase in the isomerization activity after the sulfation with increasing metal content can, therefore, only be explained by a modification of the acid character of the catalysts.

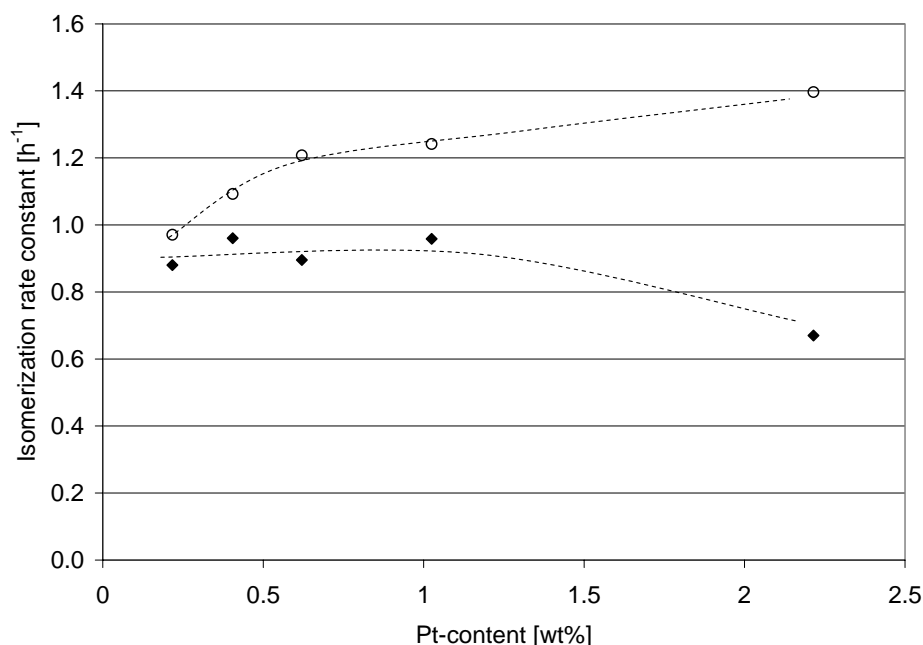


Figure 15: Isomerization activity for untreated catalysts Pt-BEA(x) (◆) and Pt-BEA(x)SA (○) at $p=4$ bar, $\text{WHSV}=30\text{ h}^{-1}$ and $T=290^{\circ}\text{C}$.

Figure 16 shows the temperature dependency of the isomerization activity for the parent Pt-BEA and the sulfated samples for different metal loading. The isomerization reaction was carried out at $p=4$ bar and a $\text{WHSV}=30\text{ h}^{-1}$ in a temperature range between 260 and 350°C . The apparent activation energies measured in the kinetic regime are summarized in the Figure caption. Only minor changes in the apparent activation energies were observed. However a significant difference in the pre-exponential factors indicates

that the concentration of active sites changes especially for the sulfated samples with a high metal loading.

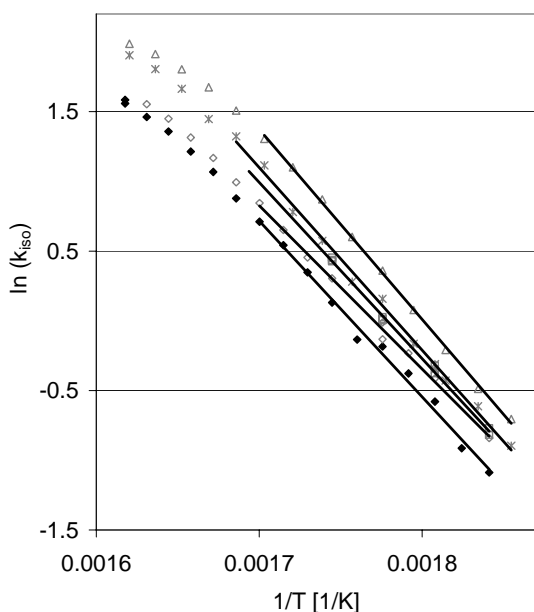


Figure 16: Isomerization activity for Pt-BEA(0.2) (◆), Pt-BEA(0.2)SA (◇), Pt-BEA(0.4)SA (□), Pt-BEA(1.0)SA (×) and Pt-BEA(2.2)SA (△).

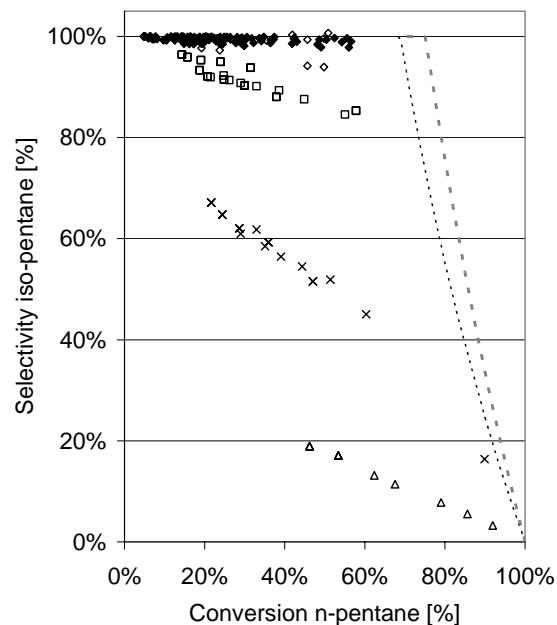


Figure 17: Isomerization selectivity for Pt-BEA(0.2) (◇), Pt-BEA(0.4) (□), Pt-BEA(1.0) (×), Pt-BEA (2.3) (△) and Pt-BEA(x)SA (●) at 4bar and thermodynamic equilibrium at 200°C (---) and 300 °C (.....).

Figure 17 shows the selectivity of the H-BEA samples with different metal loadings at 300°C and a total pressure of 4 bar (the WHSV was varied between 2 and 30 h⁻¹) The variation of the contact time enables to compare the selectivities of the catalyst at the same conversion level and hence the same distance to the equilibrium. The thermodynamic equilibrium between n- and iso-pentane, which is the upper limit for the selectivity achievable, is included for a temperature of 200 and 300°C. A decrease of the selectivity to iso-pentane with increasing metal loading was observed for the Pt-BEA samples, while after the sulfur treatment the selectivity did not show any influence on the metal loading. Note that the selectivities to iso-pentane were close to 100% after the sulfation process.

5.6 Discussion

5.6.1 Metallic properties

To reach high isomerization rates the availability of sufficient metal sites is essential to maintain the de/hydrogenation activity. Sulfur is one of the most common poisons for metal containing catalysts, therefore, sulfide species and H₂S both adsorbed on the Pt particles must be removed. The approach we applied here was to oxidize the sulfur species located on the Pt particles to regain the active metal surface after the reduction of the catalyst in hydrogen. Temperatures as low as 300°C were applied for the oxidation to prevent sulfur-induced metal sintering [36] (compare Chapter 4). Adsorption of CO on the catalysts after exposure to H₂S indicated that all Pt surface sites were poisoned either by sulfur species or by adsorption of H₂S. After the oxidation with air only a fraction of the initially present metal surface was recovered. XAS at the S K-edge, TPO experiments and the chemical analysis of the sulfur species agreed that after the oxidation primarily sulfate species are present on the catalysts, which cover approximately 50 % of the accessible Pt surface atoms. Besides the physical blockage of the metal sites an electronic effect was observed from the shift of the CO stretching frequency. For the sulfated samples a reduction of the electron density of the metal was observed, which can either be assigned to the presence of PtS species and/or to the formation of sulfate groups. For sulfur poisoned Pt catalysts supported on γ -alumina the shift of the CO stretching frequency to higher frequencies was explained by the presence of adsorbed H₂S, residual sulfur deposits and/or PtS species which abstract electrons from the platinum particles [37]. During the oxidation Pt catalyzes the formation of SO₃ from the SO₂ present on the catalysts [38] and, therefore, a high concentration of sulfate species is expected to be formed close to metal particles after the oxidative treatment, which interact with the Pt-particles and thus potentially modify the electronic properties of the metal.

Neo-pentane hydrogenolysis was used as probe reaction to directly investigate the activity of the metal particles. In general it can be assumed that the reduction of the electron density on the metal particles, observed during CO adsorption, should lead to a stronger adsorption of the neo-pentane molecule and hence a reduced apparent activation energy [39, 40]. However the apparent activation energy was significantly higher for the

oxidized samples compared to the parent Pt-BEA. It is therefore concluded that the reduction of the activation energy is rather caused by a sterical hindrance of the structure sensitive side reaction due to blocking sulfur species, than due to a weakening of the interaction of the reactants with the metal sites caused by the electronic effect. Foger observed an increase in the apparent activation energy for neo-pentane hydrogenolysis dependant the particle size of Pt and concluded different reaction pathways of the adsorbed intermediates [40]. It hence is conceivable that the sulfur species affect the surface geometry of the metal particles *e.g.* by changing the index crystallite facets, thus leading to a different catalytic behavior.

5.6.2 Acidic properties

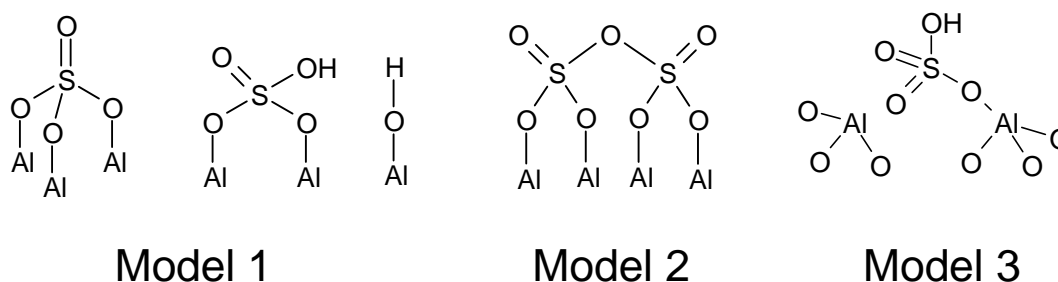
^{27}Al NMR and the formation of structural defects detected by IR (band at 3733 cm^{-1}) showed that the zeolite framework was partially dealuminated when exposed to H_2S . The removal of Al^{3+} from framework led to a reduction of the concentration of bridging hydroxy groups (3608 cm^{-1}) and to the formation of octahedrally coordinated alumina species which possessed Lewis acidity. ^{27}Al NMR indicates a reduction of the tetrahedral Al of 10%, which should lead to an equal reduction in the concentration of bridging hydroxy groups. However, the concentration of the SiOHAl groups decreased about 25 % after the H_2S treatment. Hydrogen bonding of H_2S with SiOHAl groups of zeolites leads to the formation of a broad band at 3100 cm^{-1} [10]. As perturbed hydroxy bands were not observed in this region, is assumed that either residual S fragments are adsorbed on the acid sites or cationic aluminum species originating from dealumination block the acidic sites. The significantly higher ratio between tetrahedrally and octahedrally coordinated Al obtained from the ^{27}Al NMR compared with the ratio between the Brønsted and Lewis acid sites obtained by adsorption of pyridine indicates furthermore that the protons on the bridging hydroxy groups are partially exchanged by Al^{3+} species originating from the dealumination process. As these Al^{3+} species can potentially block three acid sites, not all of the lattice aluminum sites possess Brønsted acidity [41]. During oxidation the bridging hydroxy groups are increasing compared with the Pt-BEA S sample. Flexible aluminum species in octahedral position that can be converted to tetrahedrally coordinated aluminum were already observed in [42, 43]. Simultaneously CO adsorption experiments showed the formation of strong Lewis acidic Al^{3+} surface species after oxidation. Since these sites were not observed for the parent Pt-BEA(0.2) the formation of the coordinatively unsaturated Al^{3+} species are affiliated with the generation of the sulfate groups. Analogue

to sulfated zirconia the Lewis acid strength of Al^{3+} should become remarkable stronger by the inductive effect of $\text{S}=\text{O}$. It is interesting to note that for low metal loadings the initially present concentration of bridging hydroxy groups could not be restored while for high metal loadings (> 1 wt.% Pt) an increase of the bridging hydroxy groups of *ca.* 15% was observed. At the same time the samples with higher metal loadings possessed a higher concentration of sulfate species as indicated by the intensity of the $\text{S}=\text{O}$ bond observed during IR measurements. The formation of significant concentration of sulfate only occurs in the presence of Pt or if the zeolite BEA is directly exposed to SO_3 (see Figure 11). In [44] it was also shown that the oxidation of SO_2 on alumina only occurs in the presence of Pt and that the heterogeneous reaction is kinetically controlled below temperatures of 650°C (60 ppm SO_2 , air flow of 1.7 cm/s).

Although the concentration of $\text{Si}(\text{OH})\text{Al}$ groups was reduced compared with the parent Pt-BEA(0.2), an enhanced concentration of Brønsted acid sites was observed after oxidation. Furthermore the enhancement of the bridging hydroxyl groups observed for the sample with higher metal loadings does not correlate with the enhancement of the total concentration of acid sites. It is hence suggested that H_2S or sulfide species adsorbed on the zeolite framework are converted to Brønsted acidic sulfate groups which were identified by the formation of an $\text{S}=\text{O}$ bond during IR studies and the XAS measurements on the S-K edge. Enhancement of Brønsted acidity or acid catalyzed reactions were already observed in *e.g.* [45, 46] by admixture of alumina sulfates on alumina, by sulfation *via* H_2SO_4 of alumina [47] or by treatment of H-MOR with $(\text{NH}_4)_2\text{SO}_4$ [15].

The concentration of Brønsted acid sites (determined from sorption of Pyridine) are compared to the sulfate concentration in Figure 18, which shows that the enhancement of Brønsted acidity of the sulfur treated samples directly correlates with the concentration of sulfate species on the sample. For the parent Pt-BEA sample a higher concentration of Brønsted acid sites compared to the sulfur treated samples was observed, which resulted from the dealumination during the H_2S treatment. The formation of small amounts of sulfate already present after H_2S treatment can be explained by oxygen impurities on the sample. Figure 18 shows that four to five sulfur atoms are required to form one additional Brønsted acidic site, therefore it is concluded that either not all of the sulfate groups on the sample possess Brønsted acidity and/or that bisulfate species are present. According to Saur [33] the sulfate species are partially present as $(\text{M}_3\text{O}_3)\text{S}=\text{O}$ species and $(\text{M}_2\text{O}_2)\text{SOOH}$ depending on the local concentration of OH groups and degree of

hydration for which only the latter ones possess Brønsted acidity (see **Error! Reference source not found.**). As hydrogensulfate ions are not associated with well-defined $\nu(\text{OH})$ bands, due to strong hydrogen bond interaction such species are difficult to detect [48]. The result of the ^{27}Al NMR showed that the octahedrally coordinated aluminum is arranged in different local environments. It hence is also possible that (depending on the local geometry of the aluminum configuration) different sulfate species are formed. Another indication for the presence of different arranged sulfate species is the superposition of the high temperature peak in the TPO for the Pt-BEA SA samples during TPO. The observed S-XANES spectrum can rule out the presence of thio sulfate and peroxosulfate species as additional $1s \rightarrow 3p$ bounds-state transitions should be observed. However S-O-S bridging species like $\text{S}_2\text{O}_7^{2-}$ resemble that of SO_4^{2-} because each sulfur atom is surrounded by four oxygen atoms and can therefore not be excluded [49]. In [46] an anchoring system to the framework was suggested which emphasizes the role of neighboring Lewis acid sites for the formation of strong Brønsted acid sites (see **Error! Reference source not found.**-Model 3) and explains the high thermal stability of the sulfate species.



Scheme 1: Models for the structure of surface sulfate species.

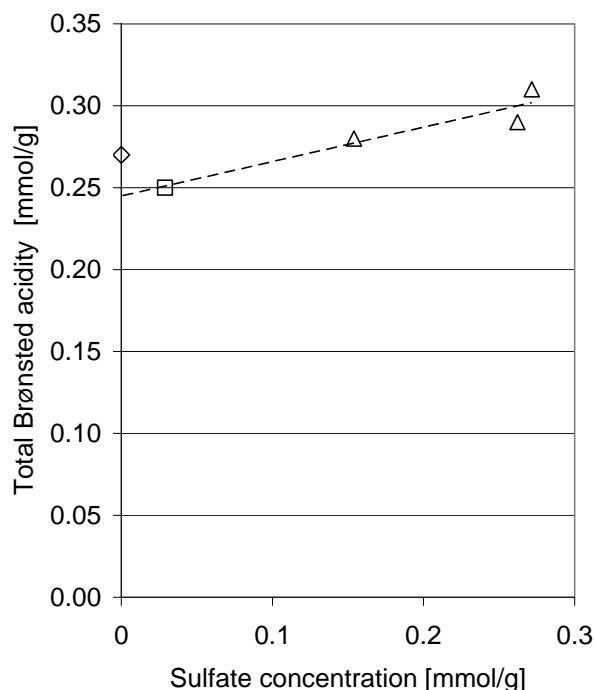


Figure 18: Correlation of sulfate content and Brønsted acidity for Pt-BEA(0.2) (◇), Pt-BEA(0.2)S (□) and Pt-BEA(0.2)SA (△).

5.6.3 Kinetic results

It was shown that the treatment with H₂S and air for sufficient oxidation times leads to the formation of additional Brønsted acid sites and to a reduction of the metal surface. The application of the sulfation procedure in the gas phase essentially reduces the ratio of accessible surface metal atoms to Brønsted acid sites (Pt_s/H^+), which favorably influences the isomerization selectivity due to the suppression of undesired metal catalyzed C-C bond breaking reactions. However, if the concentration of metal sites is too low the hydrogenation/dehydrogenation reaction might become the rate limiting step, which lowers the overall activity and can also lead to a rapid deactivation of the catalysts due to the formation of coke. Even for the catalyst containing 0.2 wt.% it was shown that the concentration of the metal sites does not influence the isomerization activity thus it can be assumed that the dehydrogenation step is equilibrated for all parent catalysts. After the H₂S treatment of Pt-BEA(0.2) (see Figure 13) a significant reduction of the isomerization activity was observed, which indicates that on this catalysts the number of available metal sites fell below the lower limit necessary to maintain the dehydrogenation activity. In the course of the oxidation the metal sites were recovered and at the same time the isomerization activity is increasing. Starting from an oxidation time of 1h the

isomerization activity of the untreated catalyst exceeds the parent material. This shows that with respect to isomerization the subsequent oxidation period is not only essential for the formation of acidic sulfate species, but also for the recovery of the metal sites.

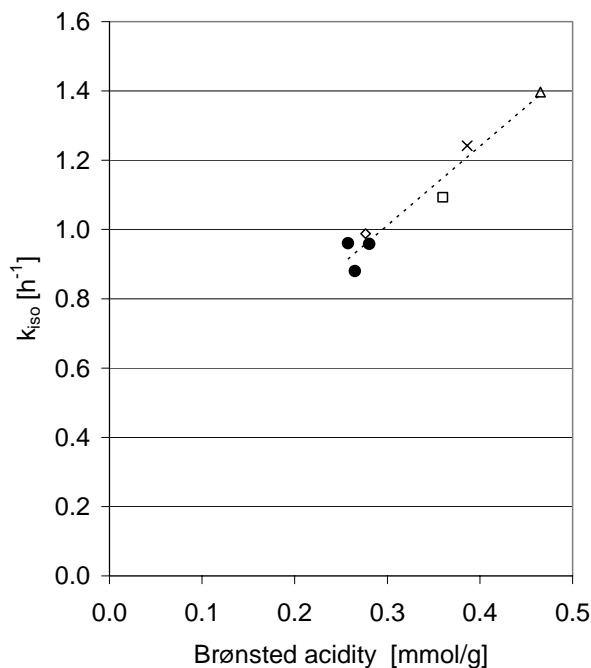


Figure 19: Isomerization acidity and activity for Pt-BEA samples (●), Pt-BEA(0.2)SA (◇), Pt-BEA(0.4)SA (□), Pt-BEA(1.0)SA (×) and Pt-BEA(2.3)SA (△).

For the Pt-BEA(x)SA samples a dependency of the metal loading on the isomerization activity was observed. Although the metal content of the sulfated samples was reduced after gasphase sulfation process the increase of the isomerization activity with increasing metal loading for the sulfated sample is rather due to the enhancement of the acidity than due to a limitation in the dehydrogenation step. The isomerization activity correlated to the concentration of Brønsted acid sites of the Pt-BEA catalyst and the gas phase sulfated samples in Figure 19. It can be seen that the samples sulfated at higher metal loadings possess a higher concentration of acid sites and hence a higher activity. The linear correlation of the acidity with the isomerization activity particularly at high metal loadings furthermore indicates that the isomerization reaction is limited on the acid sites. The increase of the concentration of acid sites for high metal loading was attributed to the catalytic oxidation of SO_2 to SO_3 which was shown to act as a sulfation precursor (Figure 11).

In addition it was shown that the metal content for the parent Pt-BEA samples significantly influences the isomerization selectivity. In general it is conceivable that the side reaction either occurs directly on the metal site (hydrogenolysis) or that the side reaction occurs on the acidic sites (acid catalyzed cracking). In both cases an enhancement of the side reaction is expected with increasing metal content. While for the metal catalyzed reaction this is evident from the increase in the (Pt_s/H^+) ratio, acid catalyzed cracking reactions (occurring *via* β -scission of the carbenium ion to an olefin and a carbenium ion/ alkoxy-group) also increase with the metal content due to the enhanced metal-catalyzed hydrogenation of the fragments obtained by β -scission. In addition for the hydrogenolysis reaction a reduction of the isomerization selectivity is expected as the dehydrogenation step is equilibrated.

Figure 17 indicate that the activity of the side reaction during n-pentane conversion on zeolite beta does not increase linearly with the exposed metal surface. The turnover frequency (TOF) for the formation of n-butane (with respect to the number of metal surface atoms) as a function of the average particle size (obtained from the metal dispersion assuming cubeoctahedral particles) is shown in Figure 21. Although the samples with different particle sizes possess different activity the turnover frequencies can be compared as the product distribution did not change with increasing conversion level. Furthermore the samples showed similar acidity, hence the differences in metal support interaction should be negligible. The results show a severe change of the turnover frequency which points to a structure sensitive side reaction. In general, for hydrogenolysis reactions over platinum on alumina a decrease in the turnover frequency (rate normalized to moles of exposed metal atoms) with decreasing particle size is observed [50]. For cyclopentane hydrogenolysis over Pt loaded Al_2O_3 [51] an enhancement of the activity of more than one order of magnitude was observed for a particle diameter between 1 nm and 2.5 nm and only for bigger particles (~5 nm) the reaction became structure insensitive. The formation of n-butane showed a similar dependence on the metal particle size, therefore, we would like to speculate that the (C-C bond breaking) side reaction occurs on the metal particles. This would further explain the significant improvement of the isomerization selectivity after sulfation as hydrogenolysis requires larger ensembles of metal atoms or the presence of highly uncoordinated metal atoms to form dehydrogenated intermediates with multiple bonds to the metal particle [52]. The constraint of the hydrogenolysis reaction after sulfation was also shown by the severe increase of the apparent activation energy. Both, larger free ensembles of Pt atoms

and highly reactive and exposed metal atoms, would be reduced dramatically by the presence of sulfur on the metal.

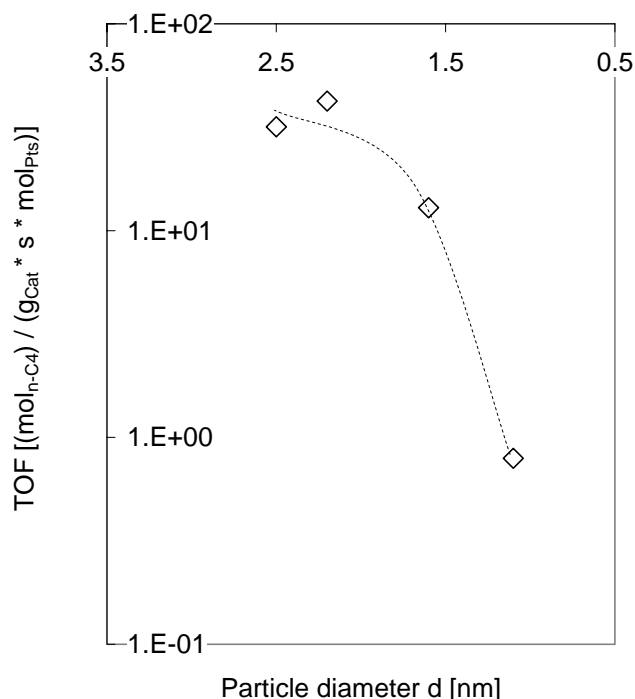


Figure 20: Turn-over frequency of n-butane formation for Pt-BEA(x) for the average metal particle sizes (6 bar, 300°C, WHSV of 14h⁻¹).

5.7 Conclusions

Gas phase sulfation on Pt loaded zeolite BEA was carried out using H₂S and air. IR studies on pyridine and CO as probe molecules showed that the acidic properties are strongly affected by the sulfur treatment. A partial dealumination of the zeolites framework was observed reducing the zeolite bridging hydroxy groups and producing Lewis sites, which can be used to anchor sulfate species. In addition aluminum species were formed which were blocking the bridging hydroxy groups of the zeolite but could be removed upon sulfation. The sulfated samples possessed a higher concentration of Brønsted acid sites with a similar acid strength thus leading to an increased isomerization activity. *In situ* XAS results combined with ion-chromatography showed that after H₂S treatment sulfur is mainly present as sulfide species on the zeolite, while after oxidation only sulfate species were observed. During the gas phase sulfation Pt was shown to be

directly involved in the formation of the sulfate species by catalyzing the formation of SO_3 . Hence the sulfated sample with high metal content possessed a higher concentration of acid sites and isomerization activity compared with the low metal loaded samples. Beside the enhancement of isomerization activity the isomerization selectivity was severely improved after gasphase sulfation. The metal content significantly enhanced the activity of the side reaction although the zeolite samples possessed similar acidity. As the size of the Pt particles influenced the turnover frequency for the side reaction hydrogenolysis was identified as mayor source of the byproducts. Neo-pentane hydrogenolysis showed a significant higher apparent activation energy on the sulfated samples. Hence it was argued that a selective reduction of the metal surface by sulfur species selectively poisons the catalyst for the structure sensitive side reaction.

5.8 Acknowledgements

The financial support by Bundesministerium für Bildung und Forschung Project (BMBF:03C0307D) is gratefully acknowledged. We acknowledge the ANKA Angstroemquelle Karlsruhe for the provision of beamtime. Specially we would like to thank Stefan Mangold for the adaptation of the ANKA-XAS beamline for the experiments at the S K-edge and for the assistance during the experiments. The authors are also grateful to M. Neukamm for the AAS measurements, X. Hecht for the hydrogen chemisorption measurements and C. Sievers for the NMR measurements.

REFERENCES

- [1] M. Guisnet, *Pol. J. Chem* 77, 637 (2003).
- [2] P.B. Weisz, *Adv. Catal.*13, 137 (1962).
- [3] G.A. Mills, H.Heinemann, T.H. Millikan, A.G. Oblad, *Ind. Eng. Chem.* 45, 134 (1953).
- [4] R. Ravishankar, S. Sivasanker, *Appl. Catal. A: Gen.* 142, 47 (1996).
- [5] A. Hollo, J. Hancsok, D. Kallo, *Appl. Catal. A: Gen.* 229, 93 (2002).
- [6] J.F. Allain, P. Magnoux, P. Schulz, M. Guisnet, *Appl. Catal. A: Gen.* 152, 221 (1997).
- [7] K. Arata, *Adv. Catal.* 37, 165 (1990).

- [8] G.B. Vicker, J.L. Kao, J.J. Ziemiak, W.E Gates, J.L. Robbins, M.M.J. Tracy, S.B. Rice, T.H. Vanderspurt, V.R. Cross, A.K. Ghosh, *J. Catal.* 139, 48 (1993).
- [9] S. Gopal, P. G. Smirniotis, *Appl. Catal. A: Gen.* 247, 113 (2003).
- [10] C.L. Garcia, J.A. Lercher, *J. Phys. Chem.* 96, 2231 (1992).
- [11] T.I. Koranyi, F. Moreau, V.V. Rozanov, E.A. Rozanova, *J. Mol. Struct.* 410, 103 (1997).
- [12] G. D. Yadav, J.J. Nair, *Micro. Meso. Mat.* 33, 1 (1999).
- [13] T. Yamaguchi, T. Jin, K. Tanabe, *J. Phys. Chem.* 90, 3148 (1986).
- [14] M.A. Babaeva, A.A. Tsyganenko, V.N. Filimonov, *Kinetics and Catalysis* 787 Vol 24, 4 (1985).
- [15] T. Lei, J.S. Xu, Z. Gao, *Mat. Chem. Phys.* 60, 177 (1999).
- [16] C. Woltz, A. Jentys and J.A. Lercher, *J. Catal.*, submitted for publication (2005).
- [17] C.P. Hubbard, K. Otto, H.S. Gandhi, K.Y.S. Ng, *J. Catal.* 144, 484 (1993).
- [18] A.F. Lee, K. Wilson, R.M. Lambert, C.P. Hubbard, R.G. Hurley, R.W. McCabe, H.S. Gandhi, *J. Catal.* 184, 491 (1999).
- [19] R. Burch, E. Haplin, M. Hayes, K. Ruth, J.A. Sullivan, *Appl. Catal. B: Environ.* 19, 199 (1998).
- [20] J.M. Jones, V.A. Dupont, R. Brydson, D.J. Fullerton, N.S. Nasri, A.B. Ross, A.V.K. Westwood, *Catal. Today* 81, 589 (2003).
- [21] H. Dathe, A. Jentys, J.A. Lercher, *Phys. Chem. Chem. Phys.* 6, 1283 (2005).
- [22] J.A. Lercher, Ch. Gründling, G. Eder-Mirth, *Catal. Today* 27, 353 (1996).
- [23] C.A. Emeis, *J. Catal.* 141, 347 (1993).
- [24] G.L. Woolery, G.H. Kuehl, H.C. Timken, A.W. Chester; J.C. Vartuli, *Zeolites* 19, 288 (1997).
- [25] S.C.B. Myneni, *Rev. Mineral. Geochem.* 49, 485 (2002).
- [26] A. Jokic, J. N. Cutler, E. Ponomarenko, G. van der Kamp, D. W. Anderson, *Geochim. Cosmochim Acta*, Vol 67, No 14, pp 2591 ff (2003).
- [27] M. Waqif, O. Saur, J.C. Lavalley, S. Perathoner, G. Centi, *J. Phys. Chem.* 95, 4051 (1991).
- [28] T. Kloprogge, J. W. Geus, J. B. H. Jansen, D. Seykens, *Thermochim acta* 209, 265 (1992)
- [29] V. Gruver, J. Fripiat, *J. Phys. Chem.* 98, 8549 (1994).
- [30] T. Ballinger, J. Yates Jr., *Langmuir* 7, 3041 (1991).
- [31] Y. Miyamoto, N. Katada, M. Niwa, *Micr. Meso Mat.* 40, 271 (2000).
- [32] I. Kiricsi, C. Flego, G. Pazzuconi, W.O. Parker, R. Millini Jr., C. Perego, G. Bellussi, *J. Phys. Chem.* 98, 4627 (1994).
- [33] O. Saur, M. Bensitel, A.B. Mohammed Saad, J.C. Lavalley, C.P. Tripp, B.A. Morrow, *J. Catal.* 99, 104 (1986).

-
- [34] M.A. Babaeva, A.A. Tsyganenko, *Kinet. Catal.* Vol. 25, 4 (1985) p. 787.
- [35] M.B. Mitchell, V. N. Sheinker, *J. Phys. Chem.* 100, 7550 (1996).
- [36] J.-R. Chang, S.-L. Chang, T.-B. Lin, *J. Catal.* 169, 338 (1997).
- [37] J.-R. Chang, S.-L. Chang, *J. Catal.* 176, 42 (1998).
- [38] H.S. Gandhi, M. Shelef, *Appl. Catal.* 77, 175 (1991).
- [39] M.K. Oudenhuijzen, J.A. van Bokhoven, D.C. Koningsberger, *J. Catal.* 219, 134 (2003).
- [40] K. Foger, J.R. Anderson, *J. Catal.* 54, 318 (1978).
- [41] G. Catana, D. Baetens, T. Mommaerts, R. A. Schoonheydt, B. M. Weckhuysen, *J. Phys. Chem. B* 105, 4904 (2001).
- [42] A. Omegna, J. A. van Bokhoven, R. Prins, *J. Phys. Chem. B* 107, 8854 (2003).
- [43] E. Bourgeat-Lami, P. Massiani, F. Di Renzo, P. Espiau, F. Fajula, T.D. Courieres, *Appl. Catal.* 72, 139 (1991).
- [44] V. Dupont, J.M. Jones, S.-H. Zhang, A. Westwood, M.V. Twigg, *Chem. Eng. Sci.* 59, 17 (2004).
- [45] W. Przystajko, R. Fiedorow, I.G. Dalla Lana, *Appl. Catal.* 15, 265 (1985).
- [46] M.L. Guzman-Castillo, E. Lopez-Salinas, J.J. Fripiat, J. Sanchez-Valente, F. Hernandez-Beltan, A. Rodriguez-Hernandez, J. Navarrete-Bolanos, *J. Catal.* 200, 317 (2003)
- [47] D.E. Gawthrope, A.F. Lee, K. Wilson, *Phys. Chem. Chem. Phys.* 6, 3907 (2004).
- [48] M. Waqif, J. Bachelier, O. Saur, J.-C. Lavalley, *J. Mol. Catal.* 72, 127 (1992).
- [49] H. Sekiyama, N. Kosugi, H. Kuroda, T. Ohta, *Bull. Chem. Soc. Jpn.* 59, 575 (1986).
- [50] M. Che and C.O. Bennett, *Advances in catalysis*, Volume 36.
- [51] J. Barbier, P. Marecot, *Nouv. J. Chim.* 5, 393 (1991).
- [52] E. H. van Broekhoven, V. Ponc, *J. Mol. Catal.* 25, 109 (1984).

Chapter 6

6 ACIDITY AND ACTIVITY ENHANCEMENT OF ZEOLITE BETA AND MORDERNITE BY SULFATION AND MODIFICATION WITH TUNGSTEN PRECURSOR

6.1 Abstract

The effect of a tungsten promoter on isomerization activity on supported Pt loaded zeolite samples was studied. The acidic properties were investigated using pyridine, ammonia and pentane as probe molecules. Tungsten significantly changes the acid properties by forming additional Lewis acidic clusters and additional Brønsted acid sites thus influencing the activity for the isomerization reaction. Subsequent sulfation of the Pt loaded tungsten promoted zeolite BEA further enhanced Brønsted acidity and isomerization activity. The adsorption properties were examined by IR and thermogravimetry showing that the additional Brønsted acid sites obtained after tungsten loading and sulfation possess different acid strength, while they do not affect the strength of the bridging hydroxy groups of the zeolite.

Additionally the effect of different sulfation precursors on the acidic properties of zeolite MOR was studied. Sulfation significantly reduces the concentration of the bridging hydroxy groups especially for high contents of sulfate on the sample. Additionally the accessibility to the acid sites is reduced which leads to pore mouth catalysis. Acidity and activity enhancement can be observed after sulfation of thermally dealuminated MOR. However the sulfation process does not have a beneficial impact on the diffusivity and accessibility of the pore structure of the dealuminated sample.

6.2 Introduction

Alkane isomerization is used for balancing the loss of octane number in gasoline which historically resulted from lead-phase out and nowadays results from restrictions of MTBE (methyl tertiary-butyl ether), oxygenates and benzene. Industrially the reaction is carried out on bifunctional catalysts, whereas the isomerization activity is typically limited to the acidity of the samples. Thus, the major task in activity enhancement is (i) the increase of the concentration of acid sites in order to get a more active catalyst per weight or volume and (ii) the increase of the acid site strength to receive a catalyst that is more active at low temperatures and hence can work at more beneficial equilibrium positions.

Alkane isomerization is industrially carried out on zeolite MOR [1]. Studies on different zeolites showed that the intrinsic acid strength and structural properties can significantly influence the isomerization activity by controlling adsorption and diffusion of the alkane molecules in the zeolite pores [2, 3]. Mostly post synthesis methods in zeolites, such as dealumination by means of steaming or leaching procedures or the modification with phosphorus compounds, are used for tailoring the concentration and strength of acid sites as well as their accessibility [4, 5].

The application of sulfur treatment under specific conditions can also significantly change the catalytic behavior of catalysts, in particular due to its change in acidity. H_2S , SO_2 , SO_3 , $(\text{NH}_4)_2\text{SO}_4$ and H_2SO_4 are the most commonly used sulfur precursors [6, 7]. Sulfation of alumina was shown to create Brønsted acid sites which show activity for cracking and isomerization reactions [8]. A promotion effect of SO_2 was observed for the double-bond migration during isomerization of *cis*-2-butene on cation exchanged zeolite X and ascribed to the generation of new acidic OH groups formed through the reaction of SO_2 with basic OH groups bonded to metal cations [9]. Calcination of an immersed ammonia sulfate solution with zeolite H-MOR also resulted in an enhancement of acidity and isomerization activity [10]. The creation of strong acid properties on sulfated and fluoridated alumina was proposed to be due to an inducing polarization of the neighboring OH groups [11,8]. On the other hand it was argued that Brønsted acidity is generated by converting covalent S=O bond to ionic SOOH species [12]. In contrast to sulfated zirconia the sulfated alumina retained weaker acid strength [7], which was shown in [8] to be comparable to silica alumina.

Furthermore, Brønsted acidity can also be formed by WO_x domains supported on Al_2O_3 , SiO_2 or SnO_2 and ZrO_2 [13]. The major advantage of (sulfur-free) WO_x - ZrO_2 over sulfated ZrO_2 is that these materials do not suffer from a partial reduction of the sulphate species under reaction conditions at which sulfur species can be released and might lead to a poisoning of the catalyst. WO_x - Al_2O_3 was furthermore shown to be active for the acid catalyzed *n*-butene skeletal isomerization [14, 15]. In [16, 17] it was proposed that for WO_x/ZrO_2 Zr^{4+} is incorporated within the polymeric WO_x clusters leading to heteropolyoxo anions, which generate Brønsted acid sites through the charge compensating protons. Similarly highly acidic heteropoly acids such as $\text{H}_5\text{PW}_{12}\text{O}_{40}$ supported on silica are known to be active for alkane isomerization [18]. In [19] it was proposed that Pd plays a unique role in heteropolyacids by the generation of H atoms which react with the

heteropoly anion ($\text{PW}_{12}\text{O}_{40}^{3-}$) to form protons and reduced forms of anions (H^+ + $\text{PW}_{12}\text{O}_{40}^{4-}$).

Bifunctional zeolites possess in general Lewis acidic extra-framework alumina species, which develop during the introduction of protons and metal cations. The question to be addressed is whether it is possible to anchor a tungsten precursor onto these alumina sites in order to create Brønsted acidity similar to binary oxides. Additionally the sample has been sulfated in order to investigate whether a combination of both additives (primarily modifying the acid character of the catalysts) may result in an enhanced catalytic activity.

The second part of this chapter deals with the application of different sulfation precursors on zeolite MOR. Zeolite MOR has a significantly lower content of extra-framework sites compared with zeolite BEA and a restricted mono-dimensional pore system. The effect of the different sulfation processes on the acidic and structural properties as well as the influence on the catalytic activity is researched.

6.3 Experimental

6.3.1 Sample preparation

Zeolite Beta with an Si/Al ratio of 12.5 (H-BEA 25) was received from Süd-Chemie AG and was loaded with 0.5 wt % Pt by ion-exchange with aqueous $\text{Pt}(\text{NH}_3)_4(\text{OH})_2$ solution. A solution containing the appropriate amount of $\text{Pt}(\text{NH}_3)_4(\text{OH})_2$ and NH_4OH (corresponding to the concentration of protons in the sample) was added dropwise to the slurry at 40°C. After the ion exchange the solid was centrifuged, washed and freeze dried. The samples were calcined in air at 350°C for 16 h (heating rate 0.5°C/min) and finally reduced in H_2 at 300°C for 4 h. The sample is referred to as Pt-BEA.

The W-promoted samples were prepared by impregnation using an 0.05 mol/l ammonia metatungstate solution ($(\text{NH}_4)_6\text{H}_2\text{W}_{12}\text{O}_{40}\cdot n\text{H}_2\text{O}$). After freeze drying the samples were calcined in air at 350°C for 6 h (heating rate 0.5°C/min). The samples are referred to as Pt-BEA-W. The characterization of the tungsten concentration by X-ray spectroscopy resulted in a tungsten loading of 5.1 wt.%.

A fraction of the Pt-BEA-W catalyst was treated by gasphase sulfation procedure carried out after heating the samples in He atmosphere to 350°C (heating rate 7.5°C/min).

with a mixture containing 1.8 vol.% H₂S in H₂ in a plug flow reactor for 3h. Subsequently the samples were oxidized in air for 3h. The sample is referred to as Pt-BEA-WS.

The MOR 400 and MOR 800 samples were obtained by loading zeolite H-MOR (Zeolyst Co. - CBV 10 A, lot No. 1822-50) with 1 wt.% Pt using an H₂PtCl₆ solution. The samples were calcined at 400°C and 800°C for 6h, respectively (heating rate of 2K/min) and subsequently reduced at 400°C in hydrogen for 2h. Atomic absorption spectroscopy resulted in a ratio Si/Al of 6.2 for MOR 400 and 7.0 for MOR 800.

For the gasphase sulfation of MOR the samples were heated up in He to 350°C with a heating rate of 7.5°C/min and then purged with 1.8 vol.% H₂S in H₂ (S1) and 5.2 vol.% SO₂ in He (S2) at 350°C for 3h. Subsequently the catalysts were oxidized in air for another 3h. The aqueous sulfation (S3) of MOR was performed by immersing the catalyst in a (NH₄)₂SO₄ solution (0.05 mol/l) for 2h. The samples were filtered, dried and calcined at 400°C for 6h.

6.3.2 N₂ adsorption

The specific surface areas and pore volumes were determined by physisorption of nitrogen using a Sorptomatic 1990 Series instrument. About 300 mg of the sample were activated in vacuum at 350 °C for 90 min before nitrogen adsorption was carried out at a temperature of -196°C. The specific surface area was calculated according to the Brunauer-Emmet- Teller (BET) method. The pore volume was determined with the t-plot method.

6.3.3 Temperature programmed desorption (TPD)

Temperature programmed desorption was performed in a home built 6-fold parallel TPD system. The catalysts were activated by heating in vacuum to 350°C (rate 10°C/min) for 2 h. Ammonia was adsorbed at 150 °C with a partial pressure of 0.6 mbar for 1 h and subsequently the samples were evacuated at 10⁻³ mbar for 2 h in order to remove physisorbed molecules. For the TPD experiments the 6 samples were (sequentially) heated from 150°C to 800°C with a rate of 10°C/min and the species desorbing were monitored by mass spectrometry (*Balzers QME 200*). In each set of experiments a reference sample with known concentration of acid sites was used for calibrating the MS signal.

6.3.4 IR spectroscopy

IR spectra of adsorbed pyridine were measured from 3800 to 1100 cm^{-1} at a resolution of 4 cm^{-1} using a Perkin Elmer 2000 spectrometer and a high vacuum IR cell described previously [20]. The samples were prepared as self supported wafers, activated by heating in vacuum with a ramp of 10 $^{\circ}\text{C}/\text{min}$ to 350 $^{\circ}\text{C}$ and keeping it at that temperature for 60 min. After cooling the sample to 150 $^{\circ}\text{C}$ the spectrum of the activated zeolite was recorded. Pyridine was adsorbed at 150 $^{\circ}\text{C}$ with a partial pressure of 0.05 mbar for 30 min and the sample was subsequently evacuated for 90 min. The weight of the wafers was used for determining the mass per surface area necessary for calculating the concentration of Brønsted and Lewis acid sites according to the method published by Emeis [21].

6.3.5 Thermal gravimetry

The sorption isotherms of pentane for the Pt-BEA, Pt-BEA-W and Pt-BEA-WS samples were measured with a Setaram TG-DSC 111 thermoanalyzer. 20 mg of sample were first activated at 350 $^{\circ}\text{C}$ for 90 min with 10 K/min under UHV condition (10^{-5} mbar). After activation, the sorbate was introduced to the system up to 0.12 mbar at 50 $^{\circ}\text{C}$ with an increment of pressure of about 0.05 mbar. After reaching the equilibrium at each pressure, the weight of the adsorbed amount and the heat of adsorption were recorded. .

6.3.6 Catalytic studies

The catalytic activity was studied with a 20-fold parallel plug flow reactor system. The reactant gas flow and pressure of each reactor was controlled by individual digital mass flow controllers and back-pressure regulators, respectively. The liquid feed was adjusted and mixed with hydrogen by a digitally controlled evaporator - mixer. For the analysis of the products a HP-MicroGC (GC M200) was used, capable of separating aliphatic C_1 to C_6 hydrocarbons (including their isomers) in less than 2 min. The total pressures, flow rates, temperatures and alkane concentrations were varied automatically. For the kinetic experiments external diffusion limitations were experimentally excluded and the activity was determined under differential reaction conditions. All data recorded was stored in a relational MS Access database.

6.4 Results

6.4.1 Influence of tungsten precursor on zeolite acidity

Figure 1 shows the IR spectra of the parent BEA sample, BEA promoted with tungstate precursor and BEA promoted with tungstate precursor which was subsequently sulfated using $\text{H}_2\text{S}/\text{air}$. The Brønsted acidic character of the sample was investigated by analysing the bridging hydroxy groups at 3608 cm^{-1} and the intensity of the pyridine adsorbed on Brønsted acidic sites at 1545 cm^{-1} . All spectra were normalized to the intensity of the structure vibrations of the zeolite between $1750 - 2100\text{ cm}^{-1}$. The parent material (1) shows intensive bands at 3733 and 3743 cm^{-1} corresponding to silanol groups at defect sites and on the outer surface of the crystals. Promotion with tungsten clearly led to a reduction of the concentration of surface silanols (3743 cm^{-1}) while after sulfation the silanol groups were restored, while a severe reduction of the silanol groups at defect sites (3733 cm^{-1}) was observed. The quantitative evaluation of the silanol groups from the subtracted spectra of Pt-BEA-W and Pt-BEA-WS indicated that loss and formation of internal and external SiOH groups occurs in equal extents. A small band at 3660 cm^{-1} was observed for the Pt-BEA-WS sample, which indicating the presence of small amounts of OH linked to extra-lattice Al species. In [22] the band was assigned to monomeric and polymeric extra-framework species. After promoting the catalyst with tungstate precursor a reduction of the bridging hydroxy groups of the zeolite of ca. 20% was observed. However pyridine adsorption showed a slight increase of the Brønsted acidity. Furthermore, an increase of the internal silanol groups was observed. The concentration of Lewis acid sites showed a reduction of about 20%. Additionally, the spectra of the sample Pt-BEA-WS is included (3) in Figure 1. Sulfation of the tungstate promoted sample clearly enhances the number of bridging SiOHAl groups compared to Pt-BEA-W. Nevertheless, the original concentration of SiOHAl groups cannot be restored. Comparing the Pt-BEA-W sample with the sulfated Pt-BEA-WS, pyridine adsorption shows an enhancement of the concentration of Brønsted acid sites while the concentration of Lewis acid sites did not markedly change. Additionally a new band appeared at 1390 cm^{-1} for the sample Pt-BEA-WS which is assigned to the S=O stretching vibrations indicating the presence of sulfate species [6,12]. The M=O and M-O vibrations of hydrated surface metal oxide species generally occur below 1000 cm^{-1} [23], thus making it impossible to detect the Keggin units of the tungstate species on the zeolite due to a complete absorbance in the low frequency region.

Table 1: Acid site characterization.

Sample	Brønsted acidity (at 1545 cm^{-1}) [mmol/g]	Lewis acidity (at 1455 cm^{-1}) [mmol/g]	Ratio BAS/LAS [mol/mol]	Reduction of Si(OH)Al (3608 cm^{-1}) [mmol/g]
Pt-BEA	0.29	0.27	1.08	-
Pt-BEA-W	0.30	0.19	1.59	22%
Pt-BEA-WS	0.33	0.20	1.61	8%

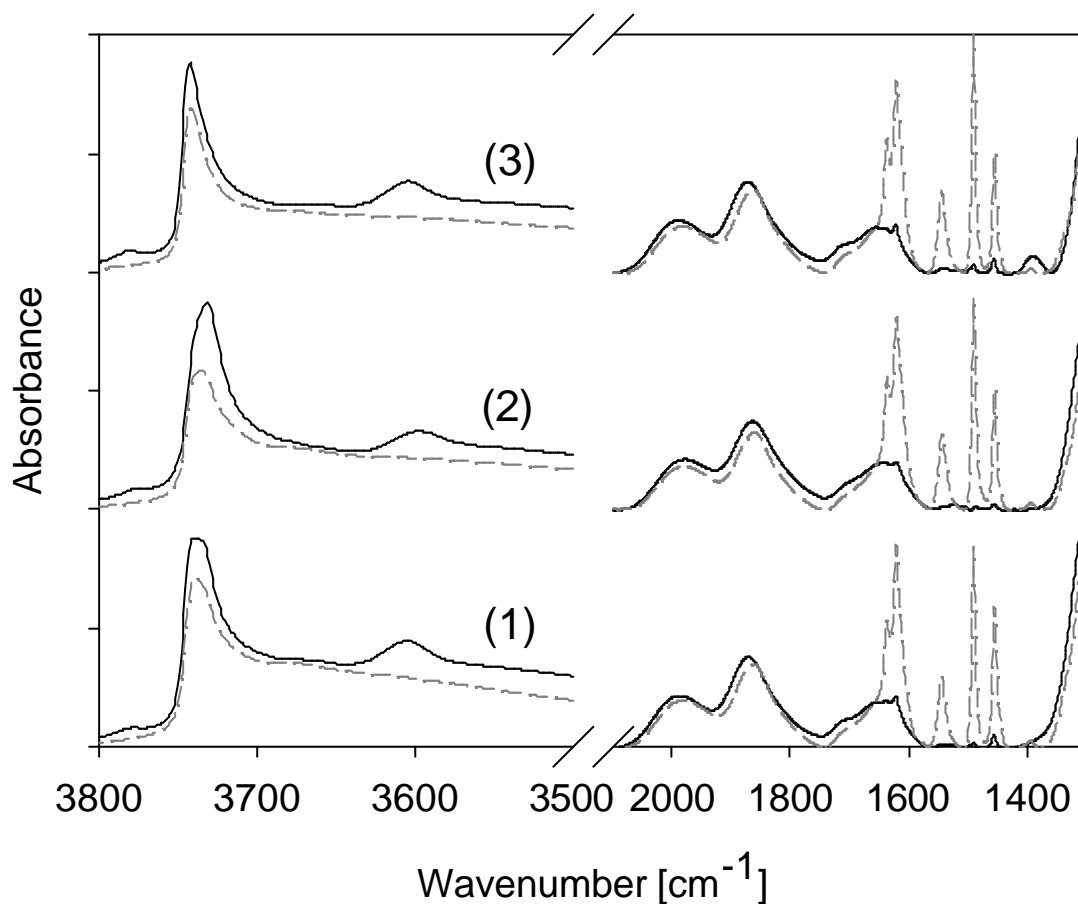


Figure 1: IR spectra for Pt-BEA (1), Pt-BEA-W (2) and Pt-BEA-WS (3) after activation (—) and after pyridine adsorption (----).

The strength of the acid sites was investigated using temperature programmed desorption of ammonia. Figure 2 shows the desorption profiles for the parent sample (Pt-BEA), the WO_x promoted sample (Pt-BEA-W) and the sample promoted with WO_x which was subsequently sulfated (Pt-BEA-WS). Two overlapping peaks for NH_3 desorption were observed indicating the presence of two sorption states of ammonia. For the parent material, the peaks were observed at *ca.* 350°C and at 550°C. The shape of the profiles

changed significantly after promoting the sample with WO_x . While the strength of the weak acid sites remained almost constant, the strength of the strong acid sites was slightly increased. Subsequent sulfation of the sample led to a reduction of the high temperature peak. However the sulfation treatment leads to an enhancement of the low temperature peak indicating a further change of the nature and strength of the acidic sites.

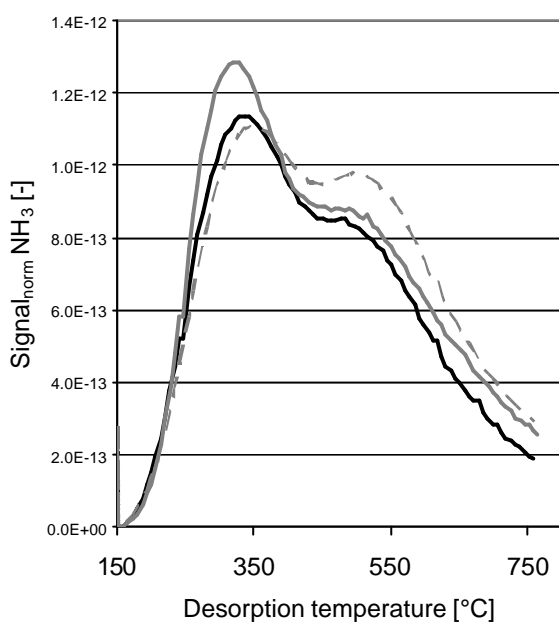


Figure 2: Ammonia TPD profiles for Pt-BEA (—), Pt-BEA-W (---) and Pt-BEA-WS (— · —).

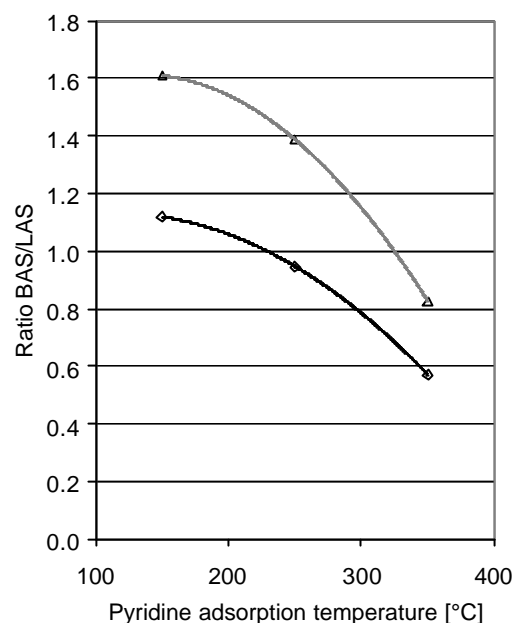


Figure 3: Ratio of Brønsted acid sites to Lewis acid sites for different adsorption temperature of pyridine for Pt-BEA (—◇—), Pt-BEA-W (---□---) and Pt-BEA-WS (—△—).

Figure 3 depicts the ratio between Brønsted and Lewis acid sites measured by pyridine adsorption ($\nu_{\text{BAS}} = 1545 \text{ cm}^{-1}$ and $\nu_{\text{LAS}} = 1455 \text{ cm}^{-1}$) at different temperatures. The results indicate that the ratio between Brønsted and Lewis acid sites is strongly increased after sulfation treatment of the promoted Pt-BEA sample. At higher adsorption temperatures the ratio of Brønsted to Lewis acid sites is generally decreasing, which indicates a lower strength of the Brønsted acid sites compared to the Lewis acid sites. The results show that the low temperature peak from the ammonia TPD corresponds to Brønsted acid sites while the high temperature peak is linked to Lewis acid sites. In addition, it is concluded that the WO_x precursor leads to the formation of additional strong Lewis acid sites which are converted to weak Brønsted acid sites after treatment with $\text{H}_2\text{S}/\text{air}$.

Pentane adsorption was followed by IR measurements for partial pressures between 0.04 and 10 mbar for Pt-BEA, Pt-BEA-W and Pt-BEA-WS. Figure 4 shows the spectra during pentane adsorption subtracted from the spectra of the activated samples. The sharp, negative bands at 3733-3743 cm^{-1} and 3608 cm^{-1} are assigned to pentane adsorbed on silanol groups and Brønsted acid sites, respectively. Pentane adsorption led to a perturbation of the hydroxy groups which lead to a shift of the frequency from 3785 to 3765 cm^{-1} for the AlOH groups from 3733-3743 cm^{-1} to *ca.* 3700 cm^{-1} for the SiOH groups and from 3608 to a (broad band) at *ca.* 3500 cm^{-1} for the SiOHAl groups. Additionally symmetric and asymmetric CH stretching vibrations (2800-3000 cm^{-1}) of CH_2 and CH_3 groups and their bending vibrations (1550-1550 cm^{-1}) were observed after sorption of pentane. Interaction of the pentane molecule with the Brønsted acid site is observed indicated by the band of the perturbed hydroxy group at around 3500 cm^{-1} .

The sorption isotherm of pentane of the SiOHAl groups was determined from the decrease of band at 3608 cm^{-1} and the maximum coverage was normalized to the concentration of the bridging hydroxy group present on the sample after the activation. Figure 5 compares the adsorption isotherms for pentane on the bridging hydroxy groups at 100°C and 250°C. Significant difference between the adsorption isotherms of the Pt-BEA, Pt-BEA-W and Pt-BEA-WS were not observed which indicates that the adsorption properties of the SiOHAl groups were similar. Additionally, the shift of the perturbed hydroxy group after adsorption of pentane was investigated for the three different materials. No perceivable difference in the strength of the hydroxy groups was observed for the Pt-BEA W and Pt-BEA-WS sample compared with the parent Pt-BEA.

For the adsorption isotherms measured at 250 °C a significantly lower coverage was observed as expected for the elevated temperatures. However, as the pressure dependant coverage (especially in the low pressure range) did not follow the expected devolution of a Langmuir isotherm, it is assumed irreversible blocking of the Brønsted acid sites occurs during pentane adsorption at the elevated temperatures. Kinetic results presented in Chapter 3 showed that the activity of BEA zeolite is significantly reduced in the absence of hydrogen. The formation of coke was shown to origin from oligomerization reaction resulting from alkenes reacting with carbenium ions. Increasing the pentane partial pressure only resulted in a slight enhancement of the coverage which levelled off for all samples at an acid site coverage of about 30%.

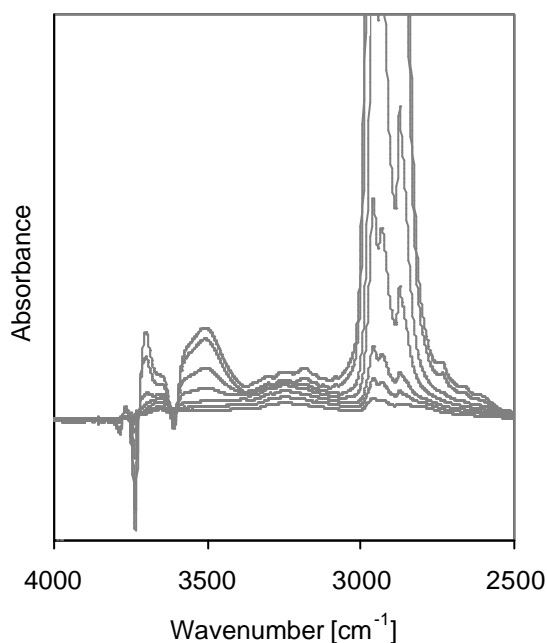


Figure 4: Subtracted IR spectra for pentane adsorbed on Pt-BEA at 100°C between 0.02-10 mbar.

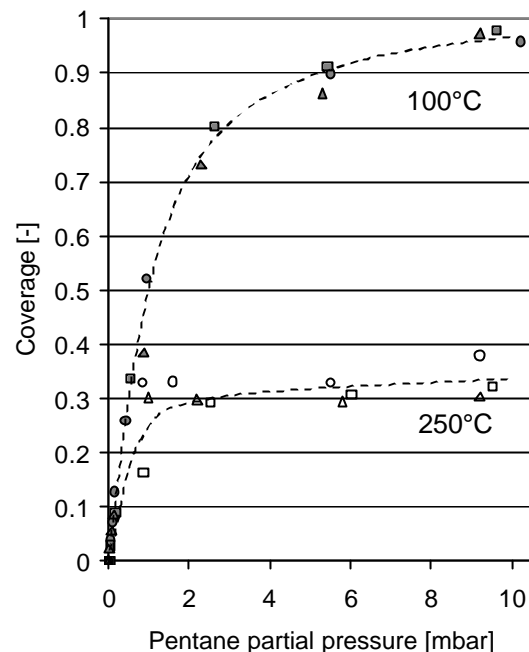


Figure 5: Adsorption isotherms for pentane adsorption on bridging hydroxy groups for Pt-BEA (●;○), Pt-BEA-W (■;□) and Pt-BEA-WS (▲;△) at (T=100°C, T=250°C).

Table 2: BET and kinetic parameters.

Sample	BET [m ² /g]	N ₂ - volume [cm ³ /g]	ΔH_{ads} [kJ/mol] ⁽¹⁾	Activation Energy (fresh) [kJ/mol]	Activation Energy (coked) [kJ/mol]
Pt-BEA	489	112	-57	133	159
Pt-BEA-W	480	110	-53	108	160
Pt-BEA-WS	464	106	-52	111	124

⁽¹⁾: measured for pentane by thermal gravimetry

6.4.2 Acidic characterization of zeolite mordenite

The surface OH and S=O groups present on the zeolite MOR 400 and MOR 800 after sulfation are shown in Figure 6 A, B and Figure 6 C, D, respectively. All spectra were normalized to the intensity of the structure vibrations of the zeolite between 1750 – 2100 cm⁻¹. For the parent MOR 400 two distinctive bands at 3743 cm⁻¹ (surface silanol groups [24]) and at 3608 cm⁻¹ (Brønsted acidic bridging hydroxy groups [24]) were observed.

Additionally a hardly noticeable band at 3785 cm^{-1} attributed to AlOH near to one or two SiOH groups was detected [25]. At lower wavenumbers (between $2050 - 1550\text{ cm}^{-1}$) the typical lattice vibration of the zeolite were observed. For the sulfated samples an intense band at 1385 cm^{-1} (S=O stretching frequency) was observed. It is interesting to note that the intensity of the band at 1385 cm^{-1} is correlated to the decrease of the concentration of the bridging hydroxy groups at 3608 cm^{-1} . The significantly higher concentration of sulfate compared with the BEA sample can be explained by a preferential adsorption of pentane in the side pockets due to an expected higher adsorption enthalpy in the narrow pores. While for the gasphase sulfation processes S1 and S2 a reduction of the intensity of the band of SiOHAl groups of 40% and 30 % was observed, the aqueous sulfation treatment S3 only reduced the concentration of the bridging hydroxy groups of about 10%. Furthermore a small band at 3660 cm^{-1} arises after the sulfation of the sample, which is assigned to OH groups linked to extra-framework Al species [26, 27] and indicates that during sulfation process the zeolite structure was partially dealuminated. The concentration of silanol groups on the outer surface was not (noticeably) affected during sulfation.

The comparison of the MOR 400 and MOR 800 sample shows that the intensity of the external silanol (3743 cm^{-1}) and AlOH groups (3785 cm^{-1}) was decreasing after calcinations at high temperature. Furthermore, the thermal treatment led to a significant reduction of the bridging hydroxy groups at 3608 cm^{-1} . Simultaneously the intensity of the OH groups linked to extra-framework Al increased (3660 cm^{-1}). Sulfation led to a minor enhancement of the band at 3608 cm^{-1} . Only a slight reduction in the region of the internal silanol groups at approximately 3733 cm^{-1} was obtained. Comparing the intensity of the band at 1385 cm^{-1} of the MOR 400 and MOR 800 sample a small reduction of the concentration of sulfate is observed for the sample calcined at high temperature.

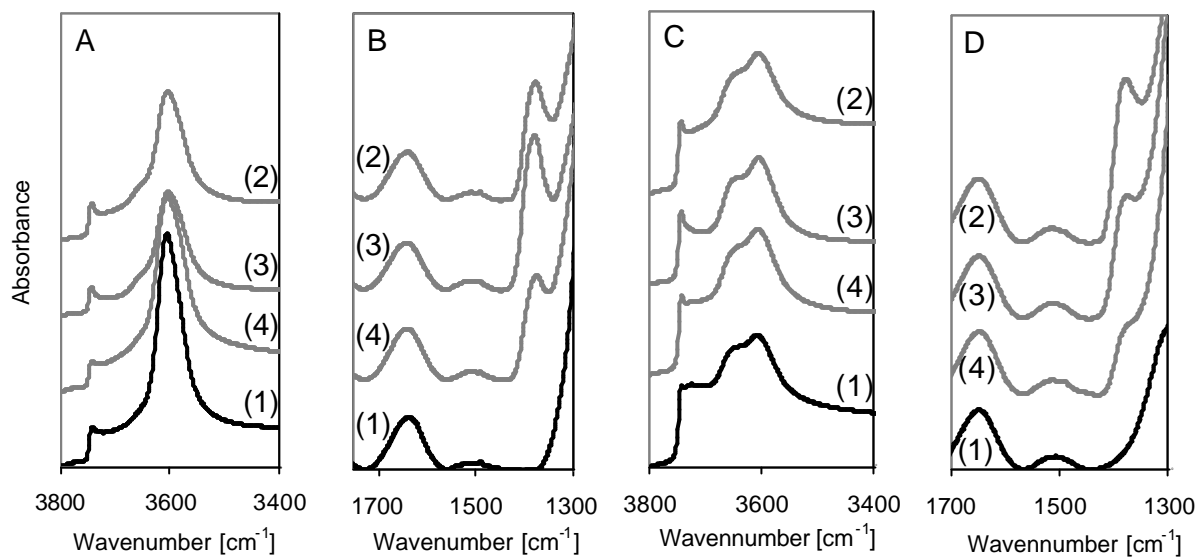


Figure 6: IR spectra for A, B: MOR 400 (1), MOR 400-S1 (2), MOR 400 S2 (3), MOR 400 S3 (4) and for C, B: MOR 800 (1), MOR 800-S1 (2), MOR 800 S2 (3) and MOR 800 S3 (4).

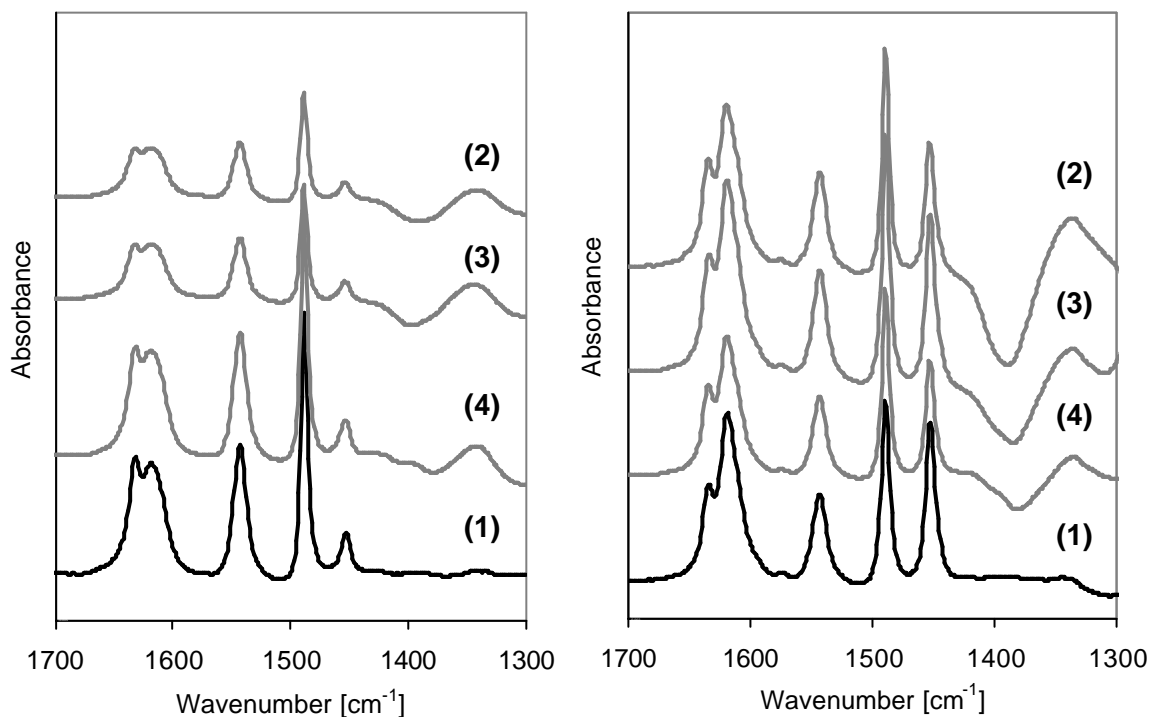


Figure 7: IR spectra for Pyridine adsorption for MOR 400 (left) and MOR 800 (right) parent MOR 400/500 (1), MOR 400/500 -S1 (2), MOR 400/500 S2 (3) and MOR 400/500 S3 (4).

The (subtracted) spectra before and after Pyridine adsorption for the sample MOR 400 and MOR 800 and the sulfated samples are compared Figure 7. Pyridine adsorption led to the typical band at 1455 cm^{-1} , 1489 cm^{-1} and 1544 cm^{-1} . The bands are assigned to coordinative bound pyridine on Lewis acid sites, to pyridine interacting with both Brønsted and Lewis acid sites and pyridine adsorbed on Brønsted acid sites. For the MOR 400 sample a significant reduction of the concentration of Brønsted acid sites was observed for sulfation via $\text{H}_2\text{S}/\text{air}$ and SO_2/air . In contrast the sample treated with aqueous $(\text{NH}_4)_2\text{SO}_4$ showed a similar intensity of the stretching vibration of the pyridinium ion at 1544 cm^{-1} . Furthermore the S=O band observed for the sulfated samples at 1385 cm^{-1} was perturbed to a stretching frequency of 1335 cm^{-1} . Comparing the intensity of the sulfate band before pyridine adsorption with the fraction that is perturbed after pyridine adsorption shows that not all of the sulfate species present on the sample interact with the probe molecule.

Table 3: Summary of characterization data for MOR samples.

	S-precursor	BAS ¹⁾ [mmol/g]	LAS ²⁾ [mmol/g]	Accessibility of Si(OH)Al groups	Apparent activation energy [kJ/mol]
MOR 400	-	0.310	0.042	40%	97
MOR 400 S1	$\text{H}_2\text{S}/\text{air}$	0.133	0.021	19%	83
MOR 400 S2	SO_2/air	0.112	0.020	17%	80
MOR 400 S3	$(\text{NH}_4)_2\text{SO}_4/\text{air}$	0.299	0.039	32%	86
MOR 800	-	0.088	0.086	45%	62
MOR 800 S1	$\text{H}_2\text{S}/\text{air}$	0.096	0.071	29%	73
MOR 800 S2	SO_2/air	0.104	0.091	22%	70
MOR 800 S3	$(\text{NH}_4)_2\text{SO}_4/\text{air}$	0.099	0.054	36%	66

¹⁾: concentration of accessible Brønsted acid sites

²⁾: concentration of accessible Lewis acid sites

For the MOR 800 sample significantly low intensities of the pyridine stretching vibrations had been observed. All sulfated samples possessed a higher concentration of Brønsted acid sites. The concentration of acid sites and the estimation of the accessibility of the bridging hydroxy groups of the zeolite are summarized in Table 3. The values had been determined by comparing the area of the band at 3608 cm^{-1} before and after the adsorption of pyridine. It is shown that for both parent materials, MOR 400 and MOR 800, only 40-45% of the Brønsted acidic SiOHAl groups are accessible for the pyridine molecule. After sulfation using the H_2S and SO_2 the access of pyridine to the SiOHAl groups was significantly reduced. The aqueous sulfation method *via* $(\text{NH}_4)_2\text{SO}_4$ led to a minor pronounced reduction of the accessibility of the SiOHAl sites for the MOR 400. A similar behaviour was observed for the MOR 800 samples.

6.4.3 Activity studies

Isomerization activity of the sample was measured in a temperature range between 250°C and 320°C at a pressure of 4 bar and a WHSV of 30 h^{-1} . The activity of the Pt-BEA, Pt-BEA-W and Pt-BEA-WS at 290°C is compared in Figure 8. An enhanced isomerization activity was observed for the sample promoted with the tungstate precursor (Pt-BEA-W) and the subsequently sulfated, tungstate promoted sample (Pt-BEA-WS). In addition poisoning experiments were carried out by treating the catalyst with pentane under helium atmosphere. Due to the lack of hydrogen all catalysts rapidly deactivated within 2 h to conversion levels below 3% at 300°C . The deactivated samples were subsequently reactivated *in situ* at a temperature of 350°C in hydrogen for 3h. After that, another temperature run for a pentane/ hydrogen mixture was performed. Figure 8 shows that the activity of the samples was severely reduced after the deactivation run pointing to an irreversible blocking of the sites. However, the same sequence of activity as before the deactivation run was observed.

The activity of the Pt-BEA, Pt-BEA-W and Pt-BEA-WS catalysts after activation (fresh condition) and after coking with pentane in helium (deactivated) are compared in Figure 9. In order to investigate the deactivation of the catalysts, the apparent activation energy were measured with increasing temperatures in the range between 250°C and 320°C followed measurements with decreasing the temperatures from 320°C to 260°C . For the fresh catalysts the activity was the same for both series of experiments during a 15 h run. The apparent activation energies for the fresh and the deactivated samples are

summarized in Table 2. It is interesting to note that the apparent activation energy was significantly reduced for the catalyst promoted with the metatungstate precursor. After deactivation the activation energy increased for all samples indicating a blockage of the strong acid sites. However, a less pronounced enhancement of the apparent activation energy was observed for the Pt-BEA-WS sample.

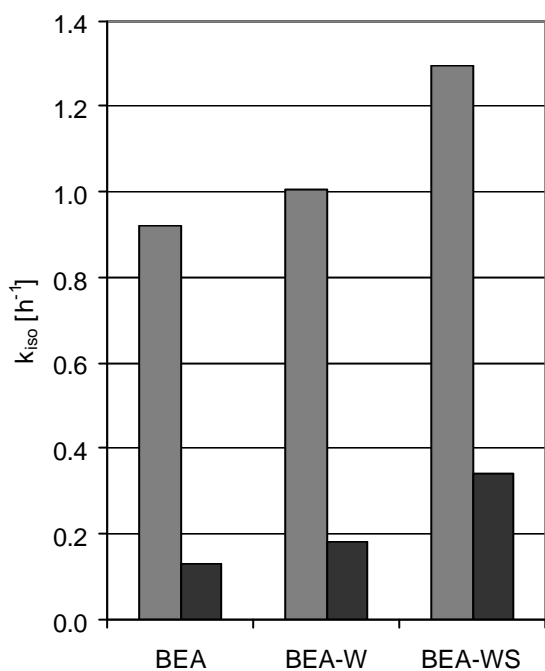


Figure 8: Isomerization activity at T=290°C for activated, fresh catalyst (\square) and samples previously deactivated (\blacksquare).

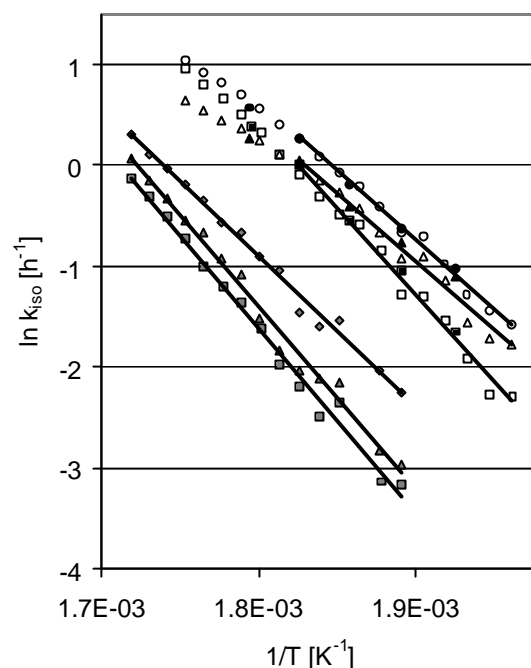


Figure 9: Arrhenius plots for Pt-BEA (\square), Pt-BEA-W (\triangle) and Pt-BEA-WS (\circ) for fresh sample during upward temperature run ($\square, \triangle, \circ$) and downward temperature run ($\blacksquare, \blacktriangle, \bullet$) and previously deactivated samples ($\square, \triangle, \diamond$).

The isomerization activity of the sulfated and non sulfated mordenite samples is compared in Figure 10. For MOR 400 and MOR 800 the temperature treatment significantly reduced the isomerization activity. The procedure applied during the sulfation process strongly influenced the isomerization activity. For the procedures S1 (H₂S/air) and S2 (SO₂/air) the isomerization activity was significantly reduced, while treatment with (NH₃)₂SO₄ led to a slight increase of the isomerization activity. Sulfation of the thermally treated MOR 800 sample enhanced furthermore the isomerization activity independently of the sulfur precursor. Figure 11 shows the temperature dependency of the isomerization activity between 250°C and 320°C. In general it can be seen that the sulfation treatment led

to a slight reduction of the apparent activation energies (summarized in Table 3), which can be rather attributed to an enhanced of the concentration of acid sites rather than to a change in adsorption properties.

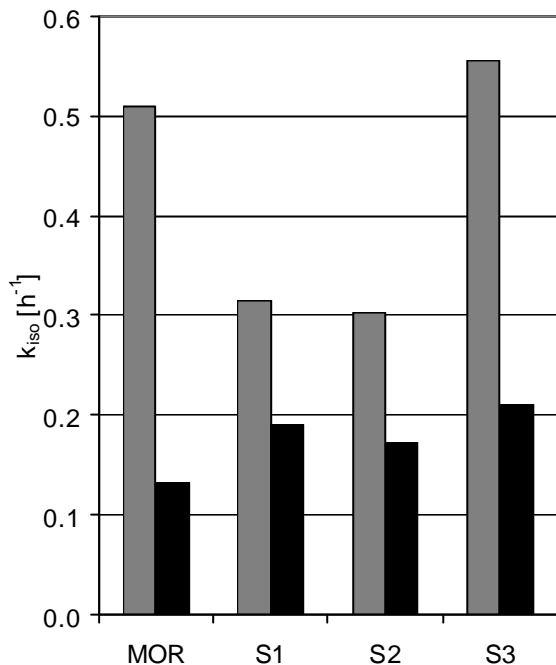


Figure 10: Isomerization activity at T=290°C for MOR 400 (□) and MOR 800 (■).

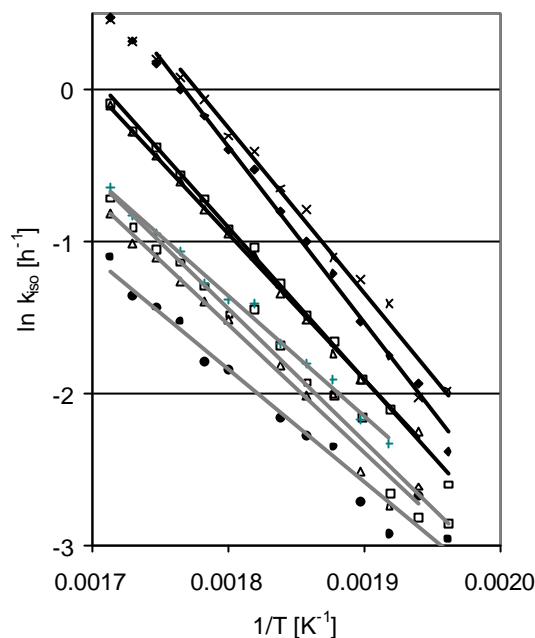


Figure 11: Arrhenius plots for MOR 400 (—) and MOR 800 (—) (◆): S1 (□), S2 (△), S3 (×).

6.5 Discussion

6.5.1 Influence of tungsten precursor and subsequent sulfation process on the acidic properties

IR studies of pyridine adsorption and ammonia temperature programmed desorption showed that the tungsten precursor does not severely influence the overall Brønsted acidity of the sample. Although the total concentration of Brønsted acid sites was slightly enhanced, the partial removal from Al³⁺ from framework positions led to a reduction of the bridging hydroxy groups. Therefore, we conclude that additional Brønsted acid sites were formed on the tungsten species, which compensates the loss Brønsted acid sites resulting from the zeolite dealumination. The concentrations of Lewis acid sites determined from the

IR and TPD experiments appear to be conflicting. Sorption of pyridine shows a reduction of the Lewis acidity, however the high temperature peak in the ammonia TPD (assigned to strong Lewis acid sites) is enhanced. Since pyridine is a considerably larger molecule than ammonia it is conceivable that the concentration of the Lewis acid sites after the tungsten impregnation is underestimated during pyridine adsorption due to sterical reasons. The BET measurements using nitrogen as probe adsorbent (molecular cross-section area of 0.162 nm^2) showed neither a significant change in surface area nor in pore volume. For the median pore radius only a minor reduction from 3.8 to 3.6 Å was observed after tungsten impregnation, indicating that the effect of pore blocking is not relevant and, therefore, it is more likely that Lewis acidic clusters have been formed and due to the different space requirements of the probe molecules (pyridine and ammonia), a different content of the Lewis acid sites are determined. We would further like to speculate that such Lewis acidic clusters might be bi- or poly tungstate species formed on the zeolite similar to those observed on tungsten oxide on alumina [28], which possess both Brønsted and Lewis acidity. The formation of extra Lewis and Brønsted sites was also observed for $\text{WO}_x\text{-CeO}_2$ [29], where the Lewis acid character was assigned to the formation of W=O species, while the formation of Brønsted acid sites was related to hydrogen attached to tetrahedral tungstate groups or to distorted octahedral groups in WO_3 . Additionally it was shown on $\text{WO}_x\text{-ZrO}_2$ that the formation of strong acid sites requires the formation of WO_x clusters [30].

Gasphase sulfation of the tungsten promoted sample showed an enhancement of the concentration of Brønsted acid sites of about 13%. The increase in acidity is attributed to the formation of sulfate species which were identified by the appearance of an S=O band in the IR spectra for the Pt-BEA-WS sample (Figure 1). The TPD results indicate that the additional Lewis acid sites of the Pt-BEA-W sample are converted to Brønsted acid sites. The fact that the sulfation process restores the Lewis acidity of the parent Pt-BEA sample suggests that the sulfation primarily occurs on the WO_x domains. For tungsten trioxide modified sulfated zirconia an increase of acidity and isomerization activity was observed compared with non-promoted sulfated zirconia [31]. However the enhanced activity was ascribed to a higher concentration of sulfate species rather than an interaction of the sulfate ion with WO_3 . Laperdrix [32] concluded from the fact that the sulphate content on tungsten promoted alumina is reduced with the reverse of the doping content, that the sulphate species are located on the uncovered alumina support. Additionally it is well known that supported tungsten catalysts present oxidation properties [33] and hence might enhance the

formation of SO_3 reacting to sulfate species. Tungsten oxide species were suggested to act as adsorption centres for SO_2 which leads to an enhanced activity for the oxidation to SO_3 [34]. Therefore it is also plausible that the primary function of the tungsten species is to catalyze the formation of sulfate species.

6.5.2 Influence of tungsten precursor and subsequent sulfation process on the adsorption and catalytic properties

Adsorption properties of the materials were studied using thermal gravimetry and IR spectroscopy. Pyridine adsorption showed that the ratio between the Brønsted and Lewis acid sites is higher for the samples Pt-BEA-W and Pt-BEA-WS (Table 1). Since pentane adsorbs stronger on the Lewis acid sites than on the Brønsted acid sites the reduction of the heat of adsorption measured by gravimetry is likely to be due to the shift of the type of acid sites. Hence the reduction of the heat of adsorption on the tungstate loaded samples is not necessarily due to a change of the strength of the kinetic relevant Brønsted acid sites. The adsorption measurements furthermore showed that for the characterization of the acid sites, the pyridine molecule (which shows an increase of the ratio between BAS /LAS) seems to be more appropriate than the ammonia molecule due to its resembling molecular size and accessibility of the reactants used.

The analysis of the hydroxy groups at 3608 cm^{-1} during pentane adsorption did not show a significant change of the strength of these sites. An induced polarization of the bridging OH groups due to the high electronegativity of the sulfur can be excluded as a shift of the hydroxy group at 3608 cm^{-1} was not observed. Additionally, the adsorption behavior of pentane on the bridging hydroxy groups was the same for Pt-BEA, Pt-BEA-W and Pt-BEA-WS. However the isomerization activity measurements showed that the apparent activation energy was reduced for the samples treated with the tungsten precursor. Since the Pt-BEA-W showed a slightly enhanced concentration of Brønsted acid sites it is concluded that the reduction of the apparent activation energy is due to an enhancement of the average strength of the kinetic relevant Brønsted acid sites, which are affiliated with the additional tungstate sites. Additionally it has to be considered that under the reducing atmosphere an enhanced concentration of OH groups might be formed on the bi- or polytungstate species due to a conversion of the Lewis acidic into Brønsted acidic species. In *o*-xylene isomerization the role of H_2 was claimed to form $\text{H}^{\delta+}(\text{WO}_3)_n^{\delta-}$ species with acidic OH groups [35]. In [36] it was proposed that on Pt promoted WO_x/ZrO_2 the role of

Pt might be both dehydrogenation activity for the alkane activation and increase in Brønsted acidity by H^+ sites generated by hydrogen spill over. Hence the tungstated species may possess different acidic properties under reaction condition during pentane hydroisomerization. In fact, for both Pt-BEA-W and Pt-BEA-WS, a higher isomerization activity was observed than is expected from the concentration of Brønsted acid sites.

Additionally, the comparison of the Pt-BEA-WS sample with the sample Pt-BEA-S shows that an enhancement of the activity is obtained by the addition of the tungsten precursor compared to the unpromoted sulfated samples. It is therefore concluded that tungsten species possess strong Brønsted acidic groups that are active for the pentane isomerization and that it is possible to combine both promoters tungsten and sulfate species for enhancing the acidic and catalytic properties for Pt loaded zeolite BEA.

6.5.3 Influence of different sulfation precursors on the acidic properties of zeolite MOR

The effect of different sulfation methods on the acidic properties of a non-optimized zeolite mordenite was investigated by IR spectroscopy. Contrary to zeolite beta, the pore system of mordenite consists of two channel types. Large channels with a 12 member oxygen ring opening of $7.0 \times 6.5 \text{ \AA}$ (main channel) and side pockets with 8 member oxygen ring opening of $3.4 \times 4.8 \text{ \AA}$. Therefore large molecules (C_3H_8 , pyridine) are only capable to diffuse mono-dimensionally through the channel system, hence diffusion limitation may be critical. For MOR 400 it was shown that it is possible to incorporate sulfate species on the zeolite for both gasphase and aqueous sulfation route. Sulfation led to a partial dealumination of the zeolite framework, which induced a reduction of the bridging hydroxy groups and the formation of AlOH groups on extra-lattice sites. For alumina treated with H_2SO_4 it was observed that the surface area strongly depends on the sulphur loading. High loadings of sulfate lead to a reduction of the surface area associated with crystallization and pore collapse upon the formation of bulk $Al_2(SO_4)_3 \cdot H_2O$ [37]. Since the reduction of the hydroxy groups was the more pronounced the higher the sulfate content it is conceivable that for the samples with high sulphur loading the sulfate species are formed by extraction of framework alumina thus leading to a reduction of bridging hydroxys. In addition a reduction of the accessibility of the remaining bridging hydroxy groups was observed which points to an additional blocking of the pore system by the sulfate species. The access to the sulfate species was limited as pyridine adsorption did not lead to a

complete perturbation of the S=O band, which furthermore confirms that the sulfation process led to a severe blocking of the channel system. The diffusion of H₂S and SO₂ into the side pockets lead to the formation of non-accessible sulfate species, which furthermore lead to the destruction of the framework in a similar way as observed for the growth of metal particles in zeolite MOR [38]. However, as already observed for the BEA samples the reduction of acidity estimated from the loss of bridging hydroxy groups due to dealumination or blocking was higher than the Brønsted acidity determined from pyridine adsorption, which indicates the presence of additional sites affiliated with the sulfate species. Brønsted acidic S-OH groups were proposed in [12, 39], which are usually strongly hydrogen-bonded to the surface leading to very broad OH bands [40, 41].

The influence of the sulfation process on thermal treated MOR 800 was distinctively different. The catalytic activity of zeolite MOR can be assumed to depend on the number of available acid sites. It is well known that upon dealumination of the zeolites, it is possible to create a secondary system of pore channels which enhance accessibility and diffusivity. Instead of the commonly applied subsequent acid leaching, the sulfation treatment was directly carried out since (i) the formed extra-framework species potentially act as sorption sites for anchoring sulfate species and (ii) in order to study whether a removal of aluminum species occurs during the sulfation, which can lead to an enhanced accessibility of the pore structure. The thermal treated MOR 800 showed a significant reduction of the bridging hydroxy and the formation of hydroxy groups on extra-framework aluminous species. Only a slight enhancement of the accessibility of the bridging hydroxy groups was observed. Sulfation led to a minor enhancement of the Si(OH)Al bands, which can be explained by the removal of blocking aluminum sites, which was also observed for zeolite BEA (see Chapter 4 and 5). However due to a reduced accessibility of the site after sulfation a slight reduction of the bridging hydroxy groups was observed. Nevertheless the total concentration of Brønsted acid sites was enhanced, which indicates that for low concentration of bridging hydroxys and probably a sufficient amount of aluminum species, the sulfation process beneficially influences the concentration of Brønsted acid sites. The reason for this is possibly also due to the fact that the dealuminated MOR possesses high contributions of γ -Al₂O₃ for which it was shown by a number of authors that incorporation of sulfate species leads to the formation Brønsted acidity [8, 42, 43]. However it was shown that neither the aqueous nor the gasphase sulfation process enables an enhanced accessibility of the acid sites though a distinctive impact of the integrity of the zeolite framework was observed.

6.5.4 Comparison of the isomerization activity of zeolite MOR treated with different sulfation precursors

The effect of the sulfation procedures on the isomerization activity and the apparent activation energies was studied for the samples MOR 400 and MOR 800. The samples showed a lower apparent activation energy compared with the zeolite BEA samples. In general the reduction of the apparent activation energy can be explained by two scenarios. (i) an enhancement of the adsorption enthalpy due to the presence of stronger acid sites and (ii) the presence of diffusion limitations in the restricted area inside the pore system of zeolite MOR, which can also lead to the occurrence of single-file diffusion, thus reducing the apparent activation energy. In [44] the acid strength on zeolite MOR was found to be higher than on BEA which would result in an increase in the adsorption enthalpy reducing the apparent activation energy. However restricted motion in zeolite MOR is likely as in the one dimensional micropores the mutual passage of the reactants is critical. Although the mordenite samples possessed a higher concentration of acid sites than the zeolite BEA a reduction of catalytic activity was observed. It is thus concluded that the reduction of the apparent activation energy is rather due to the appearance of diffusion limitations than an enhancement of acid site strength. Sulfation of MOR 400 leads to a blocking of the pore system which corresponds to a reduction in the apparent activation energy due to more pronounced diffusion restrictions. For the dealuminated MOR 800 on the other hand an increase of the apparent activation energy was observed though the access to the bridging hydroxys was reduced. It hence is proposed that the formation of active sulfate species on extra lattice alumina phases might have a less restricted access which compensated the loss of the accessibility of the few remaining bridging hydroxy groups. In Figure 12 it is shown that the improvement in isomerization activity does not linearly correlate with the concentration of acid sites. Especially for the MOR 400 samples a significant reduction of the slope in the diagram is observed which indicates a restricted access of the Brønsted acid sites. For comparison the BEA sample with a comparable acid site concentration possesses a significantly higher activity. The fact that the sample MOR 400 S3 possesses a greater activity than expected from its acidity can be explained by a partial reduction of blocking sulfate groups during the hydroisomerization run. Additionally Figure 12 shows that the curve does not intersect in the point of origin which also indicates the presence of diffusion limitations as *i.e.* reacted molecules have to pass active centers in order to give access to the educts.

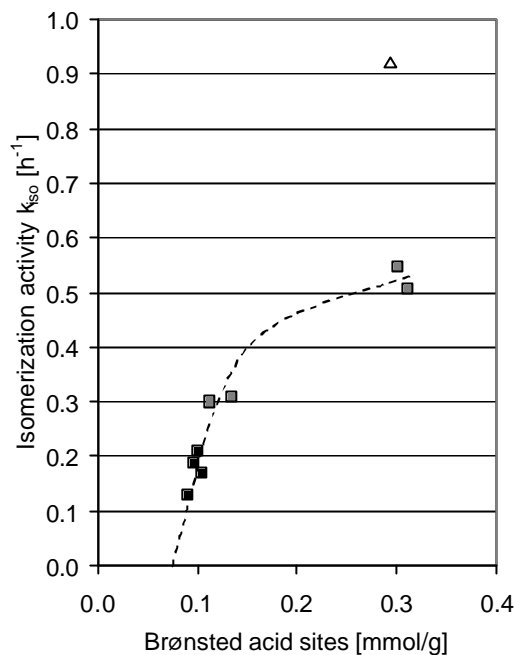


Figure 12: Correlation of isomerization activity and Brønsted acidity for MOR 400 (\square); MOR 800 (\blacksquare) and Pt-BEA (\triangle).

6.6 Conclusion

The effect of tungsten impregnation on Pt loaded zeolite BEA on isomerization activity and the gasphase sulfation process was studied. Tungsten impregnation led to an enhancement of Lewis acidity which was attributed to the formation of poly-tungstate clusters. The overall Brønsted acid sites density did not change. However as a severe reduction of the bridging hydroxy groups of the zeolite was observed it was proposed that additional, strong Brønsted acid sites are formed compensating the loss of the zeolite acid sites. During pentane hydroisomerization reaction a slightly higher isomerization activity and reduction of the apparent activation energy was observed. Furtheron it was shown that sulfation of the tungstated samples led to a further increase of the isomerization activity, which shows that both acidity promoters can be combined for the enhancement of acidity.

The isomerization activity of zeolite MOR was shown to be restricted by diffusion limitations indicated by a relatively low activity compared to its Brønsted acid site concentration and a low apparent activation energy. Sulfation of zeolite MOR was shown to severely influence the structural properties of the zeolite. The sulfation process did not improve diffusivity in the zeolite. High contents of sulfate led to a significant reduction of the bridging hydroxys due to a partial dealumination of the framework. Furthermore sulfate groups reduced the accessibility of the pore system. However for mildly sulfated

samples it was possible to slightly increase the isomerization activity by the incorporation of active sulfate species. An increase of the isomerization activity was observed for the dealuminated samples independent of sulphur precursor and content.

6.7 Acknowledgements

The financial support by Bundesministerium für Bildung und Forschung Project (BMBF:03C0307D) is gratefully acknowledged. The authors would like to thank Xaver Hecht for BET measurements and Long Jiang for the support of the characterisation of the samples.

REFERENCES

- [1] H.K. Kouwenhoven, H.J.A. van Helden, U.S. Pat. 1189850 (1970).
- [2] A. van de Runstraat, J. A. Kamp, P.J. Stobbelaar, J. Van Grondelle, S. Krijnen, R. A van Santen, *J. Catal.* 171, 77 (1997).
- [3] J.F. Allain, P. Magnoux, Ph. Schulz, M. Guisnet, *Appl. Catal. A: Gen* 152, 221 (1997).
- [4] W.W. Kaeding, C. Chu, L.B. Young, B. Weinstein, S.A. Butter, *J. Catal.* 67, 159 (1981)
- [5] A. Jentys, G. Rumpelmayr, J.A. Lercher, *Appl. Catal.* 53, 299 (1989)
- [6] T. Yamaguchi, T. Jin, K. Tanabe, *J. Phys. Chem.* 90, 3148 (1986).
- [7] D. E. Gawthorpe, A. F. Lee, K. Wilson, *Phys. Chem. Chem. Phys.* 6, 3907 (2004)
- [8] W. Przystajko, R. Fiedorow, I.G. Dalla Lana, *Appl. Catal.* 15, 265 (1985).
- [9] K. Otsuka, A. Morikawa, *J. Catal.* 56, 88 (1979).
- [10] T. Lei, J.S. Xu, Z. Gao, *Mat. Chem. Phys.* 60, 177 (1999).
- [11] R. Covini, V. Fattore, N. Giordano, *J. Catal.* 7, 126 (1967)
- [12] O. Saur, M. Bensitel, A.B. Mohammed Saad, J.C. Lavalley, C.P. Tripp, B.A. Morrow, *J. Catal.* 99, 104 (1986).
- [13] J. Macht, C.D. Baertsch, M. May-Lozano, S. L. Soled, Y. Wang, E. Iglesia, *J. Catal.* 227, 479 (2004).
- [14] A.C. Butler, C.P. Nicolaidis, *Catal. Today* 18, 443 (1993).
- [15] V.M. Benitez, C.A. Querini, N.S. Figoli, R.A. Comelli, *Appl. Catal. A: Gen.* 178, 205 (1999).
- [16] D. Scheithauer, R.K. Grasselli, H. Knoeinger, *Langmuir* 14, 3019 (1998).

-
- [17] D. Scheithauer, T.-K. Cheung, R.E. Jentoft, R.K. Grasselli, B.C. Gates, H. Knoetzing, *J. Catal.* 180, 1 (1998).
- [18] Y. Ono; *Catal. Today*, 81, 3 (2003).
- [19] Y. Ono, M. Taguchi, Gerille, S. Suzuki, T. Baba, *Stud. Catal. Surf. Sci.* 20, 167 (1985).
- [20] J.A. Lercher, Ch. Gründling, G. Eder-Mirth, *Catal. Today* 27, 353 (1996).
- [21] C.A. Emeis, *J. Catal.* 141, 347 (1993).
- [22] J.P. Marques, I. Gener, P. Ayrault, J.C. Bordado, J.M. Lopes, F.R. Ribeiro, M. Guisnet, *C.R. Chimie* 8, 399 (2005).
- [23] I.E. Wachs, *Catal. Today* 27, 437 (1996).
- [24] A. Jentys, J.A. Lercher, in *Introduction to Zeolite Science and Practice* (2nd Edition).
- [25] I. Kiricsi, C. Flego, G. Pazzuconi, W.O. Parker Jr. R. Millini, C. Perego, G. Bellussi, *J. Phys. Chem.* 98, 4627 (1999).
- [26] Guisnet, M., Ayrault, P., Datka, J., *Polish J. Chem.* 71, 1445 (1997).
- [27] J. Datka, B. Sulikowski, B. Gil, *J. Phys. Chem.* 100, 11242 (1996).
- [28] L.H. Gielgens, M.G.H. van Kampen, M.M. Broek, R. van Harveld, V. Ponc, J. *Catal.* 154, 201 (1995).
- [29] A.-S. Marnede, E. Payen, P. Grange, G. Poncelet, A. Ion, M. Alifanti, V.I. Parvulescu, *J. Catal.* 223, 1 (2004).
- [30] M. Scheithauer, T.-K. Cheung, R.E. Jentoft, R.K. Grasselli, B.C. Gates, H. Knötzinger, *J. Catal.* 180, 1 (1998).
- [31] Y.-Y. Huang, B.Y. Zhao, Y.C. Xie, *Appl. Catal. A: Gen.* 171, 75 (1998).
- [32] E. Laperdrix, A. Sahibed-dine, G. Costentin, O. Saur, M. Bensitel, C. Nedez, A.B. M. Saad, J.C. Lavalley, *Appl. Catal. B: Environ.* 26, 71 (2000).
- [33] J.P. Dunn, P.R. Koppula, H.G. Strenger, I.E. Wachs, *Appl. Catal. B: Environ.* 19, 103 (1998).
- [34] S.T. Hoo, S.D. Yim, I.-S. Nam, S.-W. Ham, J.-B. Lee, *Appl. Catal. B: Environ.* 44, 237 (2003).
- [35] C.D. Baertsch, S.L. Soled, E. Iglesia, *J. Phys. Chem. B* 105, 1320 (2001).
- [36] S.V. Filimonova, A.V. Nosov, M. Scheithauer, H. Knötzinger, *J. Catal.* 198, 89 (2001).
- [37] D.E. Gawthrope, A.F. Lee, K. Wilson, *Phys. Chem. Chem. Phys.* 4, 3907 (2004).
- [38] B.T. Carvill, B.A. Lerner, B.J. Adelman, D.C., Tomczak, W.M.H. Sachtler, *J. Catal.* 144,1 (1993).
- [39] M.L. Guzman-Castillo, E. Lopez-Salinas, J.J. Fripiat, J. Sanchez-Valente, F. Hernandez-Beltran, A. Rodriguez-Hernandez, J. Navarrete-Bolanos, *J. Catal.* 220, 317 (2003).

-
- [40] X. Li, K. Nagaoka, J.A. Lercher, *J. Catal.* 227, 130 (2004).
- [41] M. Lion, M. Maache, J.C. Lavalley, G. Ramis, G. Busca, P.F. Rossi, V. Lorenzelli, *J. Mol. Struct.* 218, 417 (1990).
- [42] M. Waqif, J. Bachelier, O. Saur, J.-C. Lavalley, *J. Mol. Catal.* 72, 127 (1992).
- [43] A. Auroux, A. Gervasini, *Ads. Scien. Techn.* Vol. 21, 8 (2003).
- [44] K.-J. Chao, H.-C. Wu, L.-J. Leu, *Appl. Catal. A: Gen* 143, 223 (1996).

Chapter 7

7.1 SUMMARY

Iso-Pentanes and hexanes are important components of high octane motor fuels, which are produced to a significant extent *via* hydroisomerization of the n-alkanes. Interest in the isomerization process heightens due to more severe environmental legislation which requires the reduction of harmful compounds such as aromatics and oxygenates, which so far were used as octane boosters. The aim of the work described was to provide a substantiated knowledge of the isomerization reaction proceeding on a bifunctional zeolite catalyst and a way of optimizing isomerization activity and selectivity.

Pentane hydroisomerization was shown to be an equilibrium limited reaction with a reaction enthalpy of -7 kJ/mol. Hence at low reaction temperatures higher isomerization yields can be achieved. In chapter 3 the role of platinum for the isomerization stability, activity and selectivity was studied. It was concluded that platinum is essential on the zeolite to activate the pentane molecule by providing dehydrogenation capability. However for high olefin concentrations catalyst deactivation occurs through oligomerization indicated by high contents of iso-butane and iso-hexanes, thus hydrogen is essential for catalyst stability by hydrogenating coke precursors and adjusting the olefin concentration. Hence stable isomerization activity was only observed in the presence of Pt and hydrogen. According to the classical mechanism a kinetic approach was derived which showed that the reaction is limited on the acidic sites for a ratio of Pt_s/H^+_{BAS} higher than 0.033. Hence for the given ratio Pt_s/H^+_{BAS} , platinum did not influence the isomerization activity. Temperature increasing and decreasing experiments did not show hysteresis curves, therefore it was concluded that no deactivation occurs on the investigated catalyst. The reaction orders of hydrogen and pentane were fitted to $n_{H_2}=-1$ and $n_{C_5}=+1$ respectively. Though Pt did not have an influence on isomerization activity a severe reduction of the isomerization selectivity was observed with increasing metal content. The origin of the side reaction was identified as metal catalyzed hydrogenolysis. The product distribution resulted in preferential cleavage of the inner carbon-carbon bond of n-pentane compared to the outer ones at which the primary products C_2 and C_3 and to a lower extent C_1 and C_4 were formed in equal measure. Secondary hydrogenolysis reactions of the formed fragments were observed only to a low content at higher conversion levels. The side reaction showed typical characteristics of structure sensitivity.

The approach applied to enhance catalyst activity was to functionalize the zeolite with sulfate anions *via* H₂S chemisorption followed by oxidation. An enhancement of isomerization activity and selectivity was achieved by choosing favorable sulfation conditions.

The treatment by H₂S and air has subtle effects on the structural, acidic and metallic properties of the zeolite. In addition the metal content plays a key role in the sulfation process. The metal properties of the sulfated samples were investigated using XAS measurements on the Pt L_{III}-edge, CO adsorption, H₂ chemisorption, TEM and hydrogenolysis reaction of neo-pentane. The acidic properties were studied by IR with different probe molecules, XAS measurements on the S K-edge, NMR and temperature programmed desorption measurements.

Gasphase sulfation potentially reduces the dehydrogenation activity of the Pt loaded zeolite through three effects: agglomeration, poisoning and reduction of adsorption properties.

Poisoning by the formation of PtS species was observed during H₂S treatment. During oxidation the number of sulfide species is severely reduced, however sulfur residues remain even though a subsequent reduction with hydrogen was applied for the poisoned catalysts. Higher oxidation temperatures reduce the sulfide content, however agglomeration occurs which outweighed the reduction of metal surface compared with the sulfation treatment at lower temperatures. Additionally the formation of sulfate species at perimeter sites of platinum was shown to abstract electrons from the metal particles. The resulting reduction of the electron density of the sulfated samples is assumed to reduce the adsorption strength and therefore the dehydrogenation activity.

Additionally it was shown that the acidic properties of the zeolite were significantly influenced. Brønsted acidic sulfate species can be anchored on the sample increasing the overall acidity and thus the isomerization activity for the Pt loaded zeolite. The additional sulfate groups possessed an acid strength similar to the acidic groups of the zeolite. Therefore the sulfated samples must be operated under reaction conditions similar to the parent zeolite samples. The experimental conditions for the sulfation process should be as mild as possible in order to maintain the structural integrity of both catalyst components. Working at low equilibrium concentrations for sulfuric acid it is possible to increase the

concentration of bridging hydroxyl groups of the zeolite during sulfation by removal of cationic alumina species blocking ion exchange sites.

The sulfation process occurs *via* the formation of sulfide species on extra framework sites during the H₂S treatment. Simultaneously a partial dealumination of the zeolite framework was observed. During oxidation these sulfide species are converted on site to form sulfate species. Furthermore it was shown that the platinum particles are necessary for catalyzing the kinetically controlled formation of SO₃. Therefore high metal loaded catalysts possess a higher acidity and isomerization activity after sulfation.

Besides activity enhancement a severe improvement of the isomerization selectivity was observed after the gasphase sulfation process. It was argued that the formation of PtS species selectively blocks the side reaction still allowing the dehydrogenation step which is required for the alkane activation to proceed. It was suggested that the sulfur species affect the surface geometry of the metal particles *e.g.* by changing the index crystallite facets, thus leading to a hindrance of the structure sensitive side reaction. Both, larger free ensembles of Pt atoms and highly reactive and exposed metal atoms, are expected to be reduced dramatically by the presence of sulfur on the metal thus preventing the hydrogenolysis reaction to occur. The selectivity enhancement after the sulfation process was independent of the metal loading.

In contrast to zeolite BEA it was shown that the isomerization activity of zeolite MOR is restricted by single file diffusion. Gasphase as well as aqueous sulfation of zeolite MOR did not improve diffusivity in the zeolite. High contents of sulfate led to a significant reduction of the bridging hydroxys due to a partial dealumination of the framework and a reduced accessibility of the pore system. However for mildly sulfated samples and thermal dealuminated samples it was possible to increase the isomerization activity through the incorporation of active sulfate species.

Finally tungsten was presented as an acidity promoter on the zeolite BEA. Although the overall Brønsted acidity was not affected by the incorporation of the formed tungstate species a distinct influence on the acidic and catalytic behavior was observed. It was argued that polytungstate clusters are formed, which possess Lewis and Brønsted acidity. Additionally the tungsten promoted sample was shown to reach a more pronounced activity enhancement after a subsequent gasphase sulfation.

7.2 Zusammenfassung

Iso-Pentan und iso-Hexane sind wichtige Komponenten von hochoktanigen Benzin, die zu einem großen Anteil durch Hydroisomerisierung von n-Alkanen hergestellt werden. Das Interesse an dem Hydroisomerisierungsprozess ist aufgrund verschärfter Umweltauflagen, welche vor allem den Gehalt von Aromaten und Oxidierungsmitteln die bisher als Oktanzahlbooster verwendet wurden reduzieren, gewachsen. Ziel dieser Arbeit war ein fundiertes Verständnis der Isomerisierungsreaktion an bifunktionellen Katalysatoren bereitzustellen sowie die Aktivität und Selektivität der Katalysatoren zu optimieren.

Durch kinetische Untersuchungen zur Pentanhydroisomerisierung konnte gezeigt werden, dass die Reaktion durch das thermodynamische Gleichgewicht limitiert ist und eine Reaktionsenthalpie von -7 kJ/mol besitzt. Die Anwendung geringer Reaktionstemperaturen ermöglicht daher höhere Isomerisierungsausbeuten zu erreichen. Kapitel 3 beschreibt den Einfluss von Platin auf die Isomerisierungsstabilität, -aktivität und -selektivität. Die Untersuchungen zeigten, dass die Dehydrierungseigenschaften von Platin zur Aktivierung des Alkans notwendig sind. Für hohe Olefinkonzentration tritt jedoch Katalysatordeaktivierung durch Oligomerisation auf, was zu hohen Anteilen von iso-Butan und iso-Hexanen führt. Für eine konstante Isomerisierungsaktivität ist daher zusätzlich Wasserstoff erforderlich, was zu einer geringeren Olefinkonzentrationen führt und zur Hydrierung von Koksprecursor. Entsprechend des klassischen Isomerisierungsmechanismus wurde ein kinetisches Modell hergeleitet. Die Anpassung der Daten an das Modell ergaben, dass bereits bei einem Verhältnis von Oberflächenplatinatomen zu Brønstedsäurezentren größer als 0.033 die Reaktion durch die Säurezentren des Zeoliths limitiert ist. Platin besitzt daher für das gegebene Verhältnis $\text{Pt}_s/\text{H}^+_{\text{BAS}}$ keinen Einfluss auf die Isomerisierungsaktivität. Da bei steigenden und anschließend sinkenden Temperaturrampen keine Hystereseerscheinungen beobachtet wurden kann angenommen werden, dass unter den untersuchten Reaktionsbedingungen keine Deaktivierung auftritt. Reaktionsordnungen von $n_{\text{C}_5}=+1$ für Pentan und $n_{\text{H}_2}=-1$ für Wasserstoff wurden bestimmt. Obwohl Platin keinen Einfluss auf die Isomerisierungsaktivität besitzt wurde eine deutliche Erniedrigung der Isomerisierungsselektivität mit zunehmendem Platingehalt beobachtet, was als eine Nebenreaktion auf den Metallzentren (Hydrogenolysereaktion) gedeutet wurde. Hierbei wurde eine bevorzugte Spaltung der inneren C-C Bindung des Pentanmoleküls beobachtet, wobei als Hauptnebenprodukte C_2 und C_3 , sowie zu

geringeren Mengen C_1 und C_4 gebildet werden. Folgereaktionen der Spaltprodukte wurden nur zu geringem Anteil bei hohen Umsätzen beobachtet. Die Nebenreaktion wies desweiteren typische Merkmale einer struktursensitiven Reaktion auf. So wurde beispielsweise eine Erhöhung der Turnover Frequency (auf Metalloberfläche normierte Aktivität) für große Metallpartikel beobachtet.

Der Ansatz, der zur Steigerung der Katalysatoraktivität verfolgt wurde, beinhaltete die Funktionalisierung der Zeolithe mit Sulfatspezies mittels H_2S Behandlung und anschließender Oxidation. Die Wahl geeigneter Sulfatisierungsbedingungen führte zu einer Verbesserung der Isomerisierungsaktivität und -selektivität.

Die Behandlung mit H_2S und Luft besitzt einen deutlichen Einfluss auf die strukturellen, aziden und metallischen Eigenschaften des Zeolithes. Des weiteren spielt Platin eine Schlüsselrolle während der Sulfatisierungsbehandlung. Die metallischen Eigenschaften der sulfatisierten Proben wurden durch XAS Messungen an der Pt-L_{III} Kante, CO Adsorption, Wasserstoffchemisorption, TEM und neo-Pentanhydrogenolyse-reaktion charakterisiert. Die aziden Eigenschaften wurden durch IR Messungen verschiedener Testmoleküle, XAS Messungen an der S-K Kante, NMR und Temperatur-programmierter Desorption untersucht.

Die Gasphasensulfatisierung bewirkt potenziell eine Reduzierung der Dehydrier-eigenschaften durch drei unterschiedliche Vorgänge: Agglomeration, Vergiftung und Reduzierung der Adsorptionseigenschaften.

Die Bildung von PtS Spezies wurde während der H_2S Behandlung beobachtet. Durch die anschließende Oxidation konnte die Anzahl der Sulfidspezies deutlich reduziert werden. Trotz anschließender Reduzierung im Wasserstoffstrom ist es jedoch nicht möglich das Auftreten von Schwefelrückständen nach dem Oxidationsvorgang zu vermeiden. Der Sulfidgehalt der Katalysatoren kann durch höhere Oxidationstemperaturen reduziert werden, was allerdings ein verstärktes Sintern der Metallpartikel verursacht, wodurch der Anteil an Oberflächenplatinatomen stärker reduziert wird als bei niedrigen Oxidationstemperaturen. Die Bildung von Sulfatspezies in der unmittelbaren Nähe von Platinpartikeln führt desweiteren zu einer Reduzierung der Elektronendichte am Metall. Dies führt zur Reduzierung der Adsorptionsstärke und damit zur Verringerung der Dehydrierungseigenschaften.

Nach der Optimierung der Sulfatisierungsbedingungen konnte gezeigt werden, dass es möglich ist Brønsted azide Sulfatspezies auf den Proben zu verankern und damit die Gesamtazidität zu steigern, was zu einer Erhöhung der Isomerisierungsaktivität führt. Die Sulfatgruppen besitzen ähnliche Zentrenstärken wie die aziden brückenbildenden Hydroxylgruppen des Zeoliths und müssen daher bei ähnlichen Reaktionsbedingungen wie die nicht behandelten Zeolithe gefahren werden. Es ist notwendig während der Schwefelbehandlung milde Reaktionsbedingungen zu wählen, um die strukturelle Integrität der beiden Katalysatorkomponenten zu erhalten. Bei der Wahl geringer Gleichgewichtskonzentrationen für Schwefelsäure ist es des weiteren durch das Entfernen von blockierenden Aluminiumkationen möglich, durch die Schwefelbehandlung die Konzentration der brückenbildenden Hydroxylgruppen des Zeolithes zu erhöhen.

Der Sulfatisierungsprozess läuft über die Bildung von Sulfidspezies auf aus dem Gitter herausgelöstem Aluminium (extra-framework Al) ab. Während der Oxidation werden diese Sulfidspezies vorort zu Sulfatspezies umgewandelt. Zusätzlich wurde gezeigt, dass die Platinpartikel notwendig sind, um die kinetisch kontrollierte Bildung von SO_3 zu katalysieren. Katalysatoren mit hohem Platingehalt besitzen daher nach der Sulfatisierungsbehandlung eine höhere Azidität und Isomerisierungsaktivität.

Neben der Aktivitätssteigerung wurde nach der Gasphasensulfatisierung ebenso eine deutliche Selektivitätssteigerung beobachtet. Es wurde argumentiert, dass Platinsulfide selektiv die Nebenreaktion unterbinden, während die Dehydrierung, die für die Aktivierung des Alkans nötig ist, weiterhin stattfinden kann. Es wurde vermutet, dass die Schwefelspezies die Oberflächengeometrie der Metallpartikel beeinflusst, beispielsweise durch Veränderung des Oberflächenindex von Facetten, was zu einer sterischen Behinderung der struktursensitiven Nebenreaktion führt. Es kann davon ausgegangen werden, dass sowohl große, freie Ensemble von Platinatomen als auch reaktive Oberflächenatome durch die Schwefelspezies drastisch reduziert werden, was das Auftreten der Hydrogenolysereaktion verhindert.

Im Unterschied zu Zeolith BEA wurde gezeigt, dass die Isomerisierungsaktivität für Zeolite MOR durch sog. „single file diffusion“ eingeschränkt ist. Weder durch Gasphasen- noch durch Flüssigphasensulfatisierung konnte eine Verbesserung der Diffusivität im Zeolith erreicht werden. Hohe Sulfatgehalte führten zu einer merklichen Reduzierung der brückenbildenden Hydroxylgruppen, verursacht durch eine partielle Dealuminierung des

Gitters und zu einer reduzierten Erreichbarkeit des Porensystems. Für Proben mit geringem Sulfatgehalt oder für stark dealuminierte Proben konnte durch die Einbringung von aktiven Sulfatspezies eine Steigerung der Isomerisierungsaktivität beobachtet werden.

Abschließend wurde Wolfram als Aziditätspromoter vorgestellt. Obwohl die gebildeten Wolframspezies die Brønsted-Gesamtazidität nicht veränderten wurde ein deutlicher Unterschied in den aziden und katalytischen Eigenschaften beobachtet. Es wurde argumentiert, dass Polywolframatclustern gebildet werden, welche zusätzlich Brønsted- und Lewisazidität besitzen. Desweiteren wurde bei den mit Wolfram behandelten Proben eine verstärkte Aktivitätssteigerung nach einer anschließenden Sulfatisierungsbehandlung festgestellt.

CURRICULUM VITAE

Christian Woltz was born in Marktheidenfeld, Germany, on November 22th, 1976. After finishing high school in Wertheim in 1996 he started his chemical engineering studies at Friedrich Alexander Universität in Erlangen. He finished his studies in 2002 after writing his diploma thesis entitled “Characterization of the fluid dynamics of a high loaded, circulating fluidized bed” at the chair of mechanical process engineering under the supervision of Prof. K.-E. Wirth. He joined the chair of catalysis and reaction engineering (TC2) of Prof. J.A. Lercher at Technical University Munich to start research on alkane hydroisomerization on bifunctional catalysts in 2002.